2007

Investigation on chemical steps of thymidylate synthase catalyzed reaction

Baoyu Hong
University of Iowa

INVESTIGATION ON CHEMICAL STEPS OF THYMIDYLATE SYNTHASE CATALYZED REACTION

by

Baoyu Hong

An Abstract

Of a thesis submitted in partial fulfillment
of the requirements for the Doctor of
Philosophy degree in Chemistry
in the Graduate College of
The University of Iowa

December 2007

Thesis Supervisor: Associate Professor Amnon Kohen

ABSTRACT

Thymidylate synthase (TS) catalyzes the reductive methylation of 2'-deoxyuridylate (dUMP) with cofactor 5,10-methylene-5, 6, 7, 8-tetrahydrofolate, forming thymidine monophosphate (dTMP) and 7, 8-dihydrofolate. The reaction pathway is comprised of at least seven covalent bond cleavage or formation, therefore, it is a very complex system for scientists to explore the mechanistic details of this reaction. In my Ph.D work, two microscopic steps in TS-catalyzed pathway were investigated by means of kinetic isotope effects (KIE), their temperature dependence and steady state initial velocity measurements. Chapter II of my thesis focuses on testing the quantum mechanical behavior of the last hydride transfer step. Chapter III is involved in studying the coupled motion between primary and secondary hydrogens for the same hydride transfer step. In Chapter IV we used same methodology to explore the mechanistic details on the last hydrogen transfer step by comparison of the temperature dependency of the intrinsic KIE using the wild type and the mutant W80M TS. The effect of the mutation on the proton abstraction was examined by comparison of the temperature dependency of the intrinsic KIE using the wild type and Y94F TS. The further examination of the subsequent hydride transfer using the wt and Y94F gave details on the reaction mechanism and on the role of tyrosine in the active site.

Abstract Approved: _____
Thesis Supervisor

_____
Title and Department

_____
Date

INVESTIGATION ON CHEMICAL STEPS OF THYMIDYLATE SYNTHASE CATALYZED REACTION

by

Baoyu Hong

A thesis submitted in partial fulfillment
of the requirements for the Doctor of
Philosophy degree in Chemistry
in the Graduate College of
The University of Iowa

December 2007

Thesis Supervisor: Associate Professor Amnon Kohen

Graduate College
The University of Iowa
Iowa City, Iowa

CERTIFICATE OF APPROVAL

_____

PH.D. THESIS

_____

This is to certify that the Ph.D. thesis of

Baoyu Hong

has been approved by the Examining Committee
for the thesis requirement for the Doctor of Philosophy
degree in Chemistry at the December 2007 graduation.

Thesis Committee: _____
Amnon Kohen, Thesis Supervisor

_____
Daniel M. Quinn

_____
Lei Geng

_____
Sarah C. Larsen

_____
S. Ramaswamy

ACKNOWLEDGMENTS

I would like to express my deep and sincere gratitude to my research adviser, Dr. Amnon Kohen, for his valuable guidance, motivation, encouragement, patience, understanding and support in all the time of my research, writing and studies at the University of Iowa. His curiosity, wide knowledge and logical way of thinking are of great value for me all the time.

I would also like to express my warm and sincere thanks to all the past and current members of Dr. Kohen's group for their kind help, support and friendship.

I would like to thank Dr. Frank Maley, our longtime collaborator, for providing enzyme plasmid, samples and constructive suggestions for publication. I thank Dr. Santhana Velupillai of the University of Iowa NMR Central Research Facility for his assistance in my research.

I would like to thank Drs. Quinn, Geng, Larsen and Rams for their instructions and advice while serving on my committee. My warm thanks are due to all the support staff in Chemistry Department- Janet, Sharon, Lin, Tim, Pete, Frank and especially to Karen (custodian) whose kind help and warmness to me. Financial support from the National Science Foundation and the National Institutes of Health is appreciated.

I also wish to thank all my friends in Iowa City, although their names could not be listed here individually.

I wish to express my thanks to my parents for their love and encouragement. I would like to give my special thanks to the most important person in my life, my husband, Chunlei, whose love and support enabled me to complete this thesis.

Finally, I would like to thank everyone who has contributed to this work by his/her time, help, and friendship.

TABLE OF CONTENTS

LIST OF TABLES

Table

LIST OF FIGURES

Figure

LIST OF SCHEMES

Scheme

LIST OF ABBREVIATIONS

TS – Thymidylate synthase

*Tb*ADH – *Thermoanaerobium Brockii* Alcohol dehydrogenase

DHFR – Dihydrofolate reductase

RP HPLC – reverse phase high performance liquid chromatography

KIE – kinetic isotope effect

5-FdUMP – 5 fluoro 2' – deoxyuridine-5'-monophosphate

dUMP – 2'- deoxyuridine-5'-monophosphate

dTMP – 2' – deoxythymidine-5'-monophosphate

H_2F – dihydrofolate

TEAA – Triethyl ammonium acetate

ACN – Acetonitrile

CH_2H_4folate - N^5, N^{10}-methylene-5, 6, 7, 8-tetrahydrofolate

PHM - peptidylglycine α- Hydroxylating Monooxygenase

LSC - liquid scintillation counter

NADPH - reduced β – nicotinamide adenine dinucleotide 2' – phosphate

ZPE - zero point energy

CHAPTER I

INTRODUCTION

Research Scope

The general interest of our research is to understand how enzymes catalyze the chemical steps in complex reactions. Such understanding may assist the rational design of drug. Thymidylate synthase has been selected as a research model and two C-H cleavage steps in its reaction pathway were studied. Several issues have been explored in our study, including: (i) the involvement of protein fluctuation for chemical steps in the active site; (ii) Coupled motions between centers of primary and secondary isotopic substitution; and (iii) the mechanism of microscopic steps and the role of highly conserved residues in catalysis.

Thesis Overview

Thymidylate synthase (TS) catalyzes the reductive methylation of 2'-deoxyuridylate (dUMP) with cofactor 5,10-methylene-5, 6, 7, 8-tetrahydrofolate (CH_2H_4folate), forming thymidine monophosphate (dTMP) and 7, 8-dihydrofolate (H_2folate) (*1, 2*). The reaction pathway is comprised of at least seven covalent bond cleavage or formation steps, therefore, it is a very complex system for scientists to explore the mechanistic details of this reaction. In the current work, two microscopic steps in the TS-catalyzed pathway were investigated by means of kinetic isotope effects (KIE), their temperature dependence and steady state initial velocity measurements. Chapter II focuses on testing the quantum mechanical behavior of the last hydride transfer step. In Chapter III we used the same methodology to explore the mechanistic details on the last hydrogen transfer step by comparison of the temperature dependency

of the intrinsic KIE using the wild type and the mutant W80M TS. Chapter IV describes studies of the coupled motion between primary and secondary hydrogens for the same hydride transfer step. The role of Tyr94 on a proton abstraction step and the subsequent hydride transfer was examined by comparison of the temperature dependency of the intrinsic KIE using the wild type and Y94F TS as described in Chapters V and VI. The studies are summarized and future studies are outlined in Chpater VII.

Background

Thymidylate Synthase

Thymidylate Synthase (TS) is one of the enzymes that catalyze DNA biosynthesis. TS catalyzes the reductive methylation of dUMP (*1*). The cofactor CH_2H_4folate serves as the donor for both hydrogen and methylene for the C7 methyl group in the product dTMP. The TS mechanism is essential for living organisms since it catalyzes the last committed step in DNA biosynthesis. Therefore, TS has long been studied as a target for chemotherapy and gene therapy (*3, 4*). The crystal structure of *E. coli* thymidylate synthase is shown in Figure 1.1 (PDB entry 2KCE). It is a homodimer with molecular weight of about 60 kDa and it is an enzyme of half-the-sites activity (*5*). The dimer interface is constructed with two 6-stranded sheets and the active site is deeply buried in each subunit (*6*). TS has been studied extensively by means of kinetic, genetic and structural methodologies due to its central role in DNA biosynthesis. Despite the wealth of information, the molecular mechanism for these proposed steps and the role of several conserved residues are still controversial.

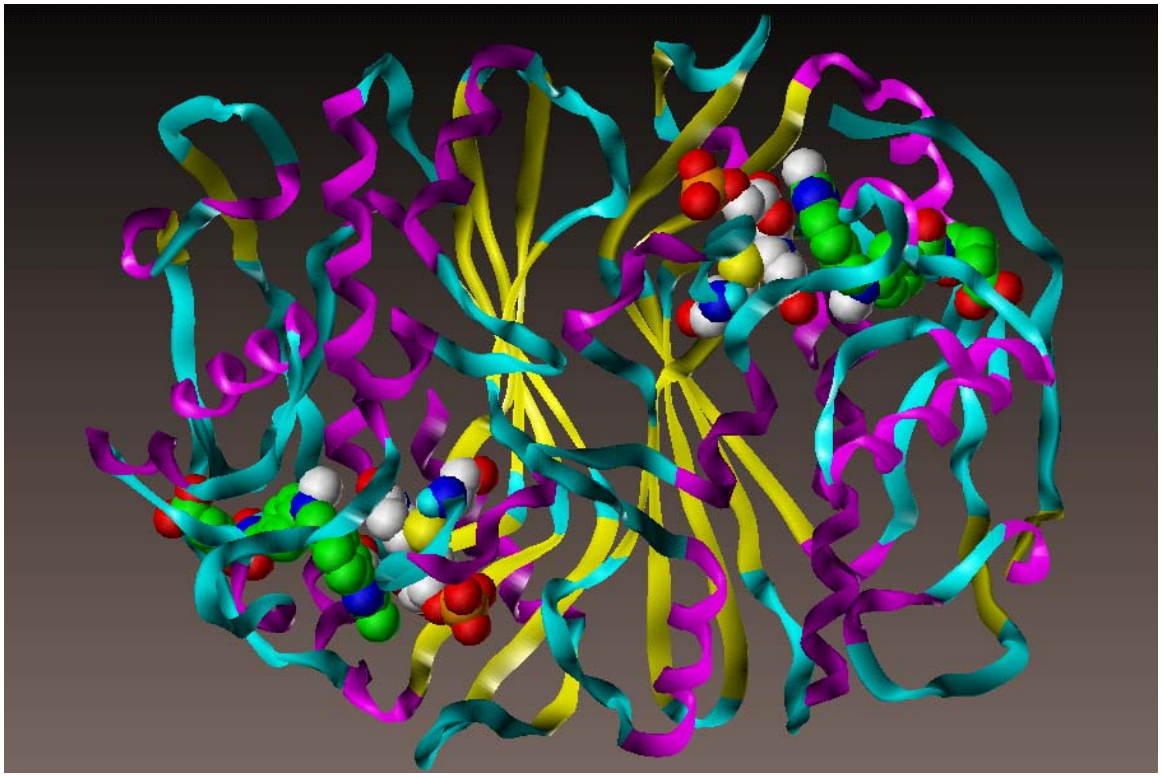

Figure 1.1 Ribbon diagram of *ec*TS dimer (PDB entry 2KCE).

Therefore, the objective of my current PhD research is to investigate the physical nature of microscopic steps of this reaction mechanism in detail.

Approaches and theoretical models

Kinetic isotope effect (KIE)

KIE is defined as the rate ratio of two reactants that only differ by their isotopic compositions (*7*). Figure 1.2 illustrates the semiclassical model for the transfers of H, D and T (the three isotopes of hydrogen) (*8-11*). It predicts that if tunneling does not contribute to the reaction rate, then the rate differences of H, D, and T will arise mostly from their different zero-point energies. When tunneling occurs, the tunneling correction is expected to be larger for H than for the heavier isotopes D or T.

Temperature dependency of kinetic isotope effect as a probe of tunneling

Kinetic isotope effects (KIE) and their temperature dependency were mainly used in our study as a measure of the nature of hydrogen transfer. Tunneling can be addressed as a correction to the transmission coefficient based on the shape of the reaction barrier (*12-14*). Such models predict temperature dependencies of reaction rates (v) that follow the empirical Arrhenius equation with temperature independent tunneling contribution: $v = A \bullet e^{-Ea/RT}$. Figure 1.3 illustrates the tunneling correction model in cases of no tunneling (I), moderate tunneling (II) and extensive tunneling (III). According to the tunneling correction of transition state model, the KIE on the Arrhenius preexponential factors should be close to unity at the region with no tunneling (I), smaller than 1 for a system with moderate tunneling (II), and larger than 1 in the case of extensive tunneling (III) (*13, 15, 16*).

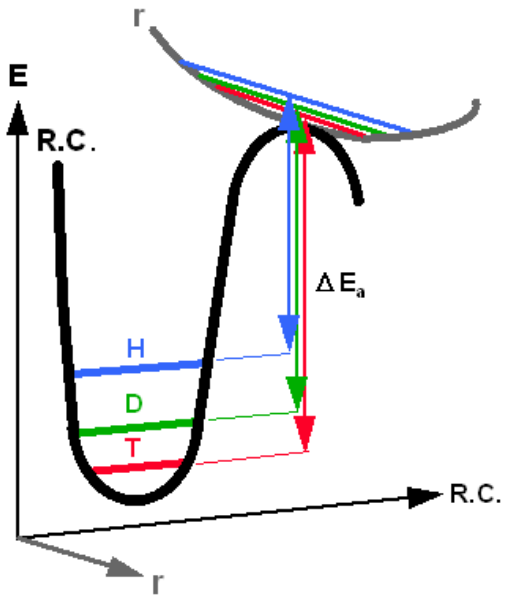

Figure 1.2 Semiclassical model. Different energies of activation (Δ*E*a) for H (blue), D (green) and T (red) result from their different zero-point energies (ZPE) at the ground state (R) and transition state (TS). R. C. reaction coordinate.

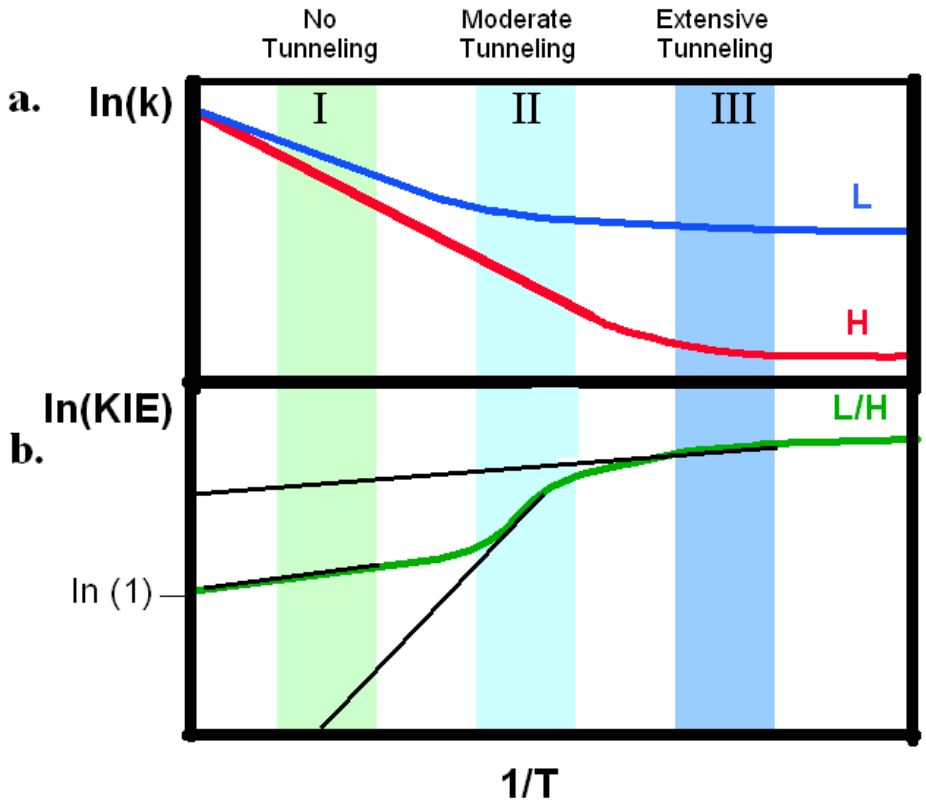

Figure 1.3 An Arrhenius plot of hydrogen transfer with a temperature independent tunneling contribution.

Dynamics and environmentally enhanced tunneling

Although the semiclassical model (Figure 1.3) has been proven to be powerful to explain the quantum mechanical behavior of many systems, there are several systems that semi-classical or rigid barrier models cannot explain. More and more experimental data need a "dynamic" model that could explain temperature independent KIEs with significant energy of activation. A number of dynamic models with a fluctuating potential surface have been proposed to rationalize these phenomena (*17-21*). Two common features of these models are the Marcus-like term and the separation of the reaction coordinate into two separate orthogonal vibrations. In such a model, the rate for hydrogen tunneling arises from the combination of two terms: one is non-isotopically sensitive but determines most of the temperature dependence of the rates, and the other (depicted as the Franck-Condon term (*22*)) is isotopically sensitive and includes a tunneling contribution and classical fluctuations between donor and acceptor. The tunneling in such a model is dominated by the symmetry of the vibration levels (reorganization energy λ and driving force ΔG^0, referred to "rearrangement" term in Marcus theory) and by the fluctuations of the distance between donor and acceptor, referred to as "gating" (*22, 23*)). Therefore, these models can explain the phenomena of temperature independences of KIEs with temperature dependences of reaction rates that cannot be explained in the frame of semi-classical models.

CHAPTER II

VIBRATIONALLY ENHANCED HYDROGEN TUNNELING IN THE *ESCHERICHIA COLI* THYMIDYLATE SYNTHASE CATALYZED REACTION

This chapter has been published in the journal *Biochemistry*. Vibrationally enhanced hydrogen tunneling in the *E. coli* thymidylate synthase catalyzed reaction. Agrawal, N., Hong, B., Mihai, C., and Kohen, A. *Biochemistry*, **2004**, 43, 1998-2006.

Summary

The enzyme thymidylate synthase (TS) catalyzes a complex reaction that involves forming and breaking at least seven covalent bonds. The physical nature of the hydride transfer step in this complex reaction cascade has been studied by means of isotope effects and their temperature dependence. Competitive kinetic isotope effects (KIEs) on the first order rate constant (*V/K*) were measured over a temperature range of 5 to 45 ˚C. The observed H/T ($^{T}V/K_{H}$) and D/T ($^{T}V/K_{D}$) KIEs were used to calculate the intrinsic KIEs throughout the temperature range. The Swain-Schaad relationships between the H/T and D/T *V/K* KIEs revealed that the hydride transfer step is the rate-determining step at the physiological temperature of *E. coli* (20-30 ˚C), but is only partly rate-determining at elevated and reduced temperatures. The H/D KIE on the first order rate constant k_{cat} (^{D}k = 3.72) has been previously reported (*27*). Additionally, the Swain-Schaad relationships between that ^{D}k and the *V/K* KIEs reported here suggested that at 20 ˚C the hydride transfer step is the rate-determining step for both rate constants. Intrinsic KIEs were calculated here and were found to be virtually temperature independent (ΔE_a = 0 within experimental error). The isotope effects on the preexponential Arrhenius factors

for the intrinsic KIEs were $A_H/A_T = 6.8 \pm 2.8$ and $A_D/A_T = 1.9 \pm 0.25$. Both effects are significantly above the semiclassical (no-tunneling) predicted values and indicate a contribution of quantum mechanical tunneling to this hydride transfer reaction. Tunneling correction to transition state theory would predict that these isotope effects on activation parameters result from no energy of activation for all isotopes. Yet, initial velocity measurements over the same temperature range indicate cofactor inhibition and result in significant activation energy on k_{cat} (4.0 ± 0.1 kcal/mol). Taken together, the temperature independent KIEs, the large isotope effects on the preexponential Arrhenius factors, and a significant energy of activation, all suggest vibrationally enhanced hydride tunneling in the TS catalyzed reaction.

Introduction

Thymidylate synthase (TS) (EC 2.1.1.45) catalyzes the last committed step in the *de novo* biosynthesis of 2'-deoxythymidine-5'-monophosphate (dTMP – one of the four building blocks of DNA). The enzyme catalyzes the reductive methylation of 2'-deoxyuridine-5'-monophosphate (dUMP) to dTMP. Apparently, two independent reactions are involved in which the cofactor N^5, N^{10}-methylene-5, 6, 7, 8-tetrahydrofolate (CH_2H_4folate) serves as a donor of both methylene and hydride (*1*). The enzyme is crucial for DNA biosynthesis and is over-expressed in actively proliferating cells such as tumor cells (*24*). TS is the target of the widely used chemotherapeutic drug 5-fluorouracil (5-FU) which, after metabolism to 5-fluoro-2'-deoxyuridine-5'- monophosphate (5F-dUMP), acts as a potent inhibitor and is active against solid tumors like those found in breast, head, neck, and colon cancers. However, to significantly inhibit large amounts of TS in tumor cells, high concentrations of TS inhibitory anticancer drugs are necessary.

This harms normal tissue cells and results in toxicity. A favorable response to anticancer TS inhibitors results in increased metabolic demand by rapidly proliferating tumors. As a result, the use of TS inhibitors commonly lead to a further increase of TS expression levels in tumor cells (*25*), making it more difficult to achieve effective treatment without side-effects and leading to drug resistance (*26*). A better understanding of the TS molecular mechanism may lead to more specific drugs that will specifically inhibit it in cancerous but not in normal cells, or alternatively, inhibit it in bacterial but not in human cells. Additionally, preferable inhibition in bacterial but not in human cells can lead to antibiotic drugs.

TS from *E. coli* (*ec*TS) has been extensively studied in terms of structure, kinetics, and mechanism (*1, 2, 27*). The enzyme is a homodimer with a molecular weight of 60 kDa. It is among the most highly conserved enzymes with approximately 18% of residues that are strictly conserved among at least 17 sequences (*6*). Numerous X-ray structures of free and bound enzyme-substrate-cofactor analogues have been determined, and several hundred mutants have been cloned and studied (*2, 6*). Steady-state kinetic studies suggest a BiBi ordered mechanism of reactants binding and products release (Scheme 2.1) (*1*).

The overall reaction catalyzed by TS can be described as methyl for proton substitution at a vinylic carbon α to a carbonyl. A multi-step reaction mechanism has been proposed in which TS transfers a methylene group from CH_2H_4folate to dUMP followed by reduction of the methylene to methyl group to yield dTMP and H_2folate (Scheme 2.2). The formation of a ternary complex between enzyme, dUMP and

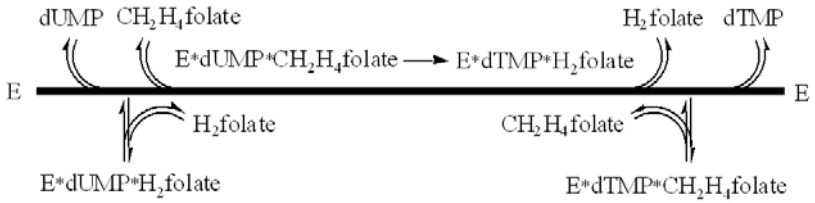

Scheme 2.1 Order of substrate binding and product release during the catalytic cycle of *E. coli* TS on the basis of initial velocity and product inhibition studies (adapted from Carreras and Santi) (1).

CH_2H_4folate aligns an overall conserved active site cysteine residue (Cys 146 in *E. coli*) that nucleophilically attacks the C-6 of dUMP (reaction 1 in Scheme 2.2). In *E. coli* TS, Glu 58 serves as a general base in the activation of the CH_2H_4folate cofactor to form an iminium ion (A). Then, the C5 carbon of the activated enol (B) nucleophilically attacks the methylene Schiff-base iminum ion (A) to form an enzyme bound covalent intermediate (C) (*28, 29*). This is followed by abstraction of a proton from C-5 of dUMP (probably by Tyr94 in *E. coli* as general base) to form the enol (D), which leads to the elimination of 5,6,7,8-tetrahydrofolate (H_4folate) to form the intermediate (E)(*30*). Finally, the exocyclic methylene intermediate is reduced by hydride from the 6*S* position of H_4folate to form dTMP and 7,8 dihydrofolate (H_2folate). It is not clear at this stage whether step 5 proceeds via another enolate intermediate or by a S_N2 fashion.

In this chapter we present mechanistic studies of the hydride transfer step (reaction 5 in Scheme 2.2), in which tools of physical chemistry were developed to examine the possible contributions of quantum mechanical H-tunneling and enzyme/environmental motion to the TS catalyzed reaction. Possible contributions of such phenomena to enzyme catalyzed reactions are a matter of intensive research and have evoked substantial debate in recent years (*15-17, 22, 31-34*). In a recent review, Benkovic and Hammes-Schiffer (*35*) summarize the current state of "our understanding or ignorance" in the field of mechanistic enzymology. As emphasized in their discussion, the ability to expose and study the chemical step of interest within any enzymatic cascade is a major challenge, and often the progress-limiting step. The work presented herein represents a study of one chemical step in such a complex chemical cascade. This work focuses on issues central to the discussion presented in Ref (*35*), namely, the

contributions of tunneling and enzyme motion to the catalyzed reaction.

The nature of the hydride transfer step is examined by means of intrinsic KIEs, their temperature dependence and activation parameters. The first temperature dependence of intrinsic KIEs has recently been reported by Francisco et al. (*36*), who studied peptidylglycine α- Hydroxylating Monooxygenase (PHM). Observed H/D and H/T KIEs were used to calculate intrinsic KIEs in a 5 to 45 ˚C temperature range. The method presented here for studying of TS is different in several aspects from that used for PHM (*36*): (i) very different chemistry (H• vs. H^-); (ii) a unique labeling pattern; (iii) a new analytical methodology; and (iv) different data analysis. Yet, both studies reveal the degree and nature of quantum mechanical tunneling in a H-transfer catalyzed reaction. Quantum mechanical tunneling is the phenomenon in which a particle transfers through a reaction barrier due to its wave-like properties (*13, 37, 38*). Quantum mechanical transfer of hydrogen at various oxidation states has been studied in several enzymatic systems, and was also associated with protein motion; its active site vibrations; or other environmental fluctuations (*16, 22, 39-49*). This effect is often depicted as "dynamics", but here we will use the terminology of Benkovic, Hammes-Schiffer, Warshel and others, in which "dynamics" are only non-equilibrium motions along the reaction coordinate (*32, 35, 50, 51*). It is important to note that similar phenomena have also been reported for non-enzymatic systems as discussed below (*52-58*).

Kinetic complexity and commitment to catalysis were also investigated and analyzed in the context of previous studies of non-competitive KIE at 20 ˚C (*27*). The research presented here involves a more complex pattern of isotopic labeling that enabled calculation of intrinsic KIEs. The current study also examines the temperature

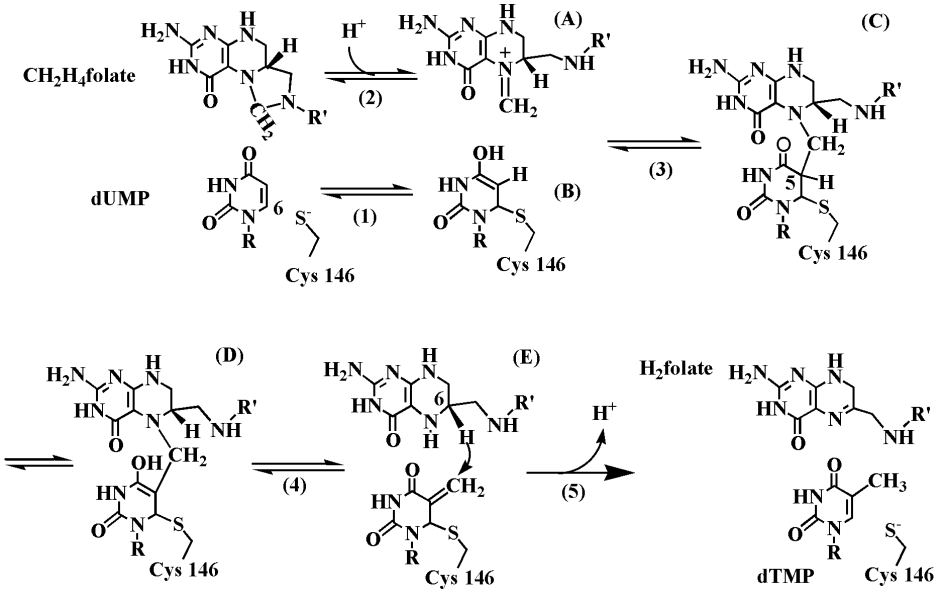

Scheme 2.2 Proposed chemical mechanism for the *E. coli* TS catalyzed reaction (adapted from Carreras and Santi (1)). R = 2' – deoxyribose 5' – phosphate and R' = (*p*-aminobenzoyl) glutamate.

dependency, the cofactor inhibition, and the activation parameters of the rate constants and the intrinsic KIEs.

Materials and Methods

Triethyl ammonium acetate (TEAA), acetonitrile (CH_3CN), dUMP, and dTMP were purchased from Sigma. CH_2H_4folate was a generous gift from Eprova Inc, Switzerland. The synthesis of *R*-[6-^{3}H]CH_2H_4folate cofactor was described in detail elsewhere (*59*). In short, labeled $NaBH_4$ reduced acetone to labeled isopropanol (*60*) that was then used to reduce $NADP^+$ to *R* labeled NADPH with alcohol dehydrogenase from *Thermoanaerobium Brockii* (*tb*ADH). This cofactor reduces H_2folate with DHFR to produce 6*S* labeled H_4folate that yields *R*-[6-^{3}H]CH_2H_4folate upon quenching with formaldehyde. The specific radioactivity used in the kinetic experiments was 375 Ci/mol, which means that ~ 1 % of the molecules were tritiated at the 6*R* position (the remainder was protonated at that position). A similar mixture of ~ 1 % *R*-[6-^{3}H]CH_2H_4folate in *R*-[6-^{2}H]CH_2H_4folate was synthesized by a similar procedure. But instead the synthesis was started from [^{3}H]-$NaBH_4$ mixed with $NaBD_4$ (> 99 % D) to the same final specific activity. [2-^{14}C]-dUMP (specific radioactivity: 60 Ci/mol) was from Moravek Biochemicals. Tris (hydroxymethyl) aminomethane, ethylene diamine tetraacetic acid (EDTA), and β-mercaptoethanol were purchased from Sigma**.** Ultima Gold Liquid Scintillation Cocktail and liquid scintillation vials were purchased from Packard Bioscience. The expression system for *E. coli* TS was a generous gift from R. Stroud (University of California at San Francisco). The enzyme was produced and purified following a published procedure (*61*). The HPLC system used was Agilent Technologies (previously HP) model 1100 equipped with an online degasser, quaternary pump,

temperature controlled column chamber, UV/VIS diode array detector and a manual injector. The column (C18, 250 X 4.6 mm, 5 μm, Discovery series) was from Supelco, and the column temperature was maintained at 25 ºC. All analytical procedures are published in detail elsewhere (*59*).

Competitive Kinetic Isotope Effects (This work was performed by Nitish Agarwal)

Primary (1°) H/T and D/T KIEs were measured competitively. All experiments were performed in 100 mM Tris Buffer (pH = 7.5, adjusted at the experimental temperature), 50 mM *β*-mercaptoethanol, 1 mM EDTA and 5 mM CH_2O. Prior to the kinetic experiments, the tritiated cofactor (trace *R*-[6-^{3}H]-CH_2H_4folate in protiated or deuterated CH_2H_4folate for H/T or D/T KIE experiments, respectively) and ^{14}C labeled substrate ([2-^{14}C]-dUMP) were mixed (typically 1.5 Mdpm T with 0.5 Mdpm ^{14}C). To enable measurement of the fractional conversion of CH_2H_4folate to dTMP (*f*), the [2-^{14}C]-dUMP was prepared in ~ 20 % molar excess over the CH_2H_4folate as described in more details elsewhere (*59*). The reaction mixture (final volume of 1.1-mL) was preequilibrated at the experimental temperature. An aliquot of 100 μL was removed and quenched in 30 μM F-dUMP (a specific inhibitor of TS with K_i = 1 nM), and used to test the radio-purity of the reactants. The reaction was then initiated by addition of the enzyme, and five time points of 100 μL each were removed at 5-minute intervals and quenched in 30 μM F-dUMP. Finally, a concentrated enzyme was added and incubated at the same temperature for 10 more minutes to achieve infinity time points. For each experiment, three infinity points were removed and quenched as described above. After quenching, all the samples were frozen and stored at -80 °C prior to RP HPLC analysis. The ratio of ^{3}H/^{14}C in the product dTMP and the fractional conversion (*f*) were

determined by RP HPLC separation followed by fraction collection and liquid scintillation counter (LSC) analysis as described elsewhere (*59*). To calculate a KIE, three values need to be measured: the ratio of $^{3}H/^{14}C$ in the product at each time point (R_t), the ratio of $^{3}H/^{14}C$ at the infinity time points (R_∞) and the fractional conversion (*f*) (*13*):

Equation 2.1 Competitive KIE equation

$$KIE = \frac{\ln(1-f)}{\ln\left(1 - f \cdot \frac{R_t}{R_\infty}\right)}$$

To determine *f*, the exact excess of [2-^{14}C]-dUMP over CH_2H_4folate was measured from the infinity time points and was defined as: $\%_{excess}$=[(total ^{14}C)-([2-^{14}C]-dTMP)$_\infty$]]/(total ^{14}C)x100. *f* was then calculated from:

Equation 2.2 Fractional conversion

$$f = \frac{[^{14}C]dTMP}{(100 - \%_{excess}) \cdot ([^{14}C]dTMP + [^{14}C]dUMP)}$$

Figure 2.1 presents a typical plot of H/T and D/T KIEs vs. fractional conversion. The fact that KIEs are *f* independent within experimental error serves as a good indication that no experimental artifact has affected the measurement (*13, 62*). The value of the observed

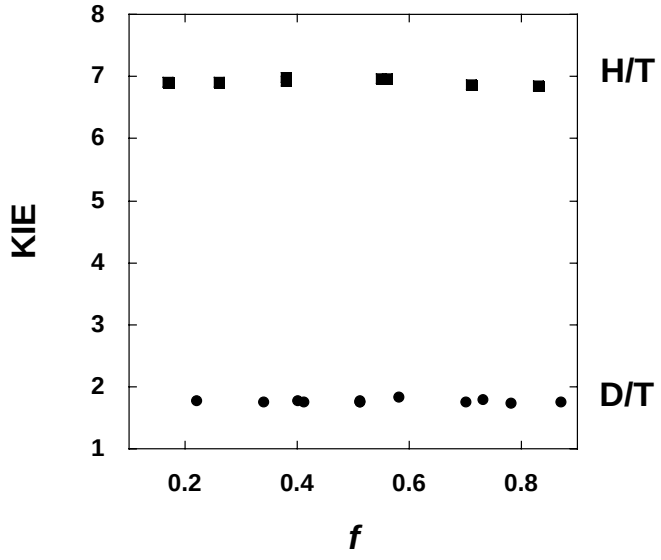

Figure 2.1 Competitive KIEs for primary $^{T}V/K_{H}$ (squares) and primary $^{T}V/K_{D}$ (circles) plotted vs fractional conversion (*f*) at 20 ºC.

KIE at each temperature was the average of at least three independent experiments with five time points and three infinity points each.

Intrinsic KIEs

The intrinsic H/T KIEs were derived using equation 2.3 (*34, 63-65*):

Equation 2.3 Northrop equation

$$\frac{{}^{T}(V/K)_{H\,obs}^{-1}-1}{{}^{T}(V/K)_{D\,obs}^{-1}-1}=\frac{k_T/k_H-1}{(k_T/k_H)^{1/3.34}-1}$$

where ${}^{T}(V/K)_{\mathrm{H\ obs}}$ and ${}^{T}(V/K)_{\mathrm{D\ obs}}$ are the observed H/T and D/T KIEs, respectively. k_T/k_H is the reciprocal of k_H/k_T, which is the intrinsic H/T KIE. The intrinsic D/T KIE is formulated as $(k_H/k_T)^{1/3.34}$ (*34, 66*). The Northrop procedure assumes that the reaction has no reverse commitment (or that EIE = 1) and that the Swain Schaad relationship holds for intrinsic 1˚ KIEs even if tunneling is involved (*34, 65*). In this context, it important to note that the TS reaction is indeed irreversible (no reverse commitment), and that in systems demonstrated to proceed with tunneling, the experimental relationship between primary D/T and H/T KIEs is valued at, or very near, the semiclassical limit (*40, 48, 49, 67, 68*). Even if the magnitude of the exponent (3.34) was altered for a full tunneling model, it would not be expected to change within the temperature range of this study, and hence, would not affect any trend in intrinsic isotope effects with temperature (*36*). The only unknown in Eq. 2.3 is the intrinsic KIE (k_H/k_T). Since this equation cannot be solved analytically a computer program was developed that solves it numerically. This program is now available on our website under tools.

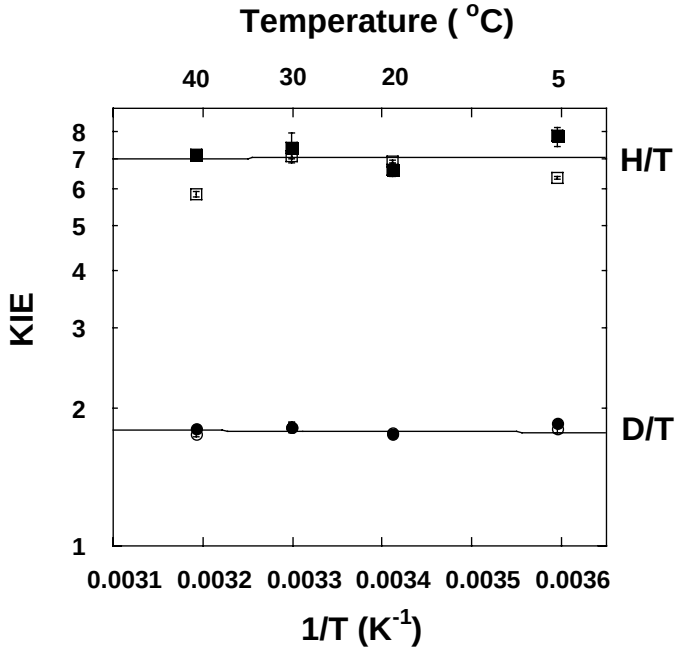

Figure 2.2 Arrhenius plot of observed (empty structures) and intrinsic (filled structures) $1^{o\ 1}V/K_H$ (squares) $1^{o\ T}V/K_D$ (circles). The intrinsic KIEs were calculated as discussed in the text. The lines are the exponential fitting of the intrinsic KIEs to Equation 2.4.

The isotope effects on the activation parameters for the intrinsic KIEs were calculated by fitting them to the Arrhenius equation for isotope effects:

Equation 2.4 Arrhenius equation for isotope effects:

$$k_L / k_T = A_L / A_T \cdot e^{\Delta E_a / RT}$$

where L is H or D, A_L/A_T is the isotope effect on the preexponential Arrhenius factors, ΔE_a is the difference in energy of activation between T and L, R is the gas constant and T is the absolute temperature (Figure 2.2).

Temperature and concentration dependence of initial rates

Initial velocities were measured by following the increase in absorbance at 340 nm which is due to the differences in absorbance between CH_2H_4folate and H_2folate ($\Delta\varepsilon_{340\ nm}$ = 6.4 $mM^{-1}cm^{-1}$ (*27*)). Measurements were conducted with a Hewlett-Packard 8453 series UV-Vis spectrophotometer equipped with a temperature controlled cuvette holder. Reaction mixtures containing various concentrations of substrate and cofactor in Tris buffer (pH = 7.5, adjusted at the experimental temperature), 50 mM DTT, 5 mM formaldehyde, and 1 mM EDTA were pre-incubated at the experimental temperature. The reaction was then initiated by addition of the enzyme. The absorbance at 340 nm (subtracted from internal reference range of 420 - 450 nm) was followed in 2 s intervals. All measurements were done in at least triplicate and data were analyzed as described below. These experiments were conducted with DTT instead of β-mercaptoethanol, since the later is an inhibitor of the reaction (*30*).

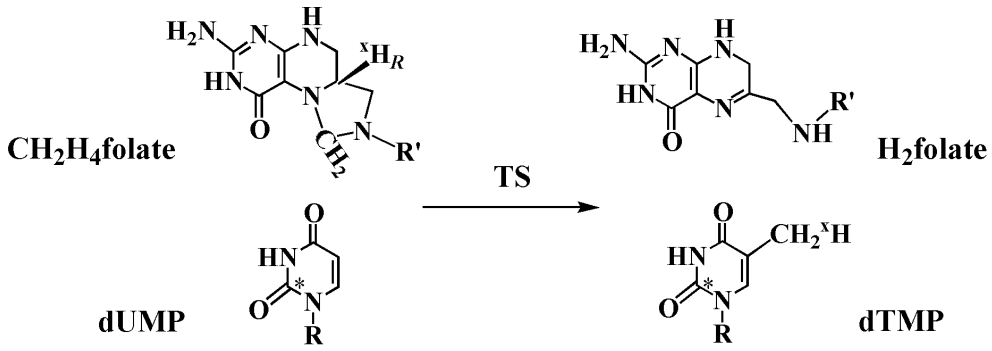

Scheme 2.3 Labeling patterns used in the competitive KIE measurements. * represents a ^{14}C labeled at C-2 position of dUMP, and ^{x}H represents H, D or T label at 6*R* position of CH_2H_4folate. R= 2'-deoxyribose-5'-phosphate and R'= (*p*-aminobenzoyl)-glutamate.

Results and Discussion

Competitive KIEs

Competitive *V/K* KIE measurements were conducted with 6*R* H, D, and T labeled CH_2H_4folate and [2-^{14}C]-dUMP. A unique feature of the competitive experiments presented here is that the remote ^{14}C label is not on the same reactant as the hydrogen isotope label (Scheme 2.3). Competitive KIE measurements of hydrogen isotopes are conducted by directly comparing the depletion or enrichment of the heavier isotope in product or reactant. For hydrogen isotopes, reactants with H or D are commonly labeled with ^{14}C or tritium at a remote position, to enable measurement of their fractional conversion (*f*) (*34, 43, 69*). The procedure presented here involves a unique remote labeling of the H-acceptor (dUMP), while the donor is labeled with H, D, or T. The conversion of [2-^{14}C]-dUMP to [2-^{14}C, 5-^{X}H]-dTMP is monitored, but the conversion of interest (*f*) is that of [6-^{X}H]-CH_2H_4folate to [2-^{14}C, 5-^{X}H]-dTMP. This requires that the [2-^{14}C]-dUMP be in excess (~20 %) over CH_2H_4folate as described recently (*59*). ^{X}H represents H, D, or T, where X is 1, 2 or 3, respectively, and is transferred from the 6*R* position of CH_2H_4folate. At 20 ˚C, competitive KIE experiments resulted in 1° $^{T}V/K_H$ and $^{T}V/K_D$ KIEs of 6.91 ± 0.05 and 1.78 ± 0.02, respectively (Figure 2.1). The Swain Schaad exponent for these KIEs is 3.35 ± 0.07 suggesting that the hydride transfer (step 5 in Scheme 2.2) is rate determining overall (*34, 65*). H/D KIE on k_{cat} (^{D}k = 3.72) has been measured at 20 ˚C by Spencer and co-workers (*27*) under the same experimental conditions as reported here. The Swain Schaad exponent for the H/T *V/K* KIEs (reported here) vs. the H/D k_{cat} KIEs (*27*) is 1.46 ± 0.04 (exp = ln($^{T}V/K_H$)/ln(^{D}k)). Taken together, the exponential relationships for k_{cat} and *V/K* KIEs suggest no kinetic complexity on

either k_{cat} or *V/K*, which strongly supports Spencer's suggestion that the hydride transfer step is rate-determining at 20 ˚C.

The reason that the observed 1˚ KIEs are often smaller than the intrinsic ones is that kinetic steps that are not isotopically sensitive "mask" the intrinsic KIEs as described in equation 2.5 (*65, 70*):

Equation 2.5 Commiment to catalysis

$$^{T}(V/K)_{L\,obs} = \frac{k_L/k_T + C}{1 + C}$$

where *C* is the commitment to catalysis, which is the ratio between the forward rate of the isotopically sensitive step ($k_{H\text{-transfer}}$) to the backward rates of the preceding isotopically non-sensitive steps. Although no commitment is present at 20 and 30 ˚C, the commitment at 5 ˚C and 40 ˚C is 0.27 ± 0.05 (calculated from Eq. 2.5). This value suggests that the hydride transfer rate at these temperatures is not much slower than the rate of the reverse steps leading to the decomposition of complex *E* in Scheme 2.2 back to dUMP and CH_2H_4folate. Obviously, this fact cannot simply be interpreted as meaning that the level of one forward step is "rate limiting" relative to other forward steps. In the current chapter we use the term "rate determining step" for cases where the isotopically sensitive step is not masked by kinetic complexity (i.e., in a case of no commitment).

Temperature dependence of intrinsic KIEs

The measured H/T and D/T KIEs ($^{T}V/K_H$ and $^{T}V/K_D$, respectively) were used to calculate the intrinsic KIEs (k_H/k_T and k_D/k_T, respectively). The method developed by Northrop (*34, 63-65*) was used to calculate the intrinsic KIE from the observed KIEs on

the three isotopes of hydrogen (Equation 2.3). Although this equation has only one unknown (k_H/k_T) it cannot be solved analytically, and a program that offers numerical solutions to any form of the Swain Schaad relationship is now available to the public on our web site as listed above. Statistical analysis of the error propagation is not trivial since Eq. 2.3 cannot be derivatized for k_H/k_T. The error propagation we chose was to avoid averaging the observed KIE. Instead the intrinsic KIEs were calculated by random combinations of the observed H/T and D/T KIEs from individual measurements under the same conditions. This solution is similar to the one applied by Francisco et al. (*36*). The average intrinsic KIE and its standard deviation were used in calculating the isotope effects on the activation parameters (Figure 2.2).

Figure 2.2 presents an Arrhenius plot (KIE on a logarithmic scale vs. the reciprocal of the absolute temperature) for the observed and intrinsic H/T and D/T KIEs. Two features are apparent from this figure: (i) The intrinsic KIEs are temperature independent over the temperature range examined and within experimental errors. (ii) The observed KIEs are close to the intrinsic values at the enzyme's physiological temperature (20 - 30 ˚C) but the observed KIEs are smaller at elevated and reduced temperatures. The first point was examined by exponential fit of the KIEs to Eq. 2.4. The isotope effects on E_a (ΔE_a) were indeed close to zero (0.02 ± 0.25 kcal/mol and –0.04 ± 0.08 kcal/mol, for H/T and D/T KIEs, respectively). The isotope effects on the Arrhenius preexponential factors were $A_H/A_T = 6.77 \pm 2.78$ and A_D/A_T 1.90 ± 0.27. Both these values lie well above the semiclassical limit (1.67 and 1.22 for H/T and D/T, respectively) and cannot be explained by a tunneling correction for the light particle (*13, 38, 55, 71, 72*). The values are, however, characteristic of a reaction in which both the

light and heavy isotopes tunnel. A number of examples of this behavior in both enzymatic reactions (*22, 49, 73*) and non-enzymatic reactions (*52-58*) now exist in the literature. Yet only one previous study has reported intrinsic KIEs that are free from complication of kinetic complexity (*36*).

Temperature dependence of Initial Rates

The steady-state initial velocities were measured within a temperature range from 5 to 40 ˚C. At each temperature, CH_2H_4folate concentrations were varied from 10 μM to 600 μM with fixed dUMP concentration of 100 μM. Alternatively, dUMP concentrations were varied from 25 μM to 600 μM at 150 μM CH_2H_4folate. The observed initial velocities were divided by the enzyme concentration prior to data analysis. The rates measured with dUMP as the variable substrate followed the Michaelis-Menten hyperbolic equation (*74*), while those measured with varying CH_2H_4folate concentrations presented substrate inhibition (Figure 2.3) and were fitted to equation 2.6 (*75*):

Equation 2.6 Michaelis-Menten equation with substrate inhibation

$$v = k_{cat}[S]/(K_M + [S]\bullet(1+[S]/K_S))$$

where [S] is the varying substrate concentration, k_{cat} is the first order rate constant, K_M is the Michaelis constant and K_S is the substrate inhibition constant. Figure 2.3 shows the rate (v) vs. CH_2H_4folate concentration at 100 μM dUMP. The lines represent the non-linear fit of the data to equation 2.6. This pattern of inhibition is in accordance with the BiBi ordered mechanism in which dUMP binds prior to CH_2H_4folate and H_2folate release precedes that of dTMP (Scheme 2.1) (*1*). In a previous report, Spencer and co-workers

(*27*) suggested that the binding constant for CH_2H_4folate might be larger than 100 μM at 20 ˚C. Fitting of the data presented here (Figure 2.3) at 20 ˚C to Eq. 2.6 results in K_S = 280 ± 24 μM, which is indeed a relatively large inhibition constant. Yet, inclusion of the cofactor inhibition while calculating k_{cat} is of substantial importance, since fitting of the observed rates to the Michaelis-Menten equation without cofactor inhibition leads to an underestimation of k_{cat}. This is especially important in the examination of the energy of activation for k_{cat}, because K_S's temperature dependence is very significant (22 ± 2 kcal/mol). If not accounted for, this affects the observed temperature dependence of k_{cat}. The first order rate constant k_{cat} at each temperature was obtained from Eq. 2.6, and the data were fit to the Arrhenius equation (Figure 2.4). The energy of activation for k_{cat} (E_a) was determined to be 4.0 ± 0.1 kcal/mol ($\Delta H^{\ddagger}_{25^{\circ}C}$ = 3.4 ± 0.08 kcal/mol and $T\Delta S^{\ddagger}$ = 24 ± 12 kcal/mol are calculated from Eyring equation). Interestingly, activation energy close to 4 kcal/mol is relatively small, and typical hydride transfer has enthalpy of activation closer to 8-15 kcal/mol (*15*). Nevertheless, this E_a is too large to fit theories that suggest no thermal activation as a source of temperature independent KIEs (*15*). The significance of this finding on the mechanism of hydride transfer in the TS catalyzed reaction is discussed below.

Environmentally enhanced tunneling

The data presented above enable close examination of the nature of the hydride transfer step (step 5, Scheme 2.2) in the complex catalytic cascade of the *ec*TS reaction. The temperature independent KIEs with large A_L/A_T taken together with E_a = 4 kcal/mol are not in accordance with theoretical models that use tunneling correction where both

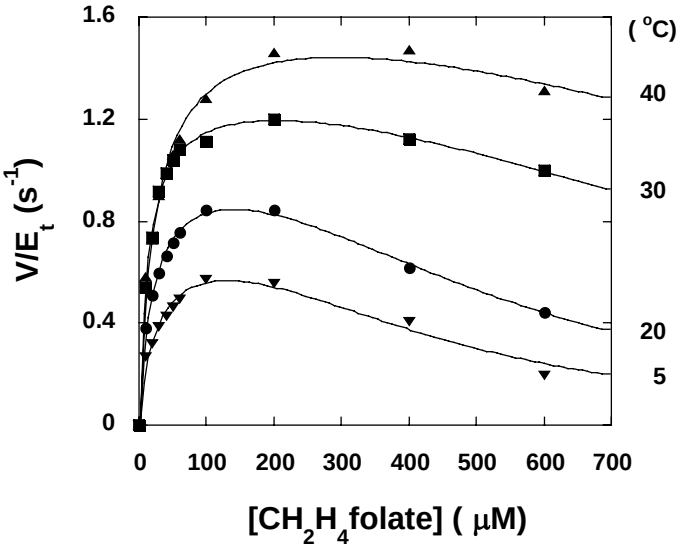

Figure 2.3 Steady-state initial rates vs. CH_2H_4folate concentration at 0.1 mM dUMP. The lines are the non-linear least squares fit to equation 2.6.

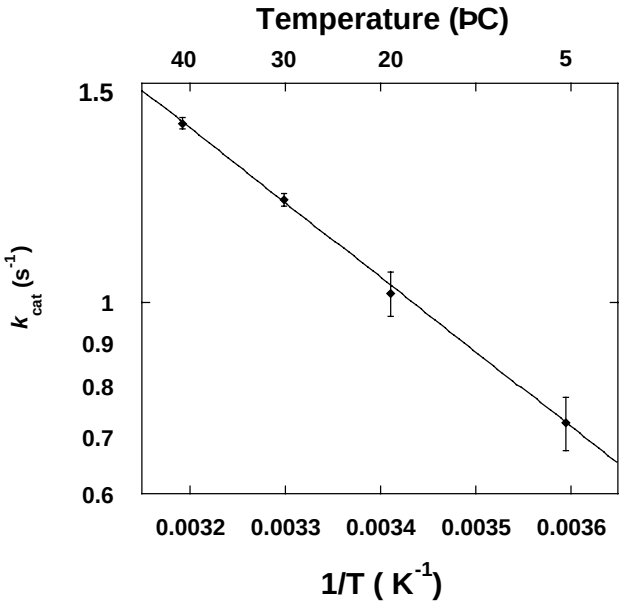

Figure 2.4 Arrhenius plot of k_{cat} (logarithmic scale) calculated from fitting the data presented in Figure 2.3 to equation 2.6. The line is the exponential fitting of the data to the Arrhenius equation.

the light and heavy isotopes tunnel (*15, 49*). This is because such models explain the lack of temperature dependence of KIEs by assuming no temperature dependence on the reaction rates for both light and heavy isotopes (full, or extensive, tunneling model (*15, 22, 34*)). The fact that E_a is significantly larger than zero might be explained by models that invoke an isotopically insensitive, thermally activated, step (e.g., environmental pre- or re-arrangement) and an isotopically sensitive but temperature independent H-transfer step (tunneling). Temperature independent KIEs with a large energy of activation have been reported in the literature (*36, 44, 46, 47, 49, 76, 77*). Those findings also could not be understood by applying a simple correction to transition state theory and a "Marcus-like" model that included an environmental motion was applied. An environmental motion can alter the probability of achieving configurations with degenerate quantum states. Such a motion can also alter the probability of tunneling at the degenerate configurations (*17, 19, 22, 73, 78-81*). These types of environmental motion modulate the tunneling barrier, typically by modulating the driving force of the reaction, the reorganization energy (ΔG° and λ in Marcus theory (*82, 83*)), and the degeneracy of the reactant and product energy levels. Several terms have been coined by models that describe such phenomenon, including: "vibrationally enhanced ground-state quantum tunneling" (*73*), "rate-promoting vibrations" (*17*), and "environmentally coupled tunneling" (*22, 79*). All of these models are phenomenological, and no molecular-level calculations have yet been reported that can reproduce such phenomena.

An alternative way to analyze the contributions of tunneling, coupled motion, dynamics and other physical phenomena to an enzymatic reaction rate would be to simulate the reaction using hybrid quantum mechanics/molecular mechanics (QM/MM)

calculations. Such calculations were preformed for several other enzymatic H-transfer reactions (e.g., references(*14, 50, 51, 81, 84-87*). Those simulations were commonly done for systems where results from KIE and other studies suggested non-classical contributions to those enzymatic reactions. Despite the medical importance of this enzyme and its interesting chemical reaction, no such calculations have been conducted for TS. This might be due to the lack of experimental information relevant to intrinsic processes along the reaction coordinate. Maybe the data presented here will encourage such studies.

Contributions to catalysis

It is of great interest to assess the contribution of non-classical phenomenon to enzyme catalysis. To address that issue the catalyzed and uncatalyzed reactions must be compared. Early attempts to address this question were carried by Kreevoy, Cleland, Schowen and their coworkers (*88-90*). Unfortunately, it is not commonly possible to measure the rate or KIE of uncatalyzed reactions that are relevant to an enzyme-catalyzed reaction. Most uncatalyzed or non-enzymatically catalyzed reactions lead to many by-products and may proceed through a transition state other than the enzymatic one. Wolfenden and co-workers (*91*) demonstrated a rare exception for hydrolytic reaction, and recently Finke and co-workers (*92, 93*) studied a model system with potential relevance to the methylmalonyl-CoA mutase reaction (*94*). In this last study, moderate tunneling (tunneling of only the light particle) was suggested for a model reaction from $A_H/A_D < 1$. That result is very different from the results presented here (A_H/A_T and $A_D/A_T > 1$) but is qualitatively similar to that reported for the methylmalonyl-CoA mutase catalyzed reaction (*94*). In their papers, Finke and co-workers suggested that their results

are in accordance with a similar degree of tunneling in both enzymatic and non-enzymatic systems. In our minds, since the H-transfer is not rate determining in that enzymatic reaction and since the uncatalyzed reaction was initiated by photolysis (potentially leading to a vibrationally excited state for the H-transfer), it is not yet clear how general that suggestion might be.

Conclusions

The hydride transfer step in the wild-type *ec*TS catalyzed reaction was examined and several significant conclusions can be drawn from the findings reported above. This work provides the first experimental evidence for a contribution of vibrationally enhanced quantum mechanical tunneling to the hydride transfer step in a TS catalyzed reaction. The temperature independence of the primary KIEs is a key evidence of non-classical behavior. The temperature dependence of intrinsic primary KIEs yields isotope effects on Arrhenius parameters that lie well outside the semiclassical limits (*13, 38, 71, 72*).

Cofactor inhibition of CH_2H_4folate was observed while measuring the steady state rate constants across the temperature range (5-40 ˚C). This phenomenon was predicted by previous publications for the reaction at 20 ˚C (*1, 27*), but has never previously been observed. This finding is in accordance with the kinetic mechanism presented in Scheme 2.1. The inhibition constant has a large binding energy (22 kcal/mol) such that inhibition almost vanishes at elevated temperature. Accounting for this inhibition enabled extraction of the first order rate constant k_{cat} at all temperatures and afforded calculation of its energy of activation (E_a = 4.0 ± 0.1 kcal/mol). This, together with the KIE activation parameters, suggests that the *ec*TS catalyzed H-transfer involves environmentally

enhanced (vibrationally coupled) tunneling.

At the current state of "our understanding or ignorance" (*35*), no one specific model that has been developed to explain temperature independent KIEs seems to be more general than others. Thus, we use the term "environmentally enhanced tunneling" (*22, 79*) while addressing "Marcus like" models. This term seems to be more comprehensive because it includes both preorganizational motion (affecting the symmetry of the H-transfer coordinate) and the "gating" fluctuation (primarily affecting the barrier's width). We hope that the new findings presented here will enable and encourage theoreticians to embark on a molecular investigation (e.g., QM/MM studies) of this interesting system.

Whether phenomena such as H-tunneling, vibrationally coupled tunneling and environmentally enhanced reaction rates contribute to enzyme catalysis is an open question. Further studies of enzymatically relevant model-reactions using the tool described here could lead to a more concrete evaluation of that seminal question.

CHAPTER III

HYDRIDE TRANSFER VS. HYDROGEN RADICAL TRANSFER IN *E.COLI* THYMIDYLATE SYNTHASE

This chapter has been published as communication in the *Journal of American Chemical Society* (JACS), Hydride transfer versus hydrogen radical transfer in thymidylate synthase, Hong, B., Haddad, M., Maley, F., Jensen, J. H., and Kohen, A.* *J. Am. Chem. Soc.* **2006**, 128, 5636 – 5637.

Summary

The nature of a H-transfer step was studied by means of intrinsic kinetic isotope effects (KIEs), their temperature dependence and other activation parameters. The temperature dependence of intrinsic KIEs provides a way to examine whether a two-step radical mechanism or a one-step hydride transfer mechanism is more likely for the rate limiting step of the TS catalyzed reaction.

Introduction

Thymidylate synthase (TS) (EC 2.1.1.45) catalyzes the last committed step in the *de novo* biosynthesis of 2'-deoxythymidine-5'-monophosphate (dTMP, one of the four building blocks of DNA). The enzyme catalyzes the reductive methylation of 2'-deoxyuridine-5'-monophosphate (dUMP) to dTMP. Two independent reactions are involved in which the cofactor N^5, N^{10}-methylene-5, 6, 7, 8- tetrahydrofolate (CH_2H_4folate) serves first as a donor of a methylene group and second as a donor of a hydride ion (*1, 2, 6*). The hydride transfer takes place between the C6 hydrogen of H_4folate and the dUMP exocyclic methylene intermediate (Scheme 3.1). While the existence of the exocyclic methylene intermediate has been reasonably supported by its

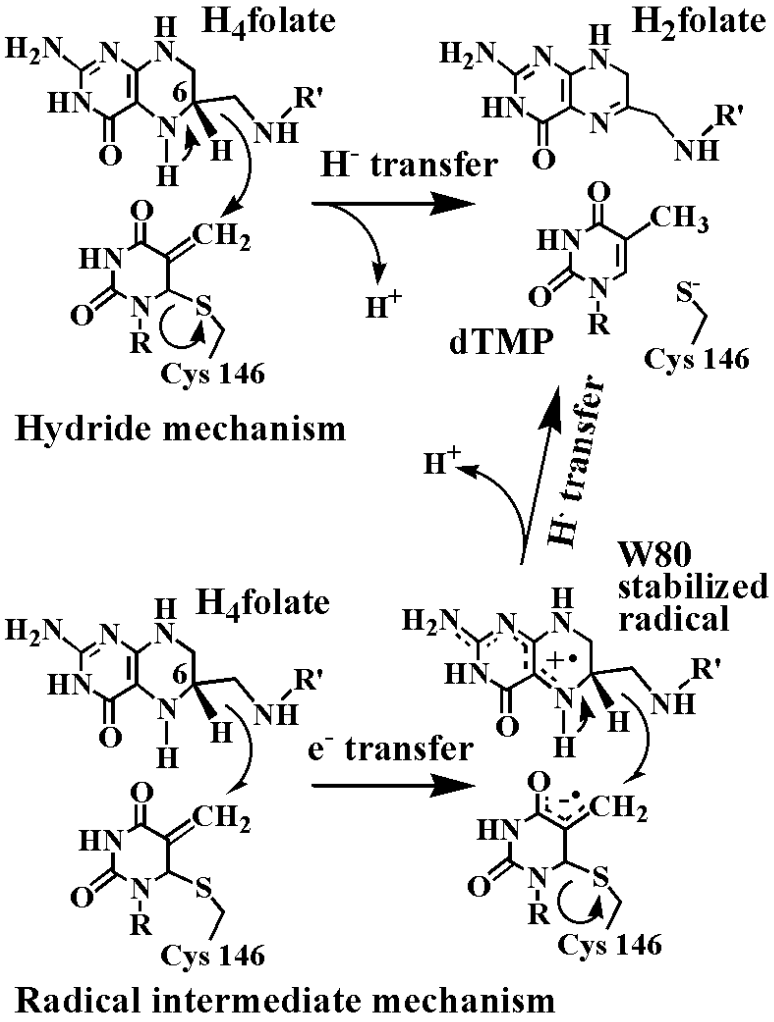

Scheme 3.1 Two Proposed Mechanisms for the H-Transfer from C6 of H_4folate to the exocyclic Methylene[a]

a. At the top, a one-step hydride transfer as proposed by refs (*2, 6, 107*). At the bottom, the two-step radical mechanism proposed by ref (*108*). Full arrows symbolize transfer of a pair of electrons, and half arrows symbolize transfer of a single electron.

trapping with *β*-mercaptoethanol ($HSCH_2$-CH_2OH) (*30*), the H-transfer step that follows has been a matter of some controversy. Different experimental data have supported two different and distinct mechanisms. Schultz and co-workers (*108*) used unnatural amino acids substituting W82 of *L. casei* TS and found a correlation between the steady-state k_{cat} for tritium release (from C5 of 5T-dUMP) and the theoretical ability of tryptophan (W) and phenylalanine (F) substituents of W82 to bind Na^+ in the gas phase. These researchers concluded that this correlation indicates that W82 stabilizes a H_4folate cation radical intermediate or transition state. They proposed that the H-transfer is initiated by an electron transfer from H_4folate to the dUMP exocyclic methylene intermediate to form anion and cation radicals (bottom of Scheme 3.1). Since crystal structures have suggested that W82 (W80 in *ec*TS) cannot stabilize such a cation at its ground state (Figure 3.1), it was proposed that the pterin ring flips closer to the tryptophan (forming charge stabilizing "stacking interactions"), and then flips back to transfer a hydrogen radical leading to products (right-hand of Scheme 3.1). Stroud and co-workers (*107*) examined the crystal structures of the wildtype (wt) and W80G mutant of *ec*TS together with other crystal structures of the enzyme with various ligands. They concluded that the flip proposed by ref (*108*) is unlikely and proposed that the role of W80 is to orient L143 and the reactants, thereby protecting the exocyclic methylene intermediate from nucleophilic attack by solutes, such as *β*-mercaptoethanol. They further concluded that the mechanism of the H-transfer is likely to be a one-step hydride transfer (top of Scheme 3.1).

The shortcoming of the methods used in refs (*108*) and (*107*) is that they could not examine the nature of the H-transfer (meaning the H-transfer step reaction's potential surface, dynamics, adiabatic reaction or non-adiabatic reaction, hydride or radical

transfer, and other physical features of the C-H-C double well system that will affect the KIEs and their temperature dependence as discussed in ref (*79, 101, 109, 110*)) step *per se* in the complex kinetic cascade of TS. As described in Chapter II, we developed a method to study the nature of that step by means of intrinsic kinetic isotope effects (KIEs) (KIE is the ratio of rates of two isotopically labeled reactants) and their temperature dependence and other activation parameters (*101*). This methodology is very sensitive even to minor changes in the reaction's potential surface and dynamics (*79, 109, 110*) and has been used to detect effects of mutations close and far from the active site on the nature of the H-transfer (*49, 111-114*). Thus, the temperature dependence of intrinsic KIEs provides a way to examine whether a two-step radical mechanism or a one-step hydride transfer mechanism is more likely.

The radical mechanism (*108*) would imply that replacing W with M, which cannot stabilize a cation radical nearly as well as the aromatic W, would substantially change the nature of the H-transfer.The hydride transfer mechanism (*107*), on the other hand, would not require significant alteration of the nature of the H-transfer even though k_{cat} is reduced (*115*).

Steady-state parameters (e.g., k_{cat} and K_M) of several mutants of W82 *lc*TS and W80 *ec*TS have been examined in the past (*30, 107, 115*). W80M *ec*TS was chosen in this work because it is still quite active relative to mutations with a smaller side chain and it is less likely to alter the entrance to the active site (*107*), but its side chain cannot stabilize a cation radical as aromatic residues can (e.g., W and F (*108*)). The ability of M to stabilize a cation radical was evaluated by the same method used by Schultz and co-workers (*108*) and extensively used to assess the ability of protein residues to stabilize

cation radicals in general (*116*). We found that the binding energy of Na^+ to dimethylthioether (the side chain of M) is 10.9 kcal/mol lower than that to indole (the side chain of W), which is a most significant difference (This value is actually a underestimation of the differences between M and W. The level of theory used by Schultz and us (RHF/6-31G(d,p)//RHF/6-31G(d,p)) following the footsteps of refs (*108*) and (*116*) do not include the additional stabilization anticipated from the π-stacking interactions between the pterin and the indole aromatic rings).

Methods

Competitive KIE measurement

All the competitive measurements are performed as described in detail for the wild type TS (*101*) except for the replacement of the reducing agent *β*-mercaptoethanol by DTT, to avoid the formation of the byproduct described in (*30*). A small amount of byproduct from the nucleophilic attack of DTT on the exocyclic methylene is observed (as a ^{14}C HPLC peak at 37 min) and the fractional conversion is corrected using equation 3.1:

Equation 3.1

$$f = ([^{14}C]dTMP\ /total^{14}C)t\ /([^{14}C]dTMP/total^{14}C)_{\infty}$$

Table 3.1 compares the observed and intrinsic KIEs (KIE_{obs} and KIE_{int}, respectively) for the wt and W80M *ec*TS, their Swain-Schaad Exponent (SS EXP) (*7, 8*) and kinetic complexity (commitment to catalysis, C). It is apparent that all the presented KIEs are "commitment free" within experimental errors.

Steady-state kinetic measurement

Initial velocities were measured as described for the wild type enzyme (*59*). The k_{cat} and K_m values were obtained by fitting rates at various substrate concentrations to the Michaelis-Menten equation. Error propagation was carried out using standard methods. The data are presented in Table 3.2. The activation energy was obtained by nonlinear fitting to the Arrhenius equation, and $\Delta H^{\ddagger}$ and $T\Delta S^{\ddagger}$ were obtained by fitting to the Eyring equation. The program KaleidaGraph was used for the analysis and regressions. The Arrhenius plot for the W80M catalyzed reaction is shown in Figure 3.3.

Discussion

To compare the nature of the H-transfer between the wt and W80M *ec*TSs, we measured the KIEs of hydrogen to tritium (H/T) and deuterium to tritium (D/T) using a competitive method as described in detail elsewhere (*59*). In this method, two isotopically labeled CH_2H_4folates at position C6 compete for the active site and yield a very accurate KIE on the second-order rate constant k_{cat}/K_M (*117*). If the relation between H/T and D/T follows the semiclassical Swain-Schaad relationship (*8*), it serves as a strong indication that the observed KIE is also the intrinsic KIE (*43, 49, 65*). If, on the other hand, the ratio of ln(H/T) to ln(D/T) is smaller than its semiclassical value, the Northrop method (*65, 117*) can be used as described previously (*101*). For the wt *ec*TS, it was found that the observed and intrinsic KIEs are the same between 20 and 30 °C, but some kinetic complexity masked the intrinsic KIE at elevated and reduced temperatures so that the observed KIE appeared smaller.

The current results for W80M indicate that the observed and intrinsic KIEs are identical from 5 to 40 °C, indicating no kinetic complexity on k_{cat}/K_M, but some on k_{cat}.

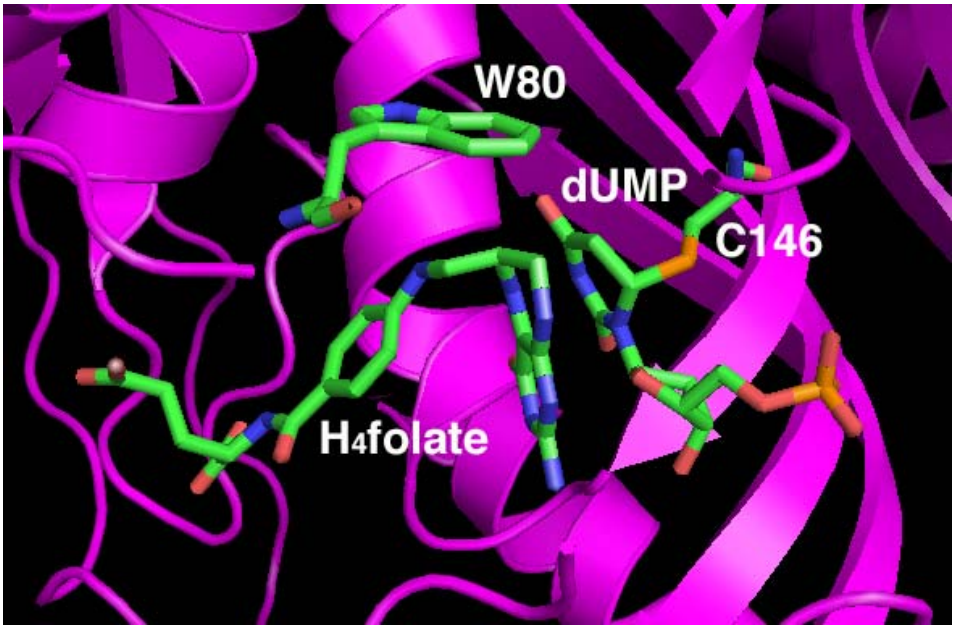

Figure 3.1 Crystal structure of *ec*TS with dUMP and H_4folate (PDB entry 1KZ17). This structure best mimics the conformation of the system prior to the H-transfer step. The C146 bound dUMP, the H_4folate, and W80 are highlighted.

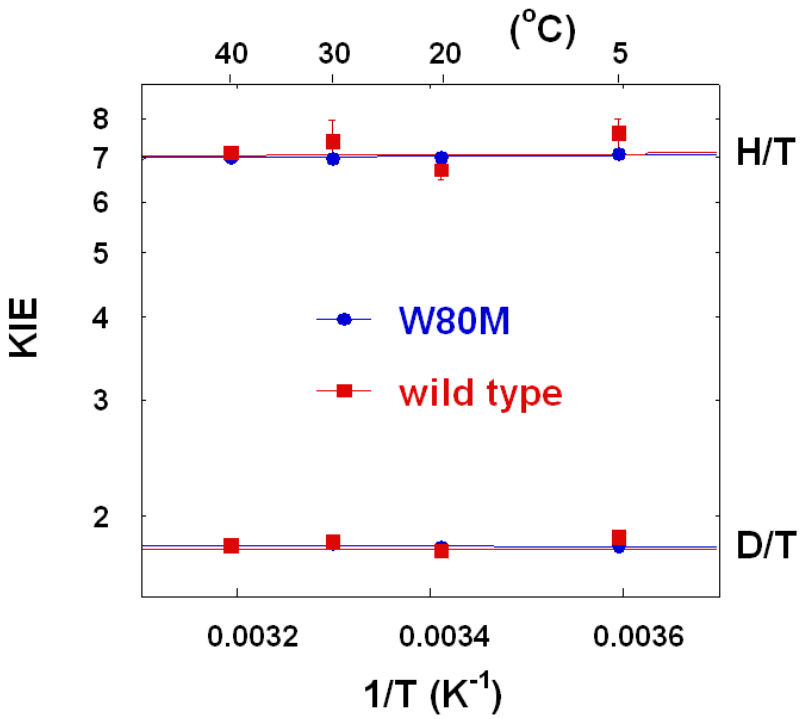

Figure 3.2 Arrhenius plots of H/T and D/T intrinsic KIEs with the wt (red squares) and W80M (blue circles) *ec*TS[a]. The lines are the exponential least squares fitting of the intrinsic KIEs to the Arrhenius equation using the package KaleidaGraph.

---

a. The errors of the W80M KIEs are much smaller than those for the wt because W80M's observed KIEs are equal to the intrinsic ones and no error propagation through Northrop's numerical solution is necessary (for details of that error propagation and regression procedures, see ref (112)).

presented in Figure 3.2 indicate no measurable change in the nature of the H-transfer between wt and W80M *ec*TS.

Figure 3.2 compares the intrinsic KIEs of the wt and W80M *ec*TSs at temperature range of 5 - 40 °C (see data in Table 3.1). Both enzymes appear to have very similar KIEs at all temperatures (within experimental error). The different theoretical models (*79, 109, 110*) that address that phenomenon would all agree that the temperature dependence of intrinsic KIEs is a very sensitive probe for the nature of the H-transfer, and that the data presented in Figure 3.2 indicate no measurable change in the nature of the H-transfer between wt and W80M *ec*TS.

The steady-state rates of the wt and W80M mutant were also compared across the same temperature range (see Table 3.2). The data indicated that the wt enzyme was 1-2 orders of magnitude faster at all temperatures, and that their activation parameters (both entropy and enthalpy) were quite different ($\Delta T\Delta S^{\ddagger}_{20°C}$ = 2.2 ± 0.9 kcal/mol and $\Delta\Delta H^{\ddagger}$ = 3.8 ± 0.9 kcal/mol). These data suggest that, in contrast to the H-transfer step, parameters affecting k_{cat} (protein rearrangements, product release, etc.) have been altered by the W to M mutation, in accordance with the conclusions of ref (*107*).

Conclusions

In summary, a sensitive probe of the nature of the H-transfer step has been applied here in search of the effect of W80 substitution to M in *ec*TS. The findings are in accordance with an alteration of the pre- and reorganization of the system toward and after the H-transfer step, but no significant change in the H-transfer step *per se*. Since M cannot stabilize a cation radical as well as W, the findings support a hydride transfer

Wide Type[a]		W80M			
20 °C		40 °C	30 °C	20 °C	5 °C
H/T KIE_{obs}	6.91±0.05	7.02±0.05	6.97±0.07	7.02±0.05	7.07±0.04
D/T KIE_{obs}	1.78±0.02	1.8 ±0.02	1.81±0.02	1.79±0.02	1.80±0.02
H/T KIE_{int}	6.91±0.35	7.21±0.40	7.19±0.32	6.91±0.35	7.30±0.33
H/D KIE_{int}	3.88±0.03	3.99±0.16	3.98±0.13	3.90±0.13	3.97±0.15
D/T KIE_{int}	1.78±0.02	1.81±0.03	1.80±0.02	1.78±0.03	1.80±0.03
SS EXP[b]	3.35±0.07	3.31±0.06	3.27±0.06	3.35±0.07	3.33±0.06
C	0.01 ±0.09	0.03 ± 0.07	0.04 ±0.06	0.00 ±0.06	0.04±0.06

Table 3.1 Intrinsic and observed KIEs for wt and W80M *ec*TS.

a. From (*101*). Data for other temperatures (5-40 °C) are also available in (*101*).

b. The Swain-Schaad Exponents were calculated using SS EXP = ln(H/T)/ln(D/T) where H/T and D/T are the KIEs of these isotopes, and their errors (ΔEXP) propagate from the standard errors on the KIEs using:

$$\Delta EXP = \sqrt{\left(\frac{\Delta(H/T)}{H/T} \Big/ \ln(D/T)\right)^2 + \left(\frac{\Delta(D/T)\ \ln(H/T)}{D/T\ \ (\ln(D/T))^2}\right)^2}$$

Temperature[a]	Wild Type[b]	W80M
40	1.62 ± 0.03	0.15 ± 0.02
30	1.32 ± 0.02	0.11 ± 0.01
20	1.02 ± 0.06	0.056 ± 0.005
5	0.73 ± 0.05	0.032 ± 0.006
E_a	4.0 ± 0.1	8.0 ± 0.8
$-T\Delta S^{\ddagger}_{20^oC}$	13.7 ± 0.1	11.5 ± 0.8
$\Delta H^{\ddagger}$	3.4 ± 0.1	7.2 ± 0.8
$\Delta G^{\ddagger}_{20^oC}$	17.1 ± 0.2	18.7 ± 1.6

Table 3.2 k_{cat} values for the wt and W80M enzyme at 5-40 °C range.

a. All temperatures are in °C, all rates are in s^{-1}, and all energies are in kcal/mol.

b. From ref (*101*).

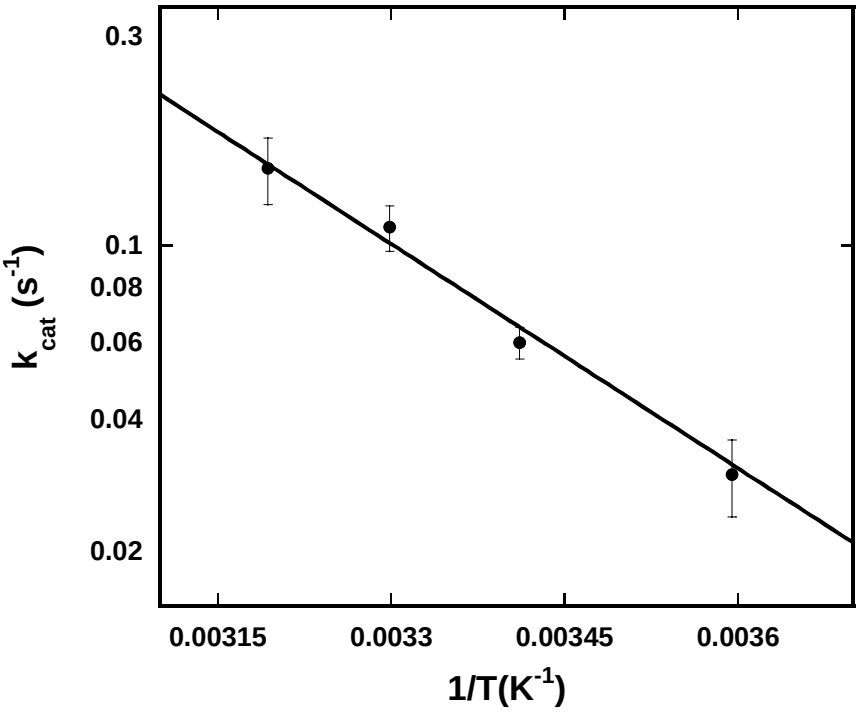

Figure 3.3 Arrhenius plot for the W80M catalyzed reaction.

mechanism (top of Scheme 3.1) dominating the reaction even for the wt enzyme. We hope that clarifying the chemical mechanism to TS will aid in rational drug design.

CHAPTER IV

MICROSCALE SYNTHESIS OF IOSTOPICALLY LABELED 6*R*-N^5,N^{10} METHYLENE-5, 6,7,8-TETRAHYDROFOLATE AS A COFACTOR FOR SECONDARY KINETIC ISOTOPE EFFECT IN THYMIDYLATE SYNTHASE CATALYZED REACTION

This chapter has been published *J. Label Compd. Radiopharm.* Hong, B. and Kohen, A., *J. Label Compd. Radiopharm.* **2005**, 48, 759 -769.

Summary

A one-pot chemo-enzymatic microscale synthesis of isotopically labeled *R*-[6-^{Y}H; 11-^{X}H] N^5, N^{10} methylene-5, 6, 7, 8-tetrahydrofolate (CH_2H_4folate) is presented, where Y = 1or 2 represents protium or deuterium, and X = 1, 2 or 3 represents protium, deuterium or tritium, respectively. In this procedure, *Thermoanaerobium brockii* alcohol dehydrogenase (TbADH) and *Escherichia coli* dihydrofolate reductase (*ec*DHFR) were used simultaneously in the reaction mixture. First *tb*ADH stereospecifically catalyzes a hydride transfer from [2-^{Y}H] iPrOH to the *re* face of C-4 of $NADP^+$, where Y is H or D. The *ec*DHFR then reduces 7, 8-dihydrofolate (H_2folate) to form 6*S* labeled H_4folate. The enzymatic reactions were followed by chemical trapping with labeled formaldehyde (HCHO) to form the final product. The preparation of deuterium- and tritium-labeled formaldehyde is also presented in this chapter. Two reverse phase HPLC methods were used in analysis and purification of product R-[6-^{Y}H; 11-^{X}H] CH_2H_4folate, where X is H, D or T. This isotopically labeled cofactor can be used to study primary and secondary kinetic isotope effects (KIEs) with any CH_2H_4folate dependent enzyme as demonstrated below by studies with *E. coli* thymidylate synthase (TS).

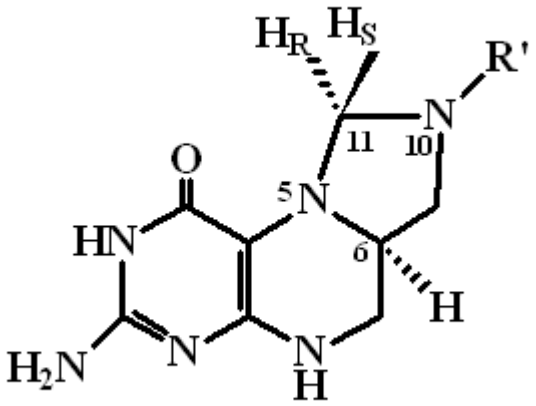

Scheme 4.1 Structure of R-N^5, N^{10}-methylene 5, 6, 7, 8-tetrahydrofolate. R'= (*p*-amino-benzoyl) glutamate.

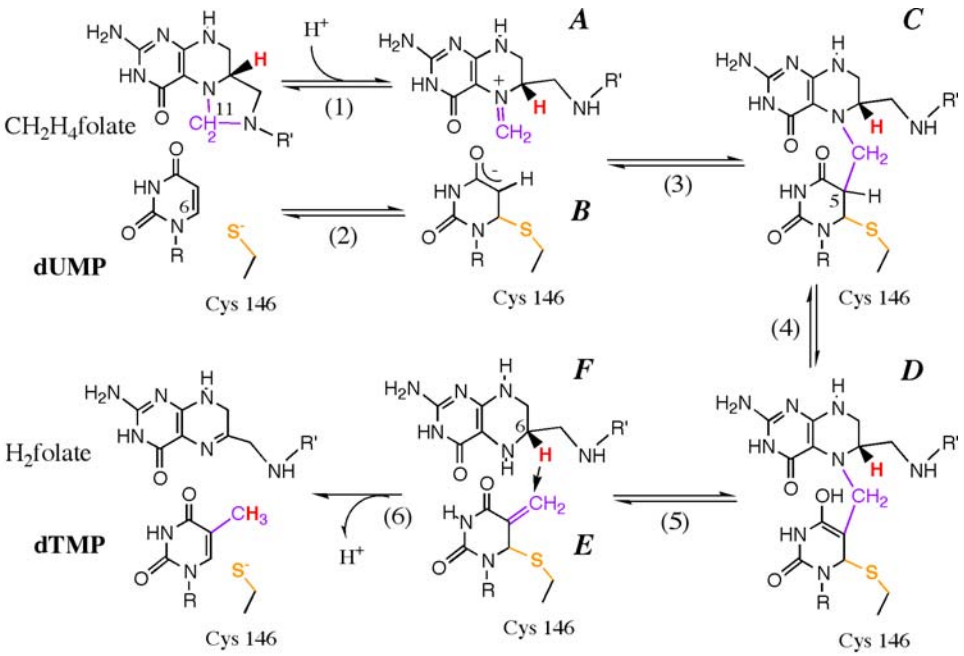

Scheme 4.2 Reaction pathway of thymidylate synthase (step 6 is target for the 2° KIE study).

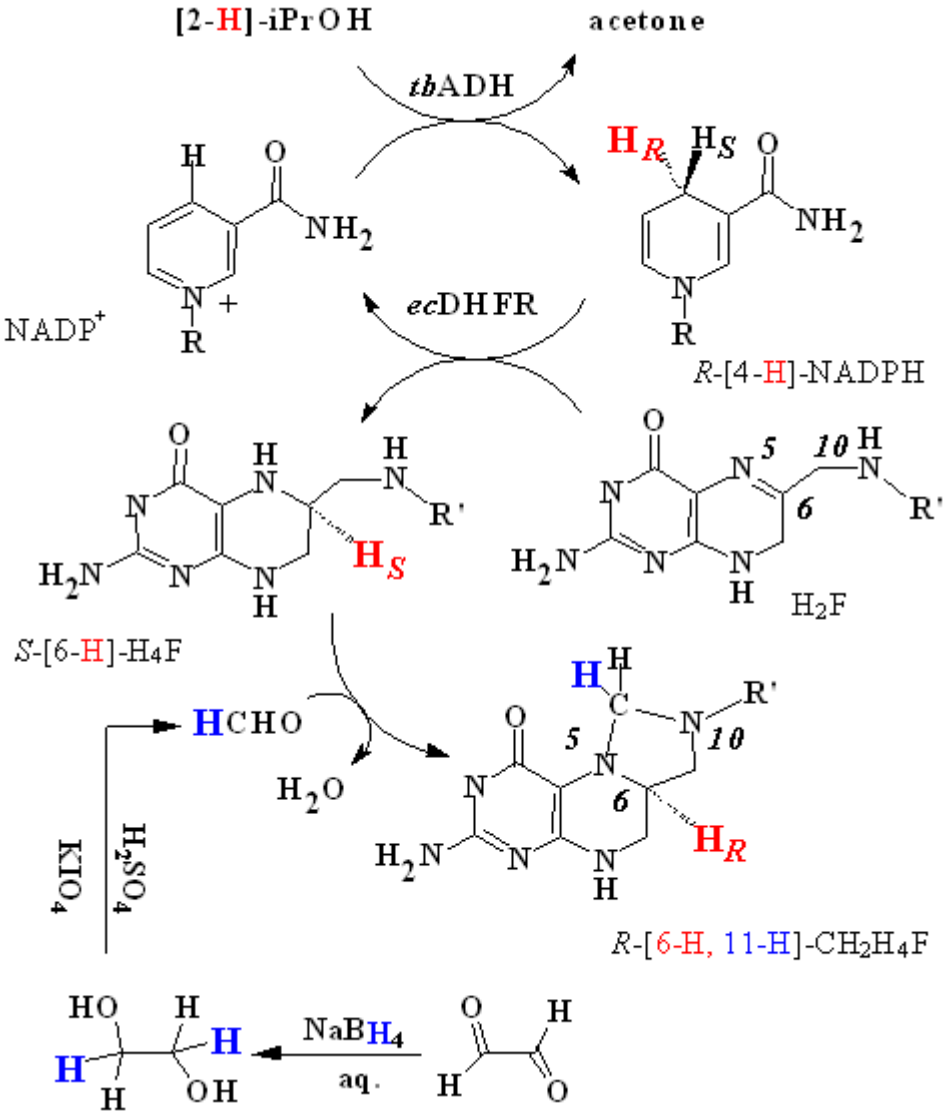

Scheme 4.3 Chemoenzymatic synthesis of isotopically labeled (*R*)-[6-^{Y}H], [11-^{X}H] CH_2H_4folate, where Y = 1, 2, X = 1, 2,or 3 represents H, D, or T, respectively. R = 2' – deoxyribose-5'-phosphate and R' = (*p*-aminobenzoyl) glutamate.

Introduction

N^5, N^{10}-methylene-5, 6, 7, 8 tetrahydrofolate (CH_2H_4folate) (Scheme 4.1) is an ubiquitous cofactor that functions in the biosynthesis of purines and pyrimidines (*95*). For example, Jaffe and Chrin (*96*) reported the presence and properties of four folate-related enzymes that are associated with this cofactor, namely serine hydroxymethyltransferase, CH_2H_4folate dehydrogenase, CH_2H_4folate reductase and thymidylate synthase (TS). In the TS-catalyzed reaction (Scheme 4.2) (*1*), CH_2H_4folate serves as the donor for both a hydride at C6 and methylene (C11) to the substrate 2'-deoxyuridine 5'-monophosphate (dUMP) forming 2'-deoxythymidine 5'-monophosphate (dTMP) and dihydrofolate (H_2folate).

Labeling substrates or cofactors at primary (1º) hydrogen (hydrogen that is involved in C-H bond cleavage) or secondary (2º) hydrogen (another hydrogen on the same carbon) with multiple hydrogen isotopes is of general interest. Such labeling has been used to measure competitive KIEs in many biological systems (*69, 97*). These studies could reveal important mechanistic features of the enzymic H-transfers including H-tunneling, coupled motion and more (*22, 34, 98*). For example, measurement of the H/T 2° KIE (k_H/k_T) with H transfer from the 1° position and the H/T 2° KIE with D transfer can directly examine possible coupling between the 1° and the 2° hydrogens along the reaction coordinate (*39, 49*). In short, this type of mutiple isotopic labeling can expose the nature of H-transfer in complex systems like enzymes.

Isotopologues (molecules that differ only in their isotopic composition) of CH_2H_4folate can be used in the mechanistic studies of any CH_2H_4folate-dependent

enzyme. The large-scale nonradioactive synthesis of CH_2H_4folate by the condensation of formaldehyde with tetrahydrofolate has been reported previously (*99, 100*). The *in situ* enzymatic synthesis of (6*R*, 11*R*)-and (6*R*, 11*S*)-5, 10-methylene [11-^{1}H, ^{2}H] tetrahydrofolate by Slieker and Benkovic (*95*) was also reported. Multiple isotopic labeling of the C6 hydrogen of 6*R*-CH_2H_4folate was used previously to study the nature of the hydride transfer step in the TS reaction through the measurement of 1° KIEs and their temperature dependence (*27, 101*).

This chapter describes a new microscale chemo-enzymatic synthesis of isotopically labeled CH_2H_4folate at positions most relevant to its role as methylene and hydride donor in many enzymatic reactions. The usage of the labeled cofactor in studies of the enzyme TS is demonstrated.

Results and discussion

***R*- [6-^{2}H; 11-^{X}H] CH_2H_4folate 5** was synthesized in two steps: preparation of *S*-[6-^{2}H] H_4folate and trapping with [^{X}H]-HCHO (Scheme 4.3). To synthesize the H_4folate with stereospecifically labeled 6C position, two enzymes were used simultaneously in the reaction mixture. *tb*ADH stereospecifically catalyzed a deuteride transfer from uniformly deuterated isopropanol **1** to the *re* face of oxidized nicotinamide adenine dinucleotide phosphate ($NADP^+$) to form *R*-[4-^{2}H]-labeled reduced nicotinamide adenine dinucleotide phosphate (NADPD) **2**. Then, *ec*DHFR was used to catalyze the transfer of the deuteride from **2** to the *si* face of 7, 8-dihydrofolate (H_2folate), forming *S*- [6-^{2}H] H_4folate **3**. The enzymatic reactions were followed by chemical trapping of **3** with labeled formaldehyde **4**.

The deuterium and/or tritium-labeled formaldehyde ([^{X}H]-HCHO) **4** used in the above procedure by a series of redox reactions initiated with [^{X}H]-$NaBH_4$. The synthetic route is shown in Scheme 4.3. In this process, glyoxal **1'** was first reduced to ethylene glycol 2' by [^{X}H]-$NaBH_4$ (*102*). When using $NaBD_4$ (> 99% D) the solvent was D_2O (99.96% D) which increase the deuterium content of the labeled formaldehyde. Then, the solution was acidified and the [1, 2-$^{X}H_2$] ethylene glycol was oxidized by potassium periodate (KIO_4) to form the product **4** [^{X}H] HCHO. The product described in the current procedure is labeled with trace tritium or > 99% protium or deuterium on one of the formaldehyde's hydrogens, while the other is always protium. This is aimed at measuring the 2º KIE of only one hydrogen and not of doubly labeled methylene of the TS intermediate. Alternative labeling patterns of formaldehyde, for different applications, can be made by usage of differently labeled glyoxal 1'.

***R*-[6-^{1}H; 11-^{X}H] CH_2H_4folate** was synthesized by incubation of *S*-[6-^{1}H] H_4folate with [^{X}H] HCHO **4**.

In all the tritiated CH_2H_4folate syntheses, a four-fold excess of [^{3}H] HCHO over CH_2H_4folate was used to form 3/1 mixture of [^{3}H] HCHO/[11-^{X}H] CH_2H_4folate. This led to complete capture of the H_4folate as labeled CH_2H_4folate. The HPLC radiogram of the tritiated CH_2H_4folate with 3:1 excess of tritiated formaldehyde is shown in Figure 4.1. Such practice was necessary due to the equilibrium between the reactants HCHO and H_4folate and the product CH_2H_4folate. Pure CH_2H_4folate (collected from HPLC separation) dissociated to free formaldehyde and H_4folate in equilibrium in about 120 min at 25 ºC. Our goal in the procedure described here was to use the labeled cofactor for measuring the 2º KIEs of the TS reaction. Thus, the limiting reagent was H_4folate that was fully (within the analytical limits) converted to the cofactor of interest

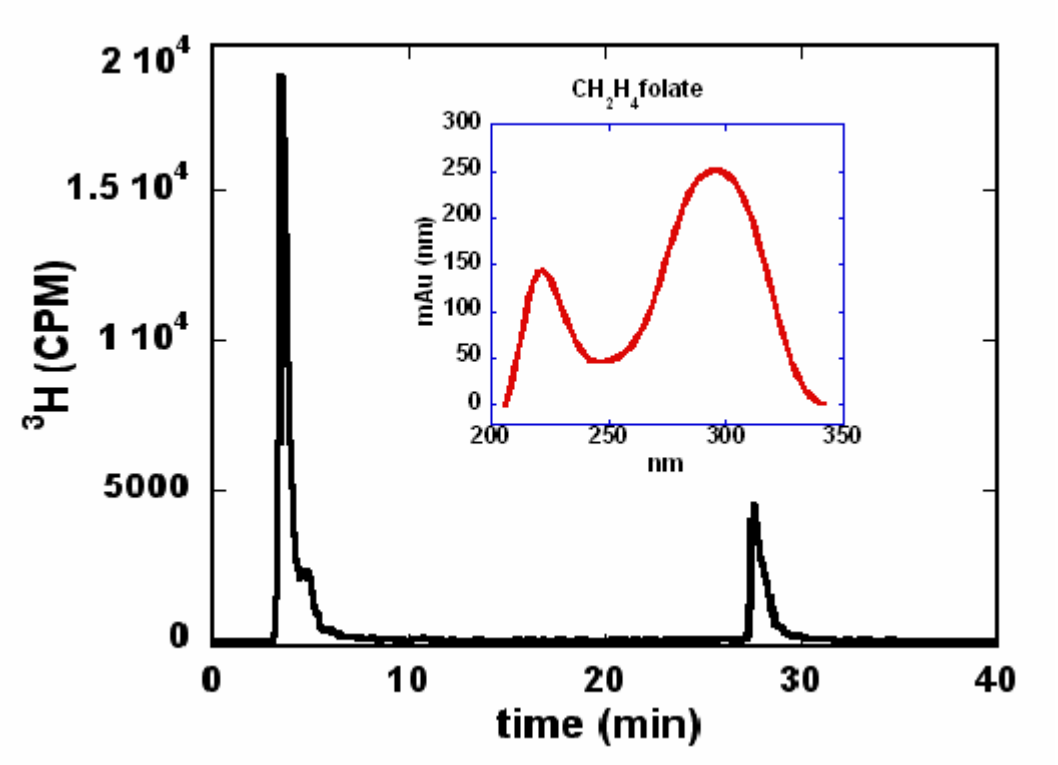

Figure 4.1 HPLC tritium radiogram of the reaction mixture of C11 labeled CH_2H_4folate in excess of [^{3}H]-HCHO under equilibrium condition. The peak of CH_2H_4folate that eluted at 26 min contained 25% of the total radioactivity. The inserted UV spectrum of this peak confirms its identity as CH_2H_4folate.

(CH_2H_4folate). Alternatively, in the case that the yield of labeled HCHO is important, an excess of H_4folate should be used under strict anaerobic conditions (H_4folate is much more sensitive to O_2 than CH_2H_4folate). While using the CH_2H_4folate in enzyme kinetic experiments, the stability of the cofactor under aerobic conditions was tested in a control experiment. In that control experiment, the reaction mixture containing all the reagents and labeled CH_2H_4folate was incubated at the experimental temperature for 40 min with no detectable degradation. The product **5** might be stable for even longer period of time, but since all the kinetic measurements were much faster (less than a few minutes), this has not been tested here.

As a result of one-hydrogen labeling of formaldehyde ([^{X}H]-HCHO), trapping of formaldehyde resulted in a mixture of (6*R*, 11*S*) and (6*R*, 11*R*) CH_2H_4folate diastereoisomers. The distribution between the two diastereoisomers was verified by NMR to be 1:1 after 120 min even when a pure diasteromer was synthesized due to epimerization at C11. The labile methylene (11C) imposes an inherent limitation on the synthesis of **5**. Stereospecifically labeled 5 at 11C epimerizes to the diastereoisomer mixture and cannot be preserved as is. Down-stream products using **5** as cofactor can be synthesized only by using coupled enzymatic mixtures that will capture stereospecifically labeled 5 as it is formed.

During the TS catalyzed reaction, the 1:1 *R: S* labeled 11C led to a1: 1 ratio of *E* and *Z* intermediates of methylene-dUMP (E in Scheme 4.2). Importantly, step 6 that reduces this intermediate is the rate limiting step in the whole TS reaction (*101*). 2º KIEs on the *E* and *Z* intermediates are expected to be very similar or identical because they both involve similar change in vibrational states along the reduction coordinate. Using

these radiolabeled cofactors, competitive measurements on the second order rate constant (*V/K*) were performed with TS. Inverse 2º KIEs (e.g. 0.76 for $^{T}V/K_{H}$) were observed for all the labeled cofactors whose synthesis is described here. The in-depth investigation of their contribution to understanding the TS mechanism will be described elsewhere.

Materials

H_4folate was a gift from Eprova Inc., Switzerland. H_2folate was synthesized according to the procedure of Blakley and its purity examined by NMR and UV as described elsewhere (*103*). Potassium periodate was from Alfa Aesar. D_2O (99.96% isotopic purity), $NaBD_4$ (> 99% D) and [U-^{2}H] isopropanol (> 99% D) were from Cambridge Isotope Laboratories Inc. [^{3}H] formaldehyde (HCTO 10 Ci/mmol) and [^{3}H] sodium borohydride ($NaBT_4$ 80 Ci/mmol) were from American Radiolabeled Chemicals Inc. [2-^{14}C] dUMP (60 Ci/mol) was from Moravek Biochemicals. The expression system for *E. coli* TS was a generous gift from R. Stroud, University of California at San Francisco. The enzyme was purified following the procedure of Changchien et al (*61*). All other materials were purchased from Sigma.

Methods

HPLC analysis and separation

Analysis of R-[6-^{Y}H; 11-^{X}H] CH_2H_4folate and its precursors The HPLC separation and analysis system has been described elsewhere (*59*). In short, the HPLC system consisted of an online degasser, quaternary pump, temperature controlled column chamber, and a UV/VIS diode array detector (Agilent 1100 series). The column (C 18, 250 mm x 4.6 mm, 5 µm, Discovery series) was from Supelco. Following the UV detector, a flow scintillation analyzer (Model RT505 from Packard, now Perkin Elmer

Biosciences) was used to analyze the radioactivity eluted from the column. The liquid scintillation flow rate was 2.4 ml/min and the HPLC flow rate was 1.0 ml/min. For purification, a splitter was set to divert 97% of the eluent to a fraction collector and 3% to the radioactivity analyzer.

For purification of labeled molecules, the separation system was used where eluent A was a mixture of 32 mM Na_2HPO_4 and 3.7 mM KH_2PO_4, pH 7.8 (Buffer A) and eluent B was a 1 : 4 mixture of MeOH: Buffer A at pH 7.8 (Buffer B). The column was preequilibrated for 5 min in Buffer A at a flow rate of 1.0 ml/min. After the injection of the sample the following gradient was applied: 0-13% B for 0-14 min, 13-85% B for 14-28 min, and 85% B for 28-30 min. The column temperature was maintained at 258 ºC and the retention times were: HCTO (5 min, λ_{max} = 210 nm), $NADP^+$ (6-7 min, λ_{max} = 258 nm), iPrOH (11.50 min), H_4folate (20 min, λ_{max} = 298 nm), H_2folate (23-24 min, λ_{max} = 284 nm) and CH_2H_4folate (26-28 min, λ_{max} = 294 nm).

Analysis of the TS catalyzed reaction

For products and reactants analysis of the TS catalyzed reaction, the previously published procedure was used (*59*). In short, eluent A comprises 20 mM triethyl ammonium acetate (TEAA), pH 6.6; Eluent B comprises 5 : 95 mixture of 20 mM TEAA (pH 5.1): acetonitrile. The column was preequilibrated for 5 min in Buffer A at a flow rate of 0.8 ml/min. After injection of the sample the following gradient was applied: 0-0.5% B for 0-10 min, 0.5-1% B for 10-30 min, 1.0-100% B for 30-35 min, and 100% B for 35-40 min; and the eluent was analyzed by RP HPLC. The retention times were: dUMP (20 min, λ_{max} = 263 nm), dTMP (28-29 min, λ_{max} = 269 nm) and CH_2H_4folate (37 min, λ_{max} = 294 nm).

Synthetic procedures

Synthesis of the mixture of [^{2}H and ^{3}H]-HCHO, ***4***

The synthesis of **4** is depicted in Scheme 3.3. First, 200 ml of a glyoxal solution (1') (83 mM in D_2O) were cooled to 0 ºC, and neutralized with NaOD (final pD = 8). This solution was then added dropwisely into a mixture of 240 ml $NaBT_4$ (80 Ci/mmol, 25 mCi) and $NaBD_4$ (33 mM, > 99% D) in D_2O. The solution was rapidly stirred at 0 ºC for 30 min. The reaction mixture was then acidified by sulfuric acid and KIO_4 (166 mM as final) was added to it. This oxidation step was carried out at room temperature for another half an hour. Finally, the pH of the product mixture solution was adjusted to 7.4 and the solution was stored at 4 ºC before use.

Synthesis of R-*[6-^{1}H; 11-^{X}H] CH_2H_4folate*

R-[6-^{1}H; 11-^{X}H] CH_2H_4folate was prepared by incubation of H_4folate with H/T or D/T formaldehyde (mixtures of trace HCTO in HCHO or HCTO in HCDO, respectively) under strict anaerobic conditions. The reaction mixture of trace T labeled CH_2H_4folate contained 500 mM H_4folate, 2.93 mM [^{3}H] HCHO (final specific activity was 1.5 Ci/mmol), and 280 mM Tris/HCl buffer. The reaction was kept at room temperature in an argon-filled glove bag for 30 min in the dark and the product was used without further purification. The synthesis of the trace C11 T in D substituted CH_2H_4folate was performed by a similar procedure.

Synthesis of R-*[6-^{2}H; 11-^{X}H] CH_2H_4folate,* ***5***

R-[6-^{2}H; 11-^{X}H] CH_2H_4folate was prepared by a modification of the procedure of Agrawal et al. The reaction mixture (total volume 700 ml) contained 54 mg $NADP^{+}$(final concentration 100 mM), 6 ml [U-^{2}H] iPrOH **1** (final concentration 111 mM), 31 mg

H_2folate (final concentration 100 mM), Tris/HCl buffer at pH 7.5 (final concentration 233 mM), and dithiothreitol (DTT, final concentration 4 mM). The pH was adjusted to 7.7 (at 37 ºC) with 10 M NaOH and the reaction was initiated by adding 50 units of *ec*DHFR and 25 units of *tb*ADH. The reaction was incubated at 37 ºC under argon atmosphere and its progress was monitored. Due to the inherent instability of H_4folate, the synthesis was performed under the same strict anaerobic conditions as the *R*-[6-^{1}H; 11-^{X}H] CH_2H_4folate. After H_4folate was obtained, labeled formaldehyde **4** was added into the reaction mixture followed by incubation for half an hour at 4 ºC. The progress of this reaction was also monitored by analytical HPLC (e.g. Figure 4.1).

The above reaction mixture was filtered through Centricell 20 (10 000 NMWL) to remove the enzymes. The mixture was then sealed under argon and preserved at –80 ºC. The identity and purity of the *R*-[6-^{2}H; 11-^{X}H] CH_2H_4folate product were verified by its use as a cofactor in the TS-catalyzed reaction. The labeled cofactor was fully consumed by excess dUMP in the presence of *E. coli* TS.

Kinetic measurements

R-[6-^{Y}H; 11-^{X}H] CH_2H_4folate **5** was used as a cofactor in the measurement of 2 º KIE with *ec*TS. 2 º KIEs were measured competitively on the first-order rate constant (*V/K*). All the measurements of H/T KIE ($^{T}(V/K)_H$ is the enzymologist's nomenclature) and D/T KIE ($^{T}(V/K)_D$) were performed in 100 mM Tris-buffer (pH 7.5), 50 mM β-mercaptoethanol and 1 mM EDTA. Prior to the kinetics experiments, the tritiated cofactor (trace *R*-[6-^{Y}H; 11-^{3}H] CH_2H_4folate in C11 protiated or deuterated CH_2H_4folate for H/T or D/T KIE experiments, respectively) and ^{l4}C-labeled substrate ([2-^{14}C] dUMP) were mixed (typically 2 Mdpm ^{3}H with 0.5 Mdpm of ^{14}C). To enable measurement of the

fractional conversion of CH_2H_4folate to dTMP, the [2-^{14}C] dUMP was in 40 – 50% molar excess over the CH_2H_4folate as described in more detail elsewhere (*59*). The reaction mixture (final volume 1.1 ml) was preequilibrated at the experimental temperature. An aliquot of 100 µl was removed and quenched in 30 mM (stock solution) 5-fluoro-2'-deoxyuridine 5'-monophosphate (F-dUMP, a specific inhibitor of TS with K_i = 1 nM) and used to test the radio purity of the reactants. The reaction was then initiated by addition of the enzyme and five 100 µl aliquots were removed at 2 min intervals and quenched in 30 mM F-dUMP. Finally, a concentrated enzyme was added to the rest of the reaction mixture and incubated at the same temperature for an additional 10 min to achieve complete conversion (infinity time points, R_∞). For each experiment, three infinity points were removed and quenched as described above. After quenching, all of the samples were frozen and stored at – 80 ºC prior to HPLC analysis. The ratio of ^{3}H/^{14}C in the product dTMP and the fractional conversion (*f*) were determined by RP HPLC separation, followed by fraction collection and liquid scintillation counting (LSC) analysis (Figure 4.2). To calculate a 2 º KIE, three values were measured: the ratio of ^{3}H/^{14}C in the product at each time point (R_t), the ratio of ^{3}H/^{14}C at the infinity time points (R_t), and the fractional conversion (*f*). The KIE was then calculated using Equation 4.1 (*13*):

Equation 4.1

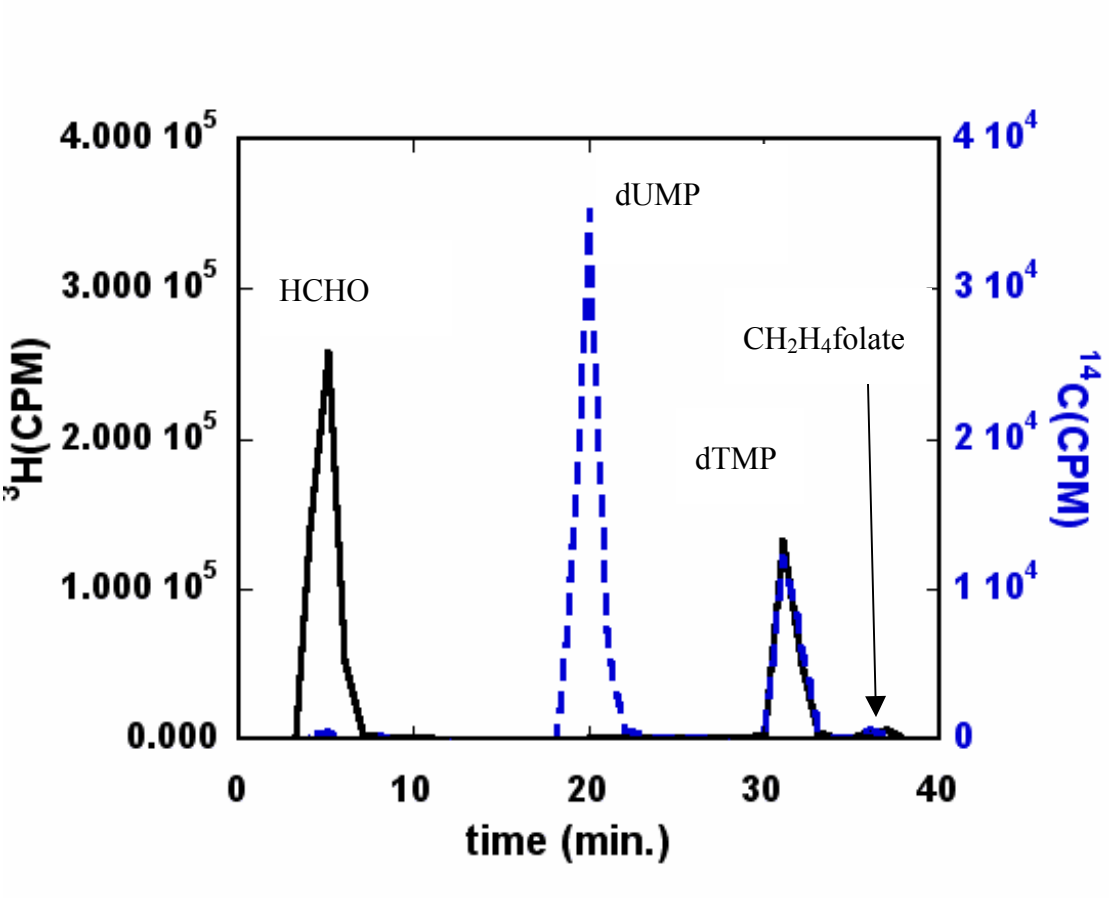

Figure 4.2 HPLC ^{3}H (solid trace) and ^{14}C (dashed trace) radiograms of *R*-[6-^{1}H; 11-^{3}H] CH_2H_4folate and [2-^{14}C]dUMP mixture 15 min after adding 0.014 units of TS.

$$KIE = \frac{\ln(1-f)}{\ln\left(1 - f \cdot \frac{R_t}{R_\infty}\right)}$$

Figure 4.3 presents a typical plot of 2º H/T KIE vs. fractional conversion. The fact that KIEs are *f* independent within experimental error serves as a good indication that no experimental artifact has affected the measurement (*13, 62*). The value of the observed KIE was the average of at least three independent experiments with five time points and three infinity points each.

Measurement of 2° KIEs of *ec*TS catalyzed reaction

The synthesized cofactors and the commercially available substrate [2-^{14}C]dUMP were used to measure the 2° KIEs on the first order rate constant *V/K* with *ec*TS. These experiments were conducted with both H transfer and D transfer at the 1° position (using *R*-[6-^{X}H; 11-^{Y}H]CH_2H_4folate where X= H or D and Y=H, D, or T). The measured 2° KIEs are summarized in Table 4.1 and Table 4.2. These findings are intriguing because a normal 2° KIE was reported by Spencer et al. (*27*). It is interesting that the 2° *V/K* KIE is inverse. These KIEs seem independent of the labeling of the 1° position, which indicates no 1°-2° coupled motion. The 2° Swain-Schaad relationships are inflated (~ 7) which is unexpected with or without tunneling contribution. Recently, QM/MM calculation (*104*) also predicted similar inverse 2 ° KIEs. We found this fact quite interesting for both us and the theoreticians. Various approaches are needed to further investigate these initial findings. Importantly, this technique is a direct probe for hybridization changes between

the ground state and the transition state of the reacting system. Resolving this puzzle is critical to understanding the nature of the TS catalyzed chemistry.

Conclusion

In this chapter, we describe a chemo-enzymatic synthesis of *R*-[6-^{Y}H], [11-^{X}H] CH_2H_4folate that results in a short, small-scale, and rather simple procedure. We also demonstrated the utility of this cofactor in measuring the 2º KIEs of the TS catalyzed reaction. The synthetic procedure described here led to four mixtures of isotopically labeled *R*-[6-^{1}H; 11-^{X}H] CH_2H_4folate cofactors. These mixtures were then used for 2º H/T and D/T KIE measurements with H-transfer or D-transfer from the 6*R* position of CH_2H_4folate (step 6 in Scheme 4.2) with the enzyme *ec*TS. These studies examine the possible contribution of H-tunneling from the breakdown of the Swain-Schaad exponential relationship as well as coupled motion (*105*) between primary and secondary hydrogens in the TS catalyzed reaction. Inverse 2°KIEs are in accordance with sp^2 to sp^3 conversion at the rate limiting step (step 6 in Scheme 4.2). The deviation from the Swan Shaad relationship suggests significant commitment on T-transfers. Lack of deviation from the rule of geometrical mean suggests no 1°-2° coupled motion. This labeling pattern may also be applied to the kinetic study of other folate-dependent enzymes (*106*). The procedure described here can easily be modified to synthesize other labeling pattern of *R*-[6-^{1}H; 11-^{X}H] CH_2H_4folate for a wide variety of experiments.

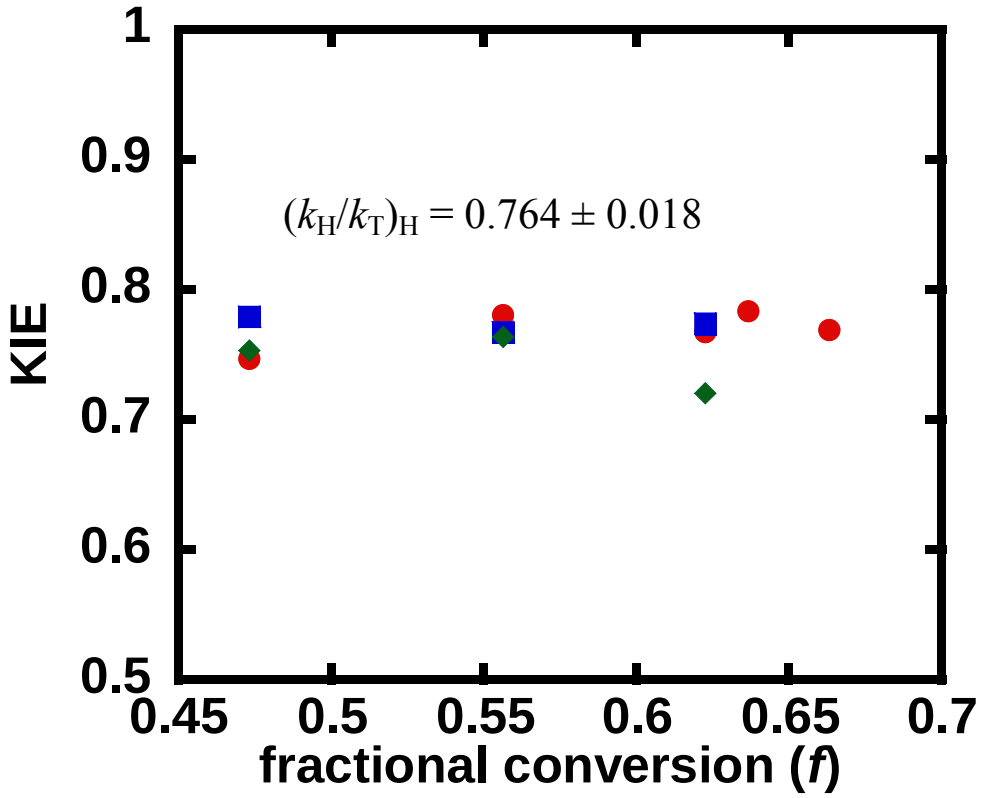

Figure 4.3 Competitive KIEs at 20 °C: 2° $^{T}V/K_H$ are plotted vs. fractional conversion (*f*). Different shapes indicate independent experiments (triplicate).

$(H/T)_H$	$(H/T)_D$	$(D/T)_H$	$(D/T)_D$
0.764 ± 0.018	0.763 ± 0.014	0.957 ± 0.007	0.962 ± 0.008

Table 4.1 Summary of all the 2˚ KIEs measured for *E. coli* TS at 20 ˚C.

Row / Column	$(H/T)_H$	$(H/T)_D$	$(D/T)_H$	$(D/T)_D$
$(H/T)_H$	1.0 ± 0.3	$RGM_{H/T}$: **1.0 ± 0.1**	$SS\text{-}EXP_H$: **6.1 ± 1.0**	Mixed SS-EXP: **6.9 ± 1.7**
$(H/T)_D$		1.0 ± 0.2	$Mixed^{-1}$ EXP: **6.1 ± 1.1**	$SS\text{-}EXP_D$: **7.0 ± 1.7**
$(D/T)_H$			1.0 ±0.1	$RGM_{D/T}$: **1.1 ± 0.3**
$(D/T)_D$				1.0 ± 0.1

Table 4.2 Summary of all possible combinations of ln (KIE_{column})/ln (KIE_{row}) for the 2˚ KIEs[a] measured for *E. coli* TS at 20 ˚C.

a. $(X/T)_p$ means 2˚ KIE of $^1(V/K)_X$ (or 2˚ k_X/k_T since chemistry is rate-limiting at 20 ˚C) with isotope P in the 1˚ position (the nucleus being transferred), where X and P are H or D.

CHAPTER V

THE ROLE OF Y94 IN PROTON TRANSFER CATALYZED BY THYMIDYLATE SYNTHASE

Summary

Thymidylate synthase (TS) catalyzes the substitution of a carbon-bound proton in a uracil base by a methyl group to yield thymine in the *de novo* biosynthesis of this DNA base. The enzymatic mechanism involves making and breaking several covalent bonds. Traditionally, a conserved tyrosine (Y94 in *E. coli*, Y146 in *L. casei*, and Y135 in human) was assumed to serve as the general base catalyzing the proton abstraction. That assumption was examined here by comparing the nature of the proton abstraction using wild type (*wt*) *E. coli* TS (*ec*TS) and its Y94F mutant (with a two orders of magnitude reduced turnover rate). The physical nature of this H-transfer step was examined by determining intrinsic kinetic isotope effects (KIEs). Surprisingly, the findings did not suggest a direct role for Y94 in the proton abstraction step. The possibility that no single residue serves as the general base in question, but rather, that the whole network of H-bonds at the active site catalyzes proton abstraction, is discussed.

Introduction

Thymidylate synthase (TS) catalyzes the reductive methylation of 2'-deoxyuridylate (dUMP) with 5,10-methylene-5, 6, 7, 8-tetrahydrofolate (CH_2H_4folate), forming thymidine monophosphate (dTMP) and 7, 8-dihydrofolate (H_2folate) (*1*). TS activity is essential to living organisms since it catalyzes the de novo synthesis of one of the DNA building blocks. Consequently, TS is a common target in cancer chemotherapy, antibiotic drugs, and gene therapy (*3, 4*). The TS-catalyzed reaction has been elucidated

in detail by a wide variety of kinetic, genetic, and structural methodologies (*1, 2, 6, 118*), which have shown that TS is a homo-dimer utilizing a half-of-the-sites-activity mechanism (*5*, *119*). Steady state measurements indicated a bi-bi ordered mechanism with substrate (dUMP) binding before the CH_2H_4folate. Kinetic and structural studies identified coherent protein motions that appear coupled to a hydride transfer step (*101, 120*), which is rate limiting for the *wt* TS.

Scheme 5.1 illustrates the two main variations proposed for the chemical mechanisms along the complex cascade of TS catalysis. In the traditional proposed mechanism (*1, 2*), E58 assists in the formation of an iminium ion (A in scheme 5.1), which is is subjected to nucleophilic attack by the C5 enolate of the C146-activated dUMP (*121*) to form a ternary intermediate (C). A proton is then abstracted from C5 of dUMP to form the enol D (step 4) (*2*). This is followed by the release of H_4folate from the ternary complex (step 5, E1CB mechanism) (*29*) to generate the exocyclic methylene intermediate (E). Finally, the product dTMP is formed in step 6 by hydride transfer from (6*S*)-H_4folate to the exocyclic methylene of the enzyme-bound nucleotide via a 1,3-S_N2 mechanism. Several experimental studies indicate that this last step is the overall rate limiting step for both first order rate constant, k_{cat}, and second order rate constant, k_{cat}/K_M (depicted below as *V/K*) (*101, 27, 122*). Recently, QM/MM calculations (*104*) suggested an alternative path with lower activation energies. In the new path, the keto-enol tautomerization at C4 of dUMP plays a minor role while the labile C6-S-Cys bond plays a major role. The differences from the traditional mechanism are: (i) Steps 2 and 3 occur concertedly; (ii) The abstraction of the proton from the C5 of dUMP involves E2 elimination of C146 (step 4'), and (iii) The dissociation of CH_2H_4folate occurs via 1,3-

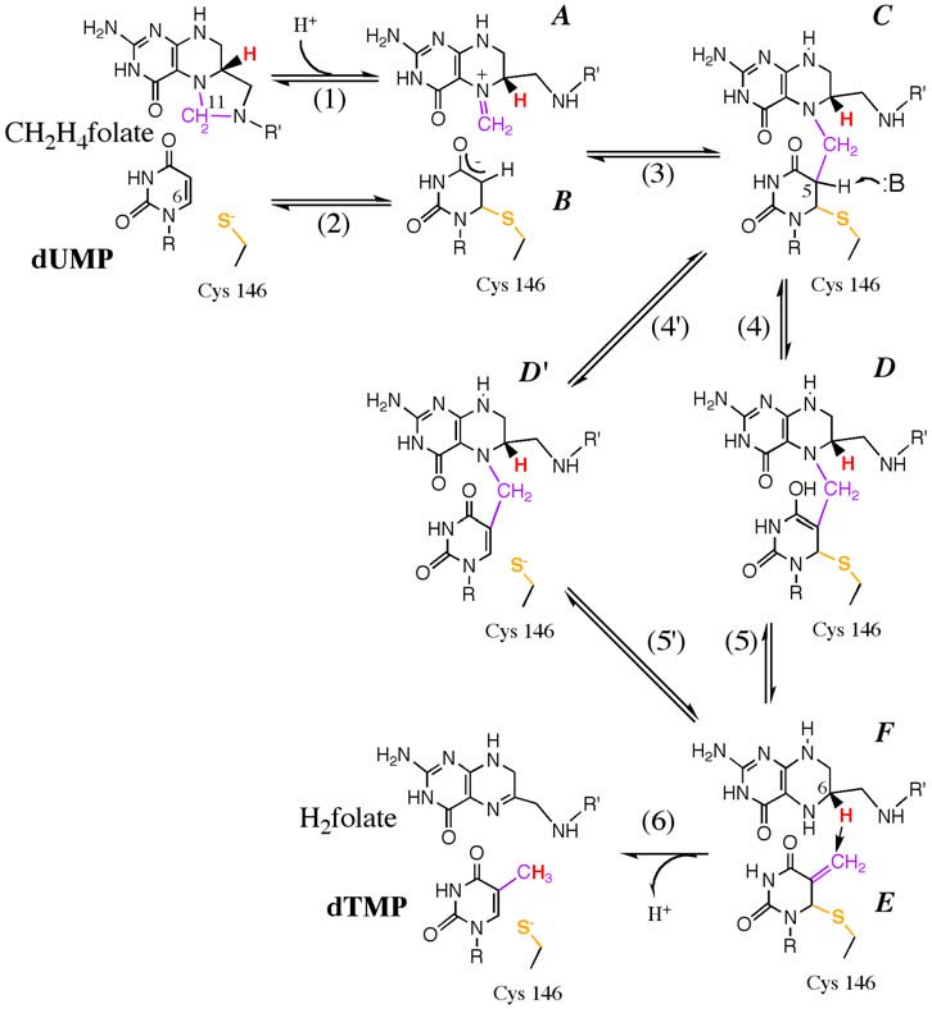

Scheme 5.1 The proposed chemical mechanisms of the TS catalyzed reaction.

S_N2 substitution with thiolate of C146 as the nucleophile and N5 of H_4folate as the leaving group (step 5').

The proton abstraction from position 5 of the pyrimidine ring is crucial in the breakdown of the ternary intermediate and is the focus of this work. The general base in the active site has been proposed to be Y94 (see ref (*2*) and many cited therein). Figure 5.1 presents the crystal structure of the *wt E. coli* TS with covalently bound dUMP and non-covalently bound folate analogue at the active site (PDB # 2KCE). The water molecule (W608) is located 2.6 Å from the oxygen of Y94 and 3.6 Å from the C5 of dUMP, and was assumed to serve as the initial acceptor of the abstracted proton in step 5 (*2, 29, 123-125*). Hardy et al. (*126*) proposed that the general base in step 4 is N5 of the H_4folate through an "H-wire", using water as conduit. Mutagenesis studies (*125*) demonstrated that several modifications of Y94 lead to loss of activity. This fact was interpreted as support of a mechanism in which Y94 assists in the proton abstraction. These issues are further examined in the current chapter.

Another interesting feature of the current work is that no isotope effects have been measured on the C5-H bond cleavage, which is not a rate limiting step for any measurable rate constant. Previous measurements monitored the ratio of ^3H to ^{14}C using [2-^{14}C, 5-^3H] dUMP as a substrate with a saturating CH_2H_4folate concentration and reported no KIE (unity) or even a slightly inverse KIE (*2*). The reason for the inverse KIEs is likely to be a fast and reversible exchange of the C5 proton through steps 1-4, prior to the irreversible and rate limiting hydride transfer in step 6. Furthermore, the high concentration of CH_2H_4folate, which binds after dUMP binds (*2, 6*), would mask a

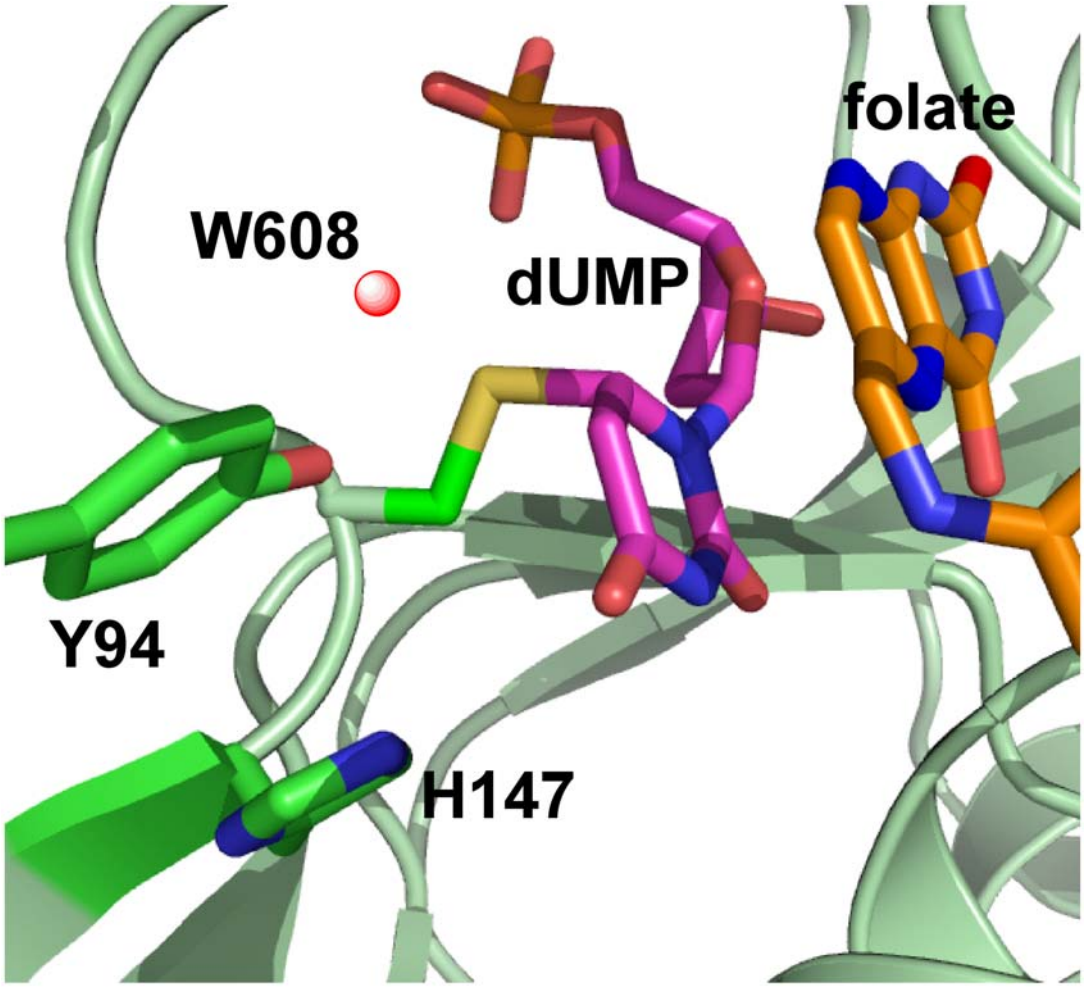

Figure 5.1 Structure of *wt E. coli* TS covalently bound to dUMP (PDB code 2KCE) with Y94 and H147 highlighted in green, the water molecule closest to the Y94 (1.7 Å) and to C5 of the dUMP is highlighted as a red ball, the dUMP in magenta is covalently bound to C146, and the pterin ring is in orange.

possible intrinsic KIE if the isotopic label is on the substrate (*126, 69,127-129*). In the current work, the KIEs on this proton abstraction were studied as a function of the concentration of CH_2H_4folate in combination with the Northrop method (*63-65, 117*). The observed KIEs versus the CH_2H_4folate concentration clearly indicated a kinetic mechanism with ordered substrate binding for the *wt* and less ordered binding for Y94F. A comparison of the intrinsic KIEs of the mutant and the *wt* served as a probe for the role of Y94 in this step.

Materials and methods

Materials

[2-^{14}C] dUMP (specific radioactivity 52 Ci/mol) and [5-^{3}H] dUMP (specific radioactivity 13.6 Ci/mmol) were from Moravek Biochemicals. [^{2}H] $NaBH_4$ (> 99.5% D) was from Cambridge Isotopes. [^{3}H] $NaBH_4$ (15 Ci/mmol) was from American Radiolabeled Chemicals. Dihydrofolate (H_2folate) was synthesized following the procedure of Blakley (*103*). [2-^{3}H] iPrOH was prepared by reduction of acetone with [^{3}H] $NaBH_4$ (specific radioactivity of 15 Ci/mmol) as described in detail elsewhere (*59*). All other materials were purchased from Sigma.

Synthesis of [2- ^{14}C, 5-D] dUMP (> 99.5% D).

[2- ^{14}C, 5-D] dUMP was prepared by modifying the method of Wataya and Hayatsu (*130-132*) using $_{L}$-cysteine in D_2O to catalyze H to D exchange at the C5 position of [2-^{14}C] dUMP . The reaction was conducted by incubation of [2-^{14}C] dUMP (~1 mM and 52 mCi/mmol) in a D_2O solution (> 99.9% D) containing 1 M of $_{L}$-cysteine at 37 °C and a pD of 8.8 for 7 days. The reaction was carried to completion as determined by ^{1}H NMR.

Enzyme

Wild-type *E. coli* TS was prepared and purified according to the procedure of ref (*61*). Y94F was prepared and purified as described in detail elsewhere (*118, 29, 125*). The mutant was stored as ammonium sulfate pellets at –80 °C, and prior to use was dissolved and dialyzed against a mixture of 25 mM potassium phosphate, 10% ethylene glycol and 2 mM DTT. *tb*ADH was purchased from Sigma.

Methods

Competitive and Intrinsic Primary Kinetic Isotope Effect (1 ° KIE) for C5 Proton Abstraction

The 1˚ KIEs on proton abstraction from the 5 position of dUMP were measured competitively. The reaction mixture contained 50 mM β-mercaptoethanol, 1 mM EDTA and 5 mM formaldehyde in 100 mM Tris buffer (pH 7.5). Prior to kinetic assay, 1.5 Mdpm [5-^{3}H] dUMP, 0.5 Mdpm of [2-^{14}C] dUMP and varied concentrations of CH_2H_4folate (2 μM to1000 μM) were added to the buffer mixture at 25 ˚C. The reaction was initiated by adding enzyme (*wt* or Y94F TS). Five aliquots of 100 μL were removed at different time points (t), quenched with 30 μM 5-fluoro-2'-deoxyuridine-5'-monophosphate (F-dUMP, a nM inhibitor of TS). Then, a concentrated solution of *wt* TS was added to the reaction mixture to a final concentration of 0.1 mM, followed by 10 more minutes of incubation to complete the reaction (t_∞). Two t_0s (reaction mixture prior to adding enzyme and used as control) and three t_∞s were obtained for each experiment and independent experiments were performed in triplicate. All the quenched samples were stored in dry ice before HPLC analysis. The method of RP HPLC separation and liquid scintillation counter (LSC) analysis of the ^{3}H/^{14}C ratio is described in detail elsewhere (59).

The competitive observed KIEs on the second order rate constant V/K were determined using equation 5.1 (*13*):

Equation 5.1

$$KIE = \frac{\ln(1-f)}{\ln\left(1 - f \cdot \frac{R_t}{R_\infty}\right)}$$

where *f* is the fractional conversion to product dTMP (typically ranging from 20 to 80 %), R_t and R_∞ are ratios of $^3H/^{14}C$ in products (water and dTMP) at each time point and time infinity. The fractional conversion *f* was calculated by equation 5.2:

Equation 5.2

$$f = \frac{[^{14}C]dTMP}{[^{14}C]dTMP + [^{14}C]dUMP}$$

Figure 5.2 presents an example of measured H/T KIEs as function of *f*. Since the KIE on the proton abstraction has not been measured before, it is important to demonstrate that the KIE is reproducible in a series of independent experiments and that there is no upward or downward trends in the KIE as function of *f*.* Figure 5.3 presents the observed H/T KIEs of the mutant and the *wt* as a function of CH_2H_4folate concentration. The analysis of the observed KIEs on the proton abstraction as function of CH_2H_4folate is presented under Results and Discussion.

* Most artifacts in a competitive experiment will result in such a trend.

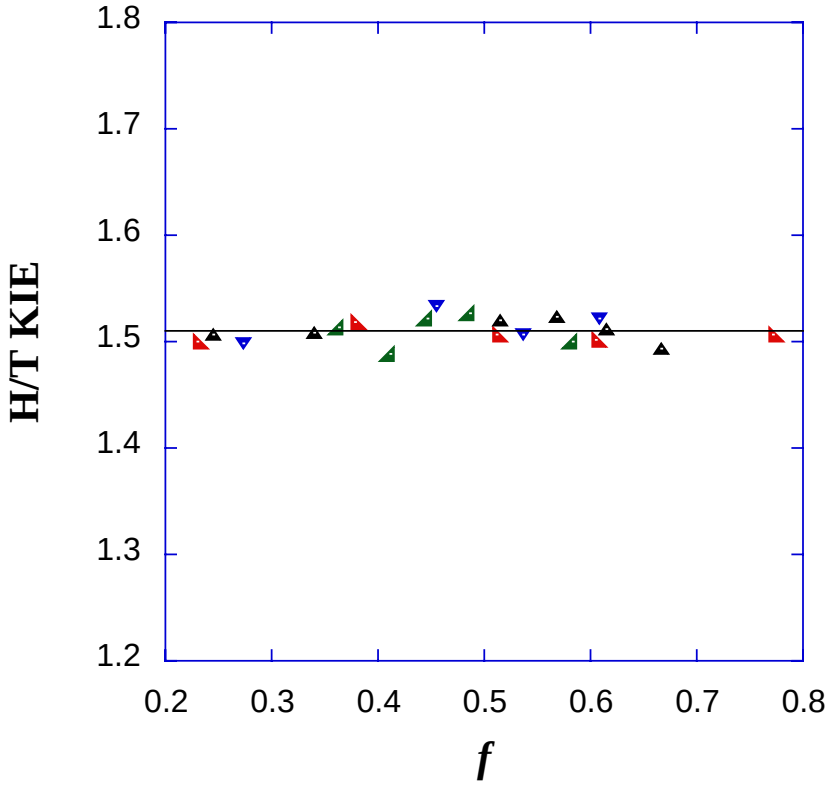

Figure 5.2 H/T KIEs as function of fractional conversion as measured for *wt* TS at 25 ˚C in 5 μM CH_2H_4folate. The different colors and shapes represent points measured in four independent experiments. The average value is 1.52 ± 0.03 and no upward or downward trend is observed within statistical error.

To determine the intrinsic KIE for this step, 5 μM CH_2H_4folate was used to measure the observed H/T and D/T KIEs. The observed D/T KIE was measured using the exact same conditions as that for the H/T KIE except the [2-^{14}C] dUMP was replaced by [2-^{14}C, 5-D] dUMP. So, the ^{14}C now represents the D-transfer rather than H-transfer. Intrinsic KIEs are calculated from equation 5.3, (*63-65, 117*):

Equation 5.3

$$\frac{{}^{T}(V/K)_{H\,obs}^{-1}-1}{{}^{T}(V/K)_{D\,obs}^{-1}-1}=\frac{k_T/k_H-1}{(k_T/k_H)^{1/3.34}-1}$$

where $^{T}(V/K)_{H,\,obs}$ and $^{T}(V/K)_{D,\,obs}$ are the observed competitive H/T and D/T KIEs; k_T/k_H represents the reciprocal of k_H/k_T (intrinsic H/T KIE). Although the intrinsic H/T KIE is the only unknown in this equation, it cannot be solved analytically. Therefore, a program has been developed to solve this equation numerically. Since error propagations in this case cannot be conducted analytically from derivatization of Eq. 5.3, the intrinsic KIEs were analyzed by calculation of the intrinsic KIEs from independent and random combinations of observed H/T and D/T KIEs (*112*). The Northrop method for a reversible step assumes $^{T}K_{eq}$ close to unity (*63-65*). We measured the $^{D}K_{eq}$ using the Cys activated dUMP as model compound for intermediate C in Scheme 5.1 (as described in the following item), and found it to be unity within experimental error. Additionally, the $^{T}K_{eq}$ for the proton abstraction can be estimated to be close to unity from fractionation factors for protons bound to similar carbons, and the fractionation factor in the product water molecule being unity since water is the reference system (*133*). Finally, since the reverse step in question involves the competition of tritium and protons from water, as

discussed below, even a larger EIE should have little effect on the outcome of the Northrop method.

Equilibrium Isotope Effect (EIE) on activated dUMP. To assess the EIE ($^{D}K_{eq}$) on the proton abstraction on C5 of dUMP, we used a model in which C6 is activated by high concentration of Cys in solution. The activated complex was allowed to exchange with 50 % H_2O/D_2O. Specifically, 270 mM dUMP and 1 M of $_{L}$-cysteine were incubated in 50 % H_2O/D_2O (mol/mol) at 37 ° C and a pH of 8.8 for 5, 7, and 9 days. The progress of the exchange reaction was monitored by ^{1}H-NMR until completion (no further change in H content at C5). For an accurate NMR examination, the samples were lyophilized and redissolved in pure D_2O at a pD of 1.5 (the exchange reaction does not proceed at this pD). Then, the ratio between the hydrogen on C6 (unexchangeable) and the one on C5 was determined by ^{1}H-NMR. The hydrogen on C3' was used as integration reference of unity and the H6/H5 ratio was determined in quintuplets. The H5/H6 values were 0.510 (±0.008) /1.010 (±0.007) indicating $^{D}K_{eq} = 0.99$ (±0.02) for the proton exchange with water.*

Results and discussion

Structural Comparison A recent X-ray crystallography study (*134*) examined the Y94F mutant at 1.6 Å and 2.0 Å resolution (without and with ligands, respectively). An overlap of crystal structures of the *wt* and the mutant (Figure 5.4) indicates a perfect overlap, including electron density for defined water molecules (r.m.s.d. = 0.014 Å (*134*)). The obvious exception is the lack of the hydroxyl at residue 94 and the water molecule

* $^{D}K_{eq} = 1$ would lead to H5/H6 ratio of 0.5 so 0.5∗1.01/0.51 = 0.99.

that is hydrogen bonded to the OH group in the *wt*. In the *wt* enzyme, Y94 is part of a H-bond network containing water molecules, H147, C146, and N5 of H_4folate. In Y94F, there is no electron density at the locations of the mutated hydroxyl and water 608. It is suggested that delocalized water molecules now occupy that space. It is also apparent that H147 in the *wt* has more than one conformation (from partial electron density), while Y94F only adopts a single conformation. This is the most substantial effect on the whole network of H-bonding at the active site.

Proton Abstraction The substrate dUMP, labeled with tritium at C5, is commonly used to measure the enzyme's activity (*2*). The use of tritium release from [5-^{3}H]-dUMP to measure the reaction rate relies on the assumption that there is no effective (observed) KIE on that step. This assumption is substantiated by the fact that the proton abstraction is not rate limiting in the overall reaction (*2, 101*) and by the ordered nature of the *wt* TS reaction. The intrinsic KIE of step 5 in Scheme 5.1 has never been measured before (to the best of our knowledge). Previous experiments that monitored the ^{3}H/^{14}C ratio in the mixture of [5-^{3}H] dUMP and [2-^{14}C] dUMP (*2, 129*), reported KIEs close to unity. This is probably due to the ordered binding mechanism of the *wt* TS (*1*) that "masked" the KIE when the labeling was on the dUMP that binds first (*69, 135, 136*). The relationship between the observed KIE on the second order rate constant $^T(V/K)$ and the KIE after the formation of the ternary complex ($^Tk_9$ in Scheme 5.2) is described in equation 5.4 (*69, 65, 137*):

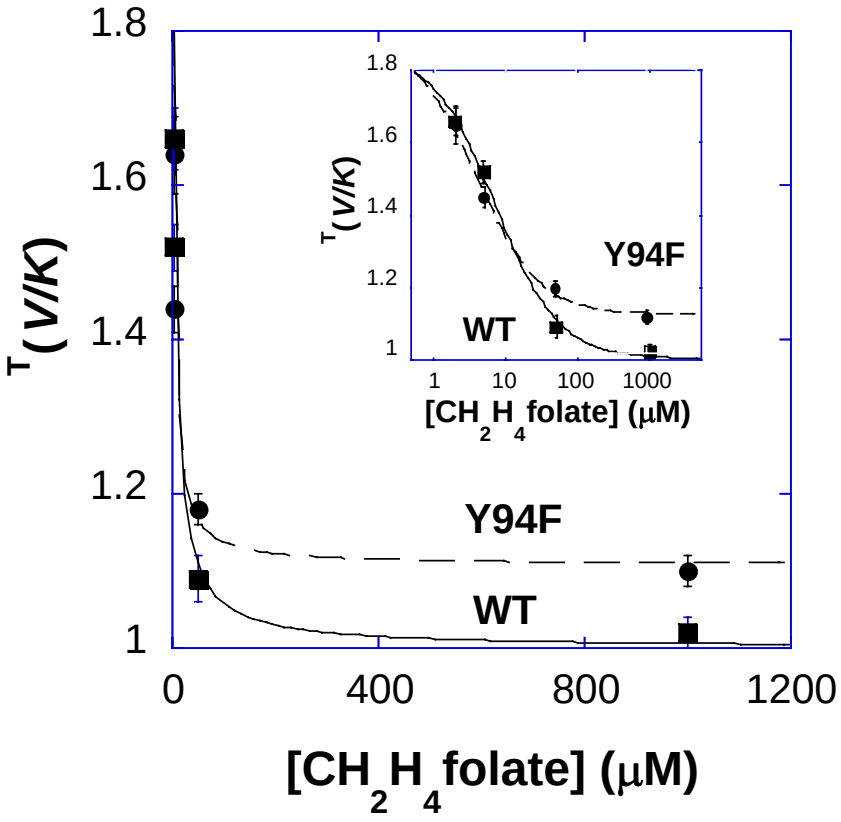

Figure 5.3 H/T KIE for proton abstraction as a function of CH_2H_4folate concentration. Data with Y94F (circles) and with *wt* (squares) are compared. Solid and dashed lines are fits to Eq. 5.4 for the *wt* and the Y94F, respectively.

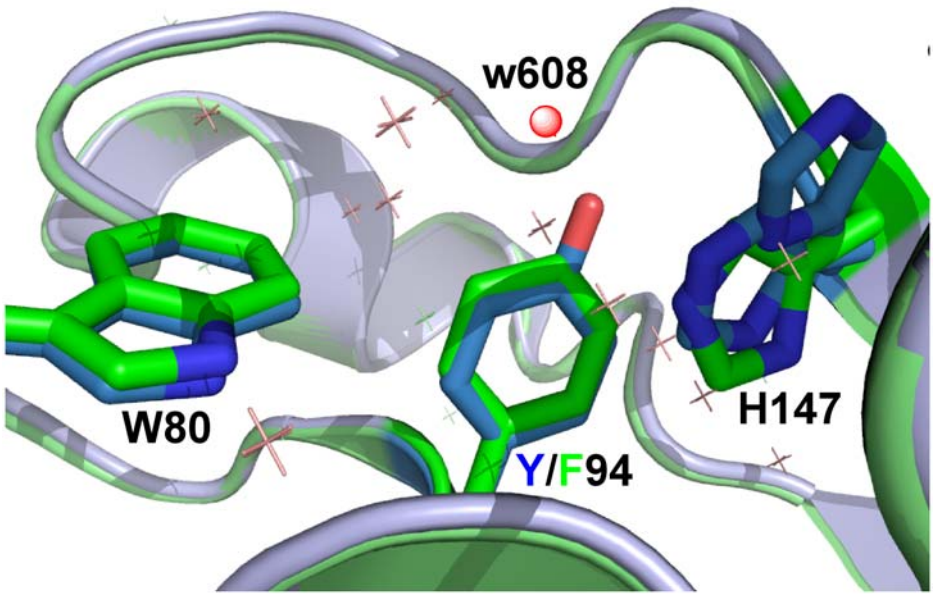

Figure 5.4 *wt* TS (blue - PDB ID # 2FTQ) and Y94F (green - PDB ID # 2FTN) with Y/F94, W80, and H147 presented as sticks. The water molecule closest to the Y94 (w608, 2.6 Å from its O) is highlighted as red ball and is missing in the mutant. All other water molecule are marked by crosses and practically overlap for the *wt* and the mutant. See also Figure 3 in ref (*134*). Note that the two-fold orientation of H147 is only apparent in the *wt* (blue), but not in Y94F (green).

Equation 5.4

$$^{T}(V/K) = \frac{^{T}k_9 + C_f + C_r\,^{T}K_{eq}}{1 + C_f + C_r}$$

where k_ns are the microscopic rate constants for the kinetic steps described in Scheme 5.2, and C_r is the reverse commitment, which in the case of the current experiments is close to zero.* $^{T}K_{eq}$ is the equilibrium isotope effect on the proton abstraction, which is expected to be close to unity. The forward commitment C_f is described by equation 5.5:

Equation 5.5

$$C_f = \frac{k_9}{k_5 + \dfrac{k_2 k_4}{k_2 + k_3[B]}}$$

where [B] is the concentration of the second substrate (CH_2H_4folate in this case).

As apparent from Eqs 5.4 and 5.5, the observed $^{T}(V/K)$ is dependent on the concentration of B and its observed value can change between two finite values (C_f changes from k_9/k_5 to $k_9/(k_5 + k_4)$ as [B] changes from infinity to zero). In contrast to the random mechanism, the C_f in an ordered mechanism in which A binds first follows:

* The reverse commitment is defined as $C_r = k_{10}/k_{11} + k_{10}k_{12}/k_{11}k_{13}$. Since C5 of dUMP is only trace labeled with tritium, k_{10} effectively represents competition between the water protons and the trace tritium. For the sake of simplicity, we follow the precedence of previous studies using [5-^{3}H]dUMP (*4*) and assume that the effective k_{10} is close to zero and thus C_r can be ignored in most of the following discussion. This assumption is further supported by comparison of the observed KIE at [B] = 0 (1.8, see Figure 5.2) with the intrinsic KIE ($^{T}k_9$ = 3.2 as calculated below). The combined commitment is only 0.45, leaving little apparent contribution for C_r alone. At any rate, C_r is independent of [B] and does not affect the conclusion regarding the effect of the mutation on the reaction order.

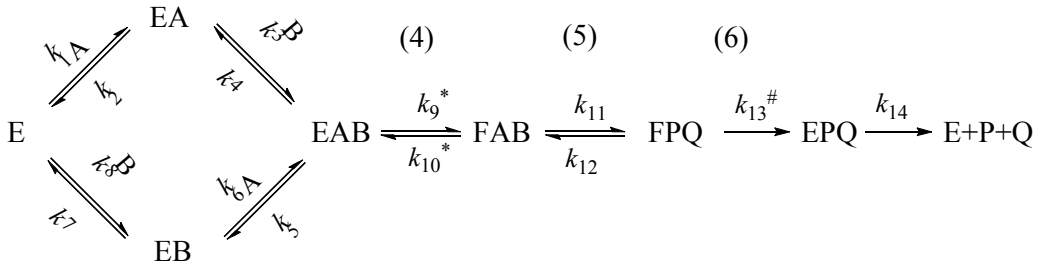

Scheme 5.2 Binding scheme for a sequential mechanism. In this case, A represents dUMP and B represents CH_2H_4folate. The relevant steps from Scheme 5.1 are presented in parenthesis. Rate constants that are isotopically sensitive in the proton abstraction experiments (using labeled dUMP) are marked with * and the one that is isotopically sensitive in the hydride transfer experiments (using labeled CH_2H_4folate) is marked with $^{\#}$.

Equation 5.6

$$C_f = \frac{k_9}{k_4} + \frac{k_3[B]}{k_2 k_4}$$

In this case, the observed $^{T}(V/K)$ is dependent on the concentration of B and its observed value can change from unity (no KIE) to a finite value (C_f changes from infinity to k_9/k_4 as [B] changes from infinity to zero (*69*)).

In the current study, the observed KIEs on the proton abstraction from C5 of dUMP were measured as a function of the CH_2H_4folate concentration to ascertain the kinetic mechanism for *wt* TS and Y94F. Figure 5.3 presents the observed KIEs as a function of CH_2H_4folate concentration. The observation that the observed H/T KIE for the *wt* approaches unity at high concentration of CH_2H_4folate (1.02 ± 0.02 at 1 mM CH_2H_4folate) while Y94F goes to an asymptote at a finite value (1.10 ± 0.02) indicates that the *wt* binding mechanism is strictly ordered (within experimental error and in agreement with previous studies (*1*)), but that of the mutant is more random (*69*). Also, the observed KIEs for the *wt* and Y94F are similar at zero [B] (1.86 ± 0.10 and 1.96 ± 0.15, respectively; Figure 5.3). This last observation, together with the intrinsic KIEs (see below), indicates a similar commitment on $^{T}(V/K)$ for the *wt* and the mutant.

To access the intrinsic KIE on the proton transfer step, we measured the D/T KIE at a low CH_2H_4folate concentration and then assessed the intrinsic KIE using the Northrop method (*63-65*). A concentration of 5 μM CH_2H_4folate was used to assure sufficient conversion of radioactive labeled dUMP on one hand, and large observed KIE values (small relative error) due to a small commitment on the other hand. The intrinsic

H/T KIE on the proton abstraction for the *wt* and Y94F are practically the same (3.25 ± 0.31 and 3.17 ± 0.22, respectively, Table 5.1).*

Conclusions

Summary of the proton abstraction step (step 4 or 4' in Scheme 5.1): An intrinsic KIE of the C5 proton abstraction from dUMP is determined here for the first time. The intrinsic KIEs for both the mutant and the *wt* are similar ($^{T}k \approx 3.2$) suggesting that the effect of Y94 mutation on this transformation was too small to be detected. Apparently, while the Y94F mutation reduced the order of binding by increasing the rate of dUMP release from the ternary complex (k_5), it did not affect the actual proton transfer step. As apparent from Figure 5.3, the level of kinetic complexity that masks the intrinsic KIE ($^{T}k_9$) on the second order rate constant $^{T}(V/K)$ at zero CH_2H_4fole appears to be small and similar for both *wt* and the mutant ($C \approx 0.45$).#

The relatively small intrinsic KIE is in accordance with a pre-activated C5-H bond and an asymmetric transition state for this transformation (*13*). QM/MM calculations (via collaboration with Moliner and co-workers) are underway to quantitatively examine this observation.

---

* At zero [B], C_f is k_9/k_4 for the *wt* and $k_9/(k_5 + k_4)$ for the mutant (see Eq. 5.5 and 5.6). Since C_f can also be calculated using the independently measured intrinsic KIE, it is tempting to calculate all the microscopic rate constants in Scheme 5.2. However, k_4 and k_9 do not have to be the same for both enzymes, and k_9 is likely to be much faster in the *wt*. Consequently the current data are insufficient for extraction of all the microscopic rate constants.

Where $C = C_f + C_r$ and $^{T}K_{eq}$ is close to unity.

KIE	Wild Type	Y94F
$^{T}(V/K)_{H}$	1.52 ± 0.03	1.44 ± 0.03
$^{T}(V/K)_{D}$	1.17 ± 0.01	1.15 ± 0.01
H/T KIE_{int}	3.2 ± 0.2	3.2 ± 0.3
D/T KIE_{int}	1.41 ± 0.03	1.42 ± 0.04
H/D KIE_{int}	2.2 ± 0.1	2.3 ± 0.2

Table 5.1 Kinetic isotope effect of the wild-type and Y94F TS on proton abstraction at 25 ºC.

CHAPTER VI

THE ROLE OF Y94 IN HYDRIDE TRANSFER CATALYZED BY THYMIDYLATE SYNTHASE

Summary

The role of a conserved tyrosine (Y94 in *E. coli*, Y146 in *L. casei*, and Y135 in human) in proton abstraction was examined in Chapter V by comparing the nature of the proton abstraction using wild type (*wt*) *E. coli* TS (*ec*TS) and its Y94F mutant. The findings did not suggest a direct role for Y94 in the proton abstraction step. In the current chapter, a subsequent hydride transfer was also studied using the *wt* and Y94F. The physical nature of this H-transfer step was examined by determining intrinsic kinetic isotope effects (KIEs). The effect of this mutation on the subsequent hydride transfer was examined by a comparison of the temperature dependency of the intrinsic KIE on both the *wt* and the mutant. The intrinsic KIEs for Y94F at physiological temperatures were slightly smaller than for *wt,* but otherwise, were as temperature independent, suggesting a perfectly pre-organized reaction coordinate for both enzymes. At reduced temperature, however, the KIE for the mutant increased with decreasing temperature, indicating a poorly pre-organized reaction coordinate. Other kinetic and structural properties were also compared and the findings suggested that Y94 is part of a H-bond network that plays a critical role at a step between the proton and the hydride transfers, presumably the dissociation of H_4folate from the covalently bound intermediate.

Introduction

Thymidylate synthase (TS) catalyzes the reductive methylation of 2'-deoxyuridylate (dUMP) with 5,10-methylene-5, 6, 7, 8-tetrahydrofolate (CH_2H_4folate),

forming thymidine monophosphate (dTMP) and 7, 8-dihydrofolate (H_2folate) (*1*). TS activity is essential to living organisms since it catalyzes the *de novo* synthesis of one of the DNA building blocks. Consequently, TS is a common target in cancer chemotherapy, antibiotic drugs, and gene therapy (*3, 4*). Scheme 6.1 illustrates the two main variations proposed for the chemical mechanisms along the complex cascade of TS catalysis and was explained in details in Chapter V. The proton abstraction from position 5 of the pyrimidine ring is crucial in the breakdown of the ternary intermediate. The general base in the active site has been proposed to be Y94 (see ref (*4*) and many cited therein). The role of Y94 in the proton abstraction was examined in Chapter V and our results suggested the proposed tyrosine (Y94, 3.6 Å from the proton donor) is not the main contributor to the proton abstraction step, but rather the whole network of H-bonds at the active site appears to serve as the general base.

In the current chapter, we investigated the effect of altering the hydrogen bond network at the active site by Y94F mutation and the nature of another chemical transformation remote from Y94, namely the hydride transfer (step 6 in scheme 6.1). The comparison of the temperature dependency of the intrinsic KIEs and activation parameters of Y94F with that of *wt* (*101*) indicated a minor effect of this mutation at physiological temperature, but a substantial distortion of the reaction's pre-organization at reduced temperature. Together, the examination of the effect of Y94F on the proton abstraction (step 4 or 4') and on the hydride transfer (step 6) indicated that a more likely role of Y94 is in the protonation of the N5 of H_4folate (the leaving group in step 5 or 5'), as discussed in detail below.

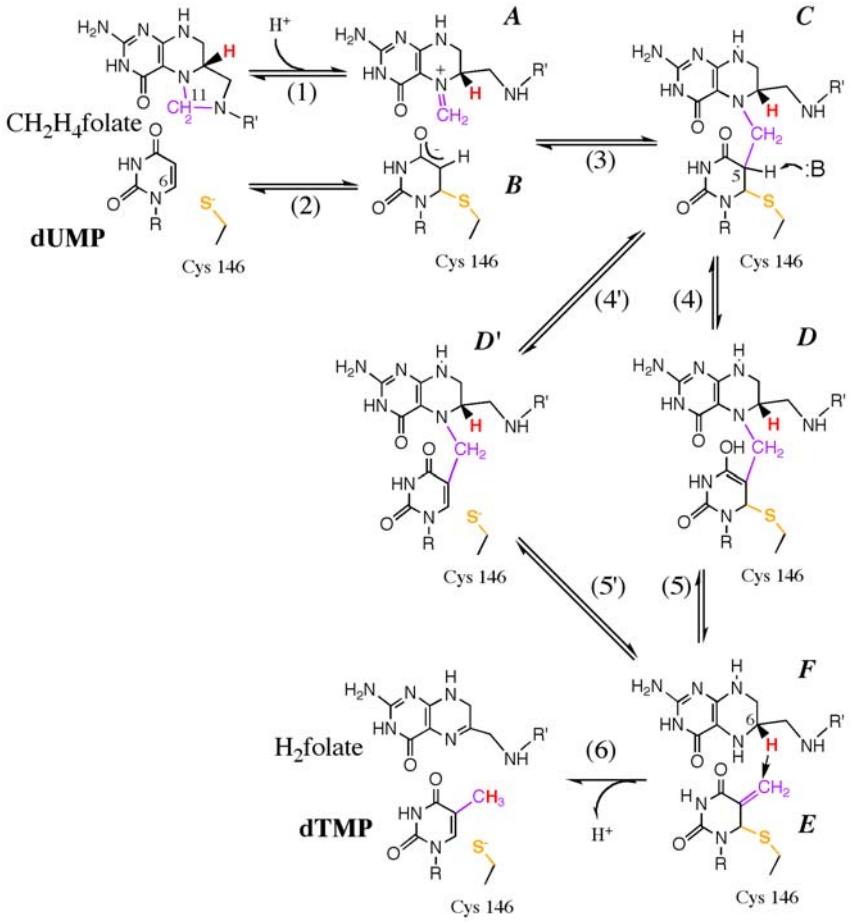

Scheme 6.1 The proposed chemical mechanisms of the TS catalyzed reaction.

Materials and methods

Materials

[2-^{14}C] dUMP (specific radioactivity 52 Ci/mol) and [5-^{3}H] dUMP (specific radioactivity 13.6 Ci/mmol) were from Moravek Biochemicals. [^{2}H] $NaBH_4$ (> 99.5% D) was from Cambridge Isotopes. [^{3}H] $NaBH_4$ (15 Ci/mmol) was from American Radiolabeled Chemicals. Dihydrofolate (H_2folate) was synthesized following the procedure of Blakley (*103*). [2-^{3}H] iPrOH was prepared by reduction of acetone with [^{3}H] $NaBH_4$ (specific radioactivity of 15 Ci/mmol) as described in detail elsewhere (*59*). All other materials were purchased from Sigma.

Synthesis of Isotopically C6 Labeled CH_2H_4folate for Measurement of KIE on Hydride Transfer

The synthesis of (*R*)-[6-^{3}H] CH_2H_4folate was performed through a combination of two enzymatic reactions as described previously (*59*). Briefly, [2-^{3}H]iPrOH was prepared by reduction of acetone with [^{3}H]$NaBH_4$. $NADP^+$ was reduced by [2-^{3}H]iPrOH to (*R*) – [4-^{3}H] NADPH by alcohol dehydrogenase from *Thermoanaerobium brockii* (*tb*ADH). DHFR catalyzed the *in situ* conversion of H_2folate to (*S*)-[6-^{3}H] H_4folate using (*R*) –[4-^{3}H] NADPH and then the isotopically labeled H_4folate was converted to (*R*)-[6-^{3}H] CH_2H_4folate upon quenching with formaldehyde. Similarly, the mixture of (*R*)-[6-^{3}H] CH_2H_4folate and (*R*)-[6-^{2}H]- CH_2H_4folate for the D/T KIE measurement was synthesized under the same conditions as for the mixture of D- and T- labeled isopropanols. The radioactively labeled CH_2H_4folate was purified by reverse phase HPLC, lyophilized and stored at -80 ˚C prior to use.

Enzyme

Wild-type *E. coli* TS was prepared and purified according to the procedure of ref (*61*). Y94F was prepared and purified as described in detail elsewhere (*118, 29, 125*). The mutant was stored as ammonium sulfate pellets at –80 °C, and prior to use was dissolved and dialyzed against a mixture of 25 mM potassium phosphate, 10% ethylene glycol and 2 mM DTT. *tb*ADH was purchased from Sigma.

Methods

Competitive and Intrinsic Primary Kinetic Isotope Effect (1 ° KIE) on Hydride Transfer from C6 (Step 6 in Scheme 6.1)

The competitive H/T and D/T KIEs for the hydride transfer from the 6 position of CH_2H_4folate with Y94F mutant were measured using the same conditions as with the *wt* TS (*101*). In short, the reaction mixture contains 1.5 Mdpm tritiated *R*- [6 - ^{3}H] CH_2H_4folate for the H/T KIE or deuterated *R*-[6-^{2}H] CH_2H_4folate for the D/T KIE, respectively, 0.5 Mdpm [2-^{14}C] dUMP, 50 mM *β*-mercaptoethanol, 1 mM EDTA and 5 mM of formaldehyde in 100 mM Tris buffer with a pH of 7.5 (adjusted at each experimental temperature). About 30 % molar excess of dUMP was used in the reaction mixture in order to ensure 100 % conversion of tritiated CH_2H_4folate at time infinity (essential for R_∞ -see below). The reaction mixture was pre-incubated at the respective experimental temperatures and initiated by adding Y94F. At five different time points, 100 µL aliquots were removed and quenched with 30 µM F-dUMP. Concentrated *wt* TS was added to the reaction mixture to achieve 100% conversion (t_∞). Two t_0s (used as control) and three t_∞s were obtained for each experiment and independent experiments were performed in at least duplicate. The competitive observed KIEs were determined by Eq. 6.1 and the fractional conversion *f* was determined from equation 6.2 (*59*):

Equation 6.1

$$KIE = \frac{\ln(1-f)}{\ln\left(1 - f \cdot \frac{R_t}{R_\infty}\right)}$$

Equation 6.2

$$f = \frac{[^{14}C]dTMP}{(100 - \%_{\text{excess}}) \cdot ([^{14}C]dTMP + [^{14}C]dUMP)}$$

where % excess = [(total ^{14}C) – ([2- ^{14}C] dTMP)$_\infty$]/(total ^{14}C) x 100.

The intrinsic H/T and D/T KIEs are calculated from Eq. 6.3

Equation 6.3

$$\frac{{}^{T}(V/K)_{H\,obs}^{-1} - 1}{{}^{T}(V/K)_{D\,obs}^{-1} - 1} = \frac{k_T/k_H - 1}{(k_T/k_H)^{1/3.34} - 1}$$

with the error propagation processed in the same way as was for the aforementioned proton abstraction step in Chapter V. The analysis of these data is described in Result and Discussion, below.

Steady-State Kinetics.

The initial velocities were measured under steady state conditions in a buffer mixture containing 50 mM DTT, 5 mM formaldehyde, 1 mM EDTA, and 100 mM Tris

with a pH of 7.5 (adjusted at each experimental temperature). The reaction was monitored by following the increase of absorbance at 340 nm upon conversion of CH_2H_4folate to H_2folate ($\Delta\varepsilon_{340nm}$ = 6.4 $mM^{-1}cm^{-1}$) (*27*). The individual reaction mixtures were pre-equilibrated at experimental temperatures and initiated by adding enzyme. Each measurement was conducted at least in duplicate and the data were analyzed as described in Results and Discussions.

Results and disscusion

Hydride Transfer

The intrinsic KIEs on the hydride transfer step (step 6 in Scheme 6.1) were measured and compared with the *wt* using CH_2H_4folate labeled with H, D, or T at its *R*-C6 position as described in ref (*101*). Since in this part, only the hydride was isotopically labeled, all the other kinetic steps are not isotopically sensitive and the kinetic equations used are not different from those used for any other system with a single isotopically sensitive step. Figure 6.1 shows both the temperature dependence of the observed and intrinsic KIEs of the *wt* and Y94F. The analysis of the temperature dependence of intrinsic KIEs proceeded by exponential fitting of the data to the Arrhenius equation (Equation 6.4) for KIEs:

Equation 6.4

$$k_L/k_T = A_L/A_T \exp [(E_T - E_L)/RT]$$

where k_L/k_T is the L/T KIE with L representing the light isotopes, A_L/A_T is the isotope effect on preexponential factors, and $E_T - E_L$ is the isotope effect on activation energy.

The biphasic behavior of the intrinsic KIEs for the mutant (Figure 6.1B) suggested an intrinsic phase transition (*49, 138*) so the data were fitted at temperature ranges of 40 - 20 °C and 20 - 5 °C independently. Above 20 °C, the KIE was temperature independent ($E_T - E_H$ = -0.03 ± 0.40 kcal/mol) and the ratio of the Arrhenius preexponential factors (Table 6.1) are well above the semiclassical values (*7, 38, 71*). At lower temperature range, the KIEs were temperature dependent and the KIE on the Arrhenius preexponential factors were inverse ($A_H/A_T < 1$) and below the semi-classical limits (Table 6.1).

Whether the temperature dependence of the KIEs can be understood within the framework of tunneling correction to transition state theory (*12, 13*) depends on the assessment of the activation parameters on the reaction rate. To assess the activation parameters for the hydride transfer step at the high and low temperature ranges, it is necessary to extract the rates of that chemical step ($k_{hydride}$) at each temperature range. We used the method developed by Klinman and coworkers (*36, 139*):

Equation 6.5

$$k_{hydride} = \frac{k_{cat}({}^{D}k - 1)}{{}^{D}k_{cat} - 1}$$

where $k_{hydride}$ is the unknown rate of the hydride transfer step; ${}^{D}k$ is the intrinsic H/D KIE for this step at each temperature (see Figure 6.1B) and ${}^{D}k_{cat}$ is the H/D KIE for k_{cat} using C6 labeled CH_2H_4folate. To assess the activation parameters for the two temperature regimes, k_{cat} was measured at 5, 20 and 40 °C, Equation 6.5 was used to assess $k_{hydride}$

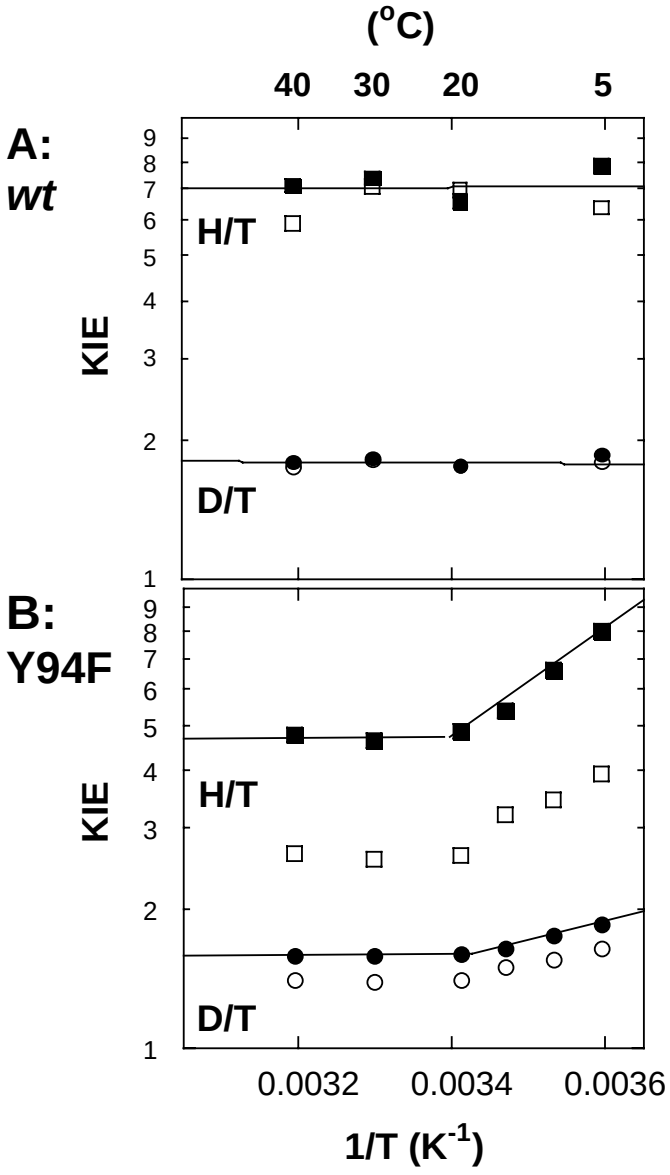

Figure 1.1 Arrhenius plots of observed (empty structures) and intrinsic (filled structures) primary H/T KIEs (squares) and primary D/T KIEs (circles). The lines are the exponential fittings of the intrinsic KIEs to Eq. 6.4. A. *wt*. and B. Y94F.

	Wild type[b]	Y94F		SC A_L/A_T[c]
	5 – 40 ° C	5 – 20 ° C	20 – 40 ° C	
A_H/A_T	6.9 ± 1.0	0.0002 ± 0.0001	4.5 ± 0.5	0.5 – 1.6
A_D/A_T	1.8 ± 0.1	0.07 ± 0.02	1.6 ± 0.1	0.9 – 1.2
ΔE_{aH-T}	0.02 ± 0.09	6.0 ± 0.5	0.03 ± 0.40	
ΔE_{aD-T}	0.01 ± 0.02	1.8 ± 0.2	0.06 ± 0.12	
E_a	4	6.2	3.1	
$\Delta H^{\ddagger}$	3.4	5.6	2.5	
$T\Delta S^{\ddagger}_{25°C}$	-13.7	-14.5	-17.6	

Table 6.1 Rates and isotope effects on Arrhenius parameters of the wild-type and Y94F TS on hydride transfer.[a]

[a.] All energy units are kcal/mol. [b] From ref. (*101*). [c] Semi-classical limits of isotope effects on preexponential factor of Arrhenius equation.(*12*, *13, 7, 34*).

	wild type[b]		Y94F	
Temp. [˚C]	k_{cat} [s^{-1}]	k_{cat} [s^{-1}]	$^{D}k_{cat}$	$k_{hydride}$ [s^{-1}]
40	1.6	0.0067	2.24	0.0109
20	1.1	0.0055	2.36	0.0080
5	0.73	0.0023	4.20	0.0026

Table 6.2 Observed k_{cat} and $^{D}k_{cat}$ used to assess the values of $k_{hydride}$ at 5, 20, and 40 ˚C using Eq. 6.5.[a]

[a.] All relative errors are under 2 % of the measured values and under 6 % of the calculated $k_{hydride}$.

[b.] From ref. (*101*).

(Table 6.2). The Arrhenius equation was used to calculate E_a for the physiological and the low temperature ranges (3.1 and 6.2 kcal/mol, respectively - Table 6.1).

The activation energy at the physiological temperature range, together with the temperature independent intrinsic KIEs suggested that, as with the wt, a Marcus-like model (*7, 22,23,140,141*) is needed to explain the findings for Y94F (*101*). In such a model, the rate for hydrogen tunneling arises from the combination of two terms: one is non-isotopically sensitive but determines most of the temperature dependence of the rates, and the other (depicted as the Franck-Condon term (*22*)) is isotopically sensitive and includes a tunneling contribution and classical fluctuations between donor and acceptor. The tunneling in such a model is dominated by the symmetry of the vibration levels (reorganization energy λ and driving force ΔG^0, the referred to "rearrangement" term in Marcus theory) and by the fluctuations of the distance between donor and acceptor, referred to as "gating") (*22, 140*). According to the Marcus-like model, lack of temperature dependence for both *wt* and Y94F at the higher temperature range indicates ideal prearrangement of the donor and acceptor prior to tunneling, which eliminates the effect of thermally activated "gating". The comparison of Y94F to *wt* suggests that the hydride transfer for both proceeds with a similar "environmentally coupled tunneling" (*140*) at the physiological temperature range. However, at lower temperature, the increase of the Y94F activation energy relative to the *wt* ($\Delta E_{a\ Y94\text{-}wt}$ is about 2.8 kcal/mol) suggests a poorly pre-organized reaction coordinate and substantial need for "gating" (*7, 22, 140*).

Examination of the activation parameters in Table 6.1 results in an interesting observation: most of the reduction in activity caused by the mutation appears to be on the entropy of activation ($\Delta T\Delta S^{\ddagger}$). The change in enthalpy of activation, $\Delta\Delta H^{\ddagger}$, was estimated to be 0.9 kcal/mol while $-\Delta T\Delta S^{\ddagger}$ was about 3.9 kcal/mol at 25 °C. Similar results were also observed for mutants of dihydrofolate reductase (*112*), but it is not clear at this stage how general this phenomenon is. We hope that attracting the community's attention to these observations will lead to more data collection addressing the effect of mutations on activation parameters, and maybe to a better rationalization of this phenomenon.

The relationship between the observed and intrinsic KIEs can be extracted from Eq. 6.6 (7, *65*):

Equation 6.6

$$^{T}(V/K) = \frac{^{T}k_9 + C_f + C_r\,^{T}K_{eq}}{1 + C_f + C_r}$$

At 20 °C, the observed H/T KIE on *V/K* of Y94F was measured to be 2.62 ± 0.01, while the intrinsic value is 4.86 ± 0.18, resulting in a commitment of 1.39 for the hydride transfer step. By contrast, the hydride transfer in the *wt* is commitment free (commitment close to zero) at room temperatures (*10*). The inflated commitment of the observed KIE on *V/K* for Y94F indicates that this hydride transfer step is no longer commitment free (rate limiting) and that a preceding step becomes rate limiting for this mutant.

Summary of the hydride transfer step (step 6 in Scheme 6.1): The Y94F enzyme exhibits biphasic behavior, with temperature independent KIEs at physiological temperature and a steep temperature dependency under 20 ˚C (Figure 6.1). At

physiological temperatures, the intrinsic KIEs were as temperature independent as the *wt*. This is in accordance with conservation of the internal dynamics and coupling of the environment to the hydride transfer step (*7, 140*), indicating only a minor role for the Y94 in step 6. At reduced temperature, the substantial temperature dependency of the KIEs with Y94F indicates a poorly pre-organized reaction coordinate and a need for thermal gating of the donor-acceptor distance (*7, 140*).

The phenomenon of intrinsic phase transition of this type has been previously reported for thermophilic enzymes (*7, 49, 77*) but not yet for a mesophilic enzyme. A possible explanation for the phase transition at 20 ˚C for Y94F (Figure 6.1) is that the removal of the "anchored" Tyr 94 hydroxyl and the lack of localization of the water molecule closest to C5 of dUMP (red ball in Figure 6.2) disrupts the H-bond network at the active site. This, in turn, may alter the structural and dynamic properties of that network (which serves as the acceptor for the C5 proton), leading to a poorly preorganized reaction coordinate and a longer effective donor-acceptor distance at reduced temperature (*7, 140*).

Kinetic analysis – Which step(s) is affected by the Y94F mutation?

Observations:

1. Hydride transfer is rate limiting for both *V/K* and k_{cat} in *wt* (the commitments on both rate constants are close to zero). In contrast, for Y94F both k_{cat} and *V/K* for dUMP are masked (the observed KIEs are smaller than the intrinsic KIEs due to non-zero commitment). This indicates that the mutation affects a kinetic step that is part of both rate constants- e.g., the affected kinetic step is between the formation of the ternary complex and the first irreversible step. Specifically:

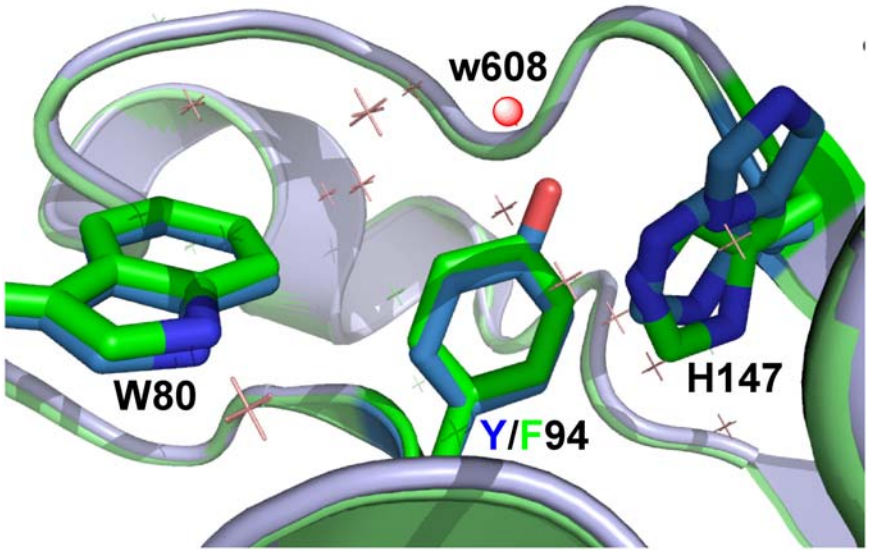

Figure 6.2 *wt* TS (blue - PDB ID # 2FTQ) and Y94F (green - PDB ID # 2FTN) with Y/F94, W80, and H147 presented as sticks. The water molecule closest to the Y94 (w608, 2.6 Å from its O) is highlighted as red ball and is missing in the mutant. All other water molecules are marked by crosses and practically overlap for the *wt* and the mutant. See also Figure 3 in ref (*134*). Note that the two-fold orientation of H147 is only apparent in the *wt* (blue), but not in Y94F (green).

a. For Y94F, the inflated commitment (relative to the *wt*) for the hydride transfer's $^{T}(V/K)$ indicates that the step affected by mutation precedes the hydride transfer.

b. For Y94F, there is a small difference in commitment for the second order rate constant $^{T}(V/K)$ of proton transfer, which indicates a small effect of mutation on the preceding steps, suggesting that most of the effect is after the proton abstraction.

2. The intrinsic KIEs for the proton transfer (using [5-^{3}H]-dUMP) are the same for *wt* and Y94F. This result suggests that the mutation does not affect the proton abstraction step per sé.

3. The K_M for dUMP is not affected by mutation but the K_M for CH_2H_4folate is increased (*125*). This is in accordance with random binding for the mutant, which is proposed here based on the dependence of the observed KIEs for proton abstraction as function of CH_2H_4folate concentration.

4. Santi, D.V., Schultz P.G. and co-workers (*125*) examined relevant mutants (Y146 in *L. casei* TS) as catalysts for CH_2H_4folate-independent dehalogenation of [5-Br]-dUMP, a reaction which simulates early steps of the normal pathway up to and including enzyme-nucleotide covalent adduct formation. Many of these mutants had activity comparable to the wild-type enzyme, indicating that the effects of the mutations occur after the initial covalent adduct is formed.

Interpretation: The effect of the mutation on steps that precede the formation of the ternary complex and proton abstraction is small, and mostly reflects the reduced binding capacity of dUMP (larger k_5 in Scheme 5.2). Most of the effect is on a step(s) that take place between the two H-transfer steps, specifically steps 5 or 5' in Scheme 6.1. Possible events that may occur along step 5 are deprotonation of the enolate in C4 and/or protonation of N5 of the H_4folate leaving group. Possible events that may occur along step 5' are deprotonation of the thiol (if protonated during the elimination step 4') and/or protonation of N5 of the H_4folate leaving group.

Conclusions on chapter V and VI

A new insight into the chemical mechanism of the thymidylate synthase catalyzed reaction is presented. Many studies have proposed that a conserved active site tyrosine (Y94 in *ec*TS) serves as a general base that enhances proton abstraction during the elimination of H_4folate (step 4 in Scheme 6.1; for review see ref (*2*)). The effect of the Y94F mutation on two distinct chemical steps has been examined. These steps were the proton abstraction step (step 4 in Scheme 6.1) and the hydride transfer step (step 6 in Scheme 6.1). The findings indicate that the proposed tyrosine (Y94, 3.6 Å from the proton donor) is not the main contributor to the proton abstraction step, but rather the whole network of H-bonds at the active site appears to serve as the general base. This conclusion is in accordance with the proposal of Hardy and coworkers (*126*) who used 5-deazatetrahydrofolate and concluded that N5 of H_4folate contributes to this general base. Additional candidates away from C5 are the imidazole and carboxylate side chains of H147 (5-6 Å) and E58 (~7 Å). Out of these we prefer the closer and more basic imidazole group. Future work will examine the H147V mutant and the *wt* TS from *B. subtilis*,

which has a Val rather than His in that position. It is of course possible that no single functional group exclusively constitutes the general base, but all three contribute to the basicity of the initial proton acceptor (a water oxygen).

What accounts for the two order of magnitude decrease in Y94F activity relative to the *wt* TS? Taken together, the findings suggest that at physiological temperature the step most affected by the mutation occurs after the proton abstraction and prior to the hydride transfer. According to the mechanism illustrated in Scheme 6.1, these are likely to be step 5 or step 5', specifically the protonation of N5 of H_4folate (in both paths) or the deprotonation of the enol in step 5. Additionally, the mutation weakens the binding and enhances the release of dUMP, which results in a random binding sequence (Scheme 5.2). QM/MM calculations comparing this mutant to the *wt* (*104*) are underway and may offer a molecular insight into the findings reported here.

CHAPTER VII

SUMMARY AND FUTURE SCOPE

Studying the chemical steps within the complex kinetic cascade of enzyme-catalyzed reactions has been a major challenge for chemists and enzymologists. Kinetic isotope effects and their temperature dependency and the activation parameters have been developed as a unique tool to reveal the molecular mechanism, quantum mechanical behavior of H transfer (tunneling), role of protein dynamics, the role of highly conserved residues in the active site and other physical features of the thymidylate synthase catalyzed reaction.

A substantial difference between previous studies and those presented in this thesis is that three different chemical transformations along the same catalytic path were examined: (i) the hydride C-H-C transfer to reduce an exocylic methylene, (ii) a proton C-H-O transfer in the tautomerization reaction, and (iii) a methylene transfer. The study on these transformations exposed the microscopic nature of bond cleavages (tunneling, coupled motion, environmental coupling and rehybridizations) and allowed the investigation of the role of various active site residues in catalyzing these transformations.

Our study on the wild type TS shows the contribution of environmentally coupled tunneling to the rate of hydride transfer. In addition, cofactor inhibition of CH_2H_4folate was observed while measuring the steady state initial velocities across the temperature range of 5 to 40 °C. The data indicated that the inhibition constant has a large binding energy (22 kcal/mol) such that inhibition almost vanishes at elevated temperatures (CHAPTER II).

The sensitivity of the temperature dependence of KIEs to the reaction mechanism has been used to detect effects of mutations close and far from the active site on the nature of the H-transfer(*23*). We applied this method in examination of the H-transfer mechanism (step 6 in Scheme 7.1) by comparison of the temperature dependency of the intrinsic KIEs of the mutant W80M with the wild type (CHAPTER III). Since Met cannot stabilize cation radicals as well as Trp, our findings support a one-step hydride transfer mechanism dominating the reaction for both the mutant and the wild type enzyme.

Experimental methods have been developed to examine the nature of the proton abstraction step that precedes the hydride transfer in the TS reaction pathway. Traditionally, a conserved tyrosine (Y94 in *E. coli*, Y146 in *L. casei*, and Y135 in human) was assumed to serve as the general base catalyzing the proton abstraction. That assumption was examined in Chapter V by comparing the nature of the proton abstraction using wild type (*wt*) *E. coli* TS (*ec*TS) and its Y94F mutant (with a 420-fold reduced turnover rate). Surprisingly, the findings did not suggest a direct role for Y94 in the proton abstraction step. Instead, the whole network of H-bonds at the active site catalyzes the proton abstraction and the cofactor elimination.

Studying on the subsequent hydride transfer step indicated an intrinsic phase transition at 20 °C for the mutant Y94F, suggesing the removal of the “anchored” Tyr 94 hydroxyl and the lack of localization of the water molecule closest to C5 of dUMP disrupted the H-bond network at the active site (Chapter VI). Further study on the temperature dependency of the C5 proton abstraction step is underway. QM/MM study is also underway to gain the molecular insight of this mutation. Significantly, this is also the first time tunneling is examined for two distinct mechanistic steps in one enzymatic

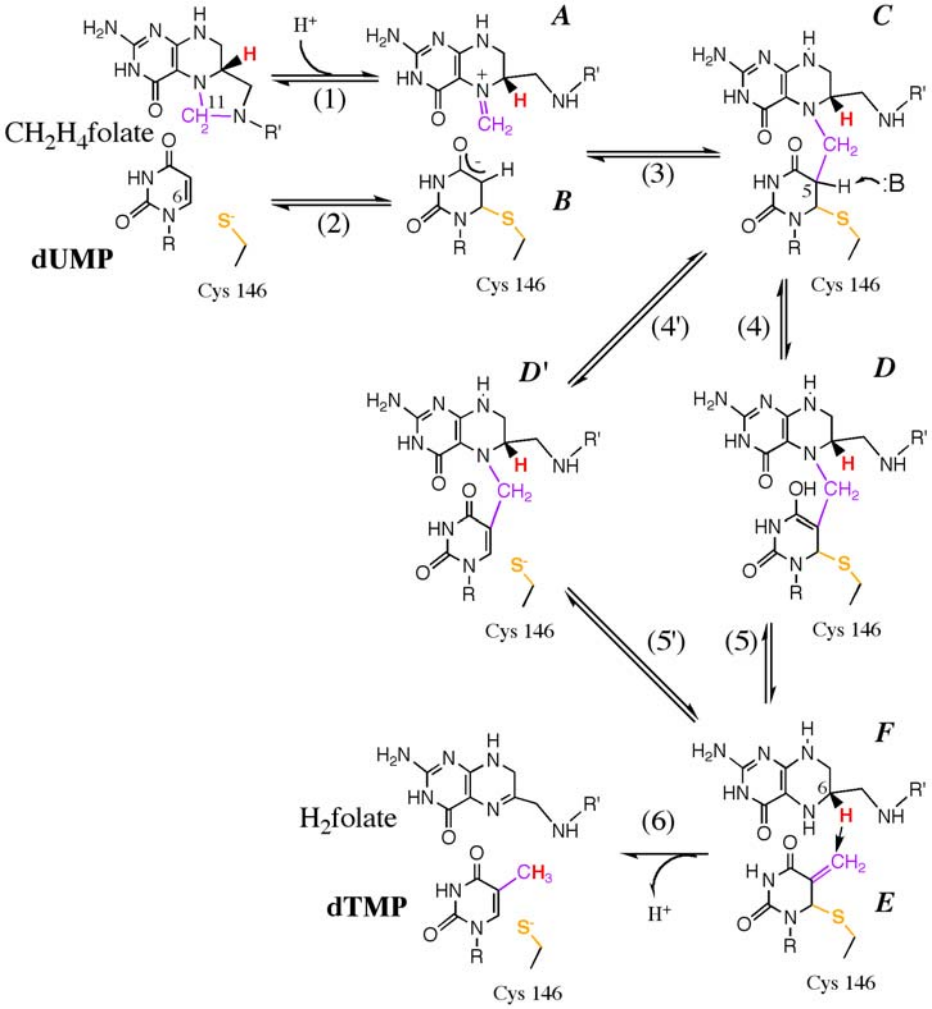

Scheme 7.1 The proposed chemical mechanisms of the TS catalyzed reaction.

reaction. It is interesting to observe whether the enzyme facilitates all chemical transformations through tunneling or only the rate-limiting ones.

Labeling methods have been developed for the 2°KIE study (CHAPTER IV). Our findings indicated no 1° - 2° coupled motion. Inverse values were found for the *V/K* KIE, in accordance with sp^2 to sp^3 at the rate limiting step. Interestingly, Spencer et al. (*27*) found normal values of 2°KIE on k_{cat} measurements, while it is expected to be inverse in that case. Further investigation is needed to understand the nature of this chemical transformation.

In summary, methods have been developed to expose the physical nature of critical steps along the complex reaction coordinate in TS catalyzed reaction (hydride, proton, and methylene). These studies may lead to deeper understanding of enzymatic catalysis and advances in enzymology.

BIBLIOGRAPHY

1. Carreras, C. W., and Santi, D. V. (1995) *Annu. Rev. Biochem. 64*, 721-762.

2. Finer-Moore, J. S., Santi, D. V., and Stroud, R. M. (2003) *Biochemistry 42*, 248-256.

3. Phan, J., Steadman, D. J., Koli, S., Ding, W. C., Minor, W., Dunlap, R. B., Berger, S. H., and Lebioda, L. (2001) *The Journal of Biological Chemistry 276*, 14170-14177.

4. Sergeeva, O. A., Khambatta, H. G., Cathers, B. E., and Sergeeva, M. V. (2003) *Biochemical and Biophysical Research Communications 307*, 297-300.

5. Maley, F., Pedersen-Lane, J., and Changchien, L. (1995) *Biochemistry 34*, 1469-1474.

6. Stroud, R. M., and Finer-Moore, J. S. (2003) *Biochemistry 42*, 239-247.

7. Kohen, A. (2006) in *Isotope Effects in Chemistry and Biology* (Kohen, A. L., H.H. Eds., Ed.) pp 743-764, Taylor & Francis -CRC Press, Boca Raton,FL.

8. Swain, C. G., Stivers, E. C., Reuwer, J. F., and Schaad, L. J. (1958) *J. Am. Chem. Soc. 80*, 5885-5893.

9. Saunders, W. H. (1985) *J. Am. Chem. Soc. 107*, 164-169.

10. Saunders, W. H. (1992) *Croat. Chem. Acta. 65*, 505-515.

11. Lin, S., and Saunders, W. H. (1994) *J. Am. Chem. Soc. 116*, 6107-6110.

12. Bell, R. P. (1980), NY: Chapman & Hall., London, UK and New York,.

13. Melander, L., and Saunders, W. H. (1987) *Krieger, R. E., Ed.) Malabar, FL*.

14. Alhambra, C., Corchado, J. C., Sanchez, M. L., Gao, J., and Truhlar, D. J. (2000) *J. Am. Chem. Soc. 122*, 8197-8203.

15. Kohen, A., and Klinman, J. P. (1998) *Acc. Chem. Res. 31*, 397-404.

16. Kohen, A., and Klinman, J. P. (1999) *Chem. Biol. 6*, 191-198.

17. Antoniou, D., Caratzoulas, S., Kalyanaraman, C., Mincer, J. S., and Schwartz, S. D. (2002) *Eur. J. Biochem. 269*, 3103-3112.

18. Borgis, D. C., and Hynes, J. T. (1991) *J. Chem. Phys. 94*, 3619-3628.

19. Borgis, D. C., and Hynes, J. T. (1993) *Chem. Phys. 170*, 315-346.

20. Bruice, T. C., and Benkovic, S. J. (2000) *Biochemistry 39*, 6267-6274.

21. Kuznetsov, A. M., and Ulstrup, J. (1999) *Can. J. Chem. 77*, 1085-1096.

22. Knapp, M. J., and Klinman, J. P. (2002) *Eur. J. Biochem. 269*, 3113-3121.

23. Wang, L., Goodey, N. M., Benkovic, S. J., and Kohen, A. (2006) *Proc. Natl. Acad. Sci. USA 103*, 15753-15758.

24. Von Laar, J. A., Rustum, Y. M., Ackland, S. P., van Groeningen, C. J., and Peters, G. J. (1998) *Eur.J. Cancer 34*, 296-306.

25. Salonga, D., Danenberg, K. D., Johnson, M. M., R., Groshen, S., Tsao-Wei, D. D., Lenz, H. J., Leichman, C. G., Leichman, L., Diasio, R. B., and Danenberg, P. V. (2000) *Clin. Cancer Res.*, 1322-1327.

26. Copur, S., Aiba, K., Drake, J. C., Allegra, C. J., and Chu, E. (1995) *Biochem. Pharmacol. 49*, 1419-1426.

27. Spencer, H. T., Villafranca, J. E., and Appleman, J. R. (1997) *Biochemistry 36*, 4212-4222.

28. Moore, M. A., Ahmed, F., and Dunlap, R. B. (1986) *Biochemistry 25*, 3311-3317.

29. Hyatt, D. C., Maley, F., and Monfort, W. R. (1997) *Biochemistry 36*, 4585-4594.

30. Barrett, J. E., Maltby, D. A., D.V.Santi, and P.G.Schultz. (1998) *J. AM. CHEM. SOC. 120*, 449-450.

31. Warshel, A., Jen, C. Y., and Villa, J. (2001) *Biophys. J. 80*, 144-151.

32. Warshel, A., and Parson, W. W. (2001) *Q. Rev. Biophys. 34*, 563-679.

33. Klinman, J. P. (2003) *Pure Appl. Chem. 75*, 601-608.

34. Kohen, A. (2003) *Progress in reaction kinetics and mechanism 28*, 119-156.

35. Benkovic, S. J., and Hammes-Schiffer, S. (2003) *Science 301*, 1196-1202.

36. Francisco, W. A., Knapp, M. J., Blackburn, N. J., and Klinman, J. P. (2002) *J. Am. Chem. Soc. 124*, 8194-8195.

37. Atkins, P., and De-Paula, J. (2002) *Physical Chemistry*, 7th Ed., Oxford University Press, Oxford.

38. Bell, R. P. (1980) *Chapman and Hall: London*.

39. Cha, Y., Murray, C. J., and Klinman, J. P. (1989) *Science 243*, 1325-1330.

40. Grant, K. L., and Klinman, J. P. (1989) *Biochemistry 28*, 6597-6605.

41. Glickman, M. H., Wiseman, J. S., and Klinman, J. P. (1994) *J. Am. CHem. Soc. 116*, 793-794.

42. Bahnson, B. J., Park, D.-H., Kim, K., Plapp, B. V., and Klinman, J. P. (1993) *Biochemistry 32*, 5503-5507.

43. Bahnson, B. J., and Klinman, J. P. (1995) *Methods in Enzymology 249*, 373-397.

44. Basran, J., Sutcliffe, M. J., Hille, R., and Scrutton, N. S. (1999) *Biochem. J. 341*, 307-314.

45. Basran, J., Sutcliffe, M. J., and Scrutton, N. S. (1999) *Biochemistry 38*, 3218-3222.

46. Harris, R. J., Meskys, R., Sutcliffe, M. J., and Scrutton, N. S. (2000) *Biochemistry 39*, 1189-1198.

47. Basran, J., Patel, S., Sutcliffe, M. J., and Scrutton, N. S. (2001) *J. Biol. Chem. 276*, 6234-6242.

48. Jonsson, T., Edmondson, D. E., and Klinman, J. P. (1994) *Biochemistry 33*, 14871-14878.

49. Kohen, A., Cannio, R., Bartolucci, S., and Klinman, J. P. (1999) *Nature 399*, 496-499.

50. Hwang, J. K., Chu, Z. T., Yadav, A., and Warshel, A. (1991) *J. Phys. Chem. 95*, 8445-8448.

51. Villa, J., and Warshel, A. (2001) *J. Phys. Chem. B 105*, 7887-7907.

52. Kwart, H. (1982) *Acc. Chem. Res. 15*, 401-408.

53. Anhede, B., and Bergman, N. A. (1984) *J. Am. Chem. Soc. 106*, 7634-7636.

54. Braun, J., Schwesinger, R., Williams, P. G., Morimoto, H., Wemmer, D. E., and Limbach, H. H. (1996) *J. Am. Chem. Soc. 118*, 11101-11110.

55. Brunton, G., Griller, D., Barclay, L. R. C., and Ingold, K. U. (1976) *J. AM. CHEM. SOC. 98*, 6803-6811.

56. Koch, H. F., Dahlberg, D. B., McEntee, M. F., and Klecha, C. J. (1976) *J. AM. CHEM. SOC. 98*, 1060-1061.

57. Kresge, A. J., and Powell, M. F. (1981) *J. Am. Chem. Soc. 103*, 201-202.

58. Butenhoff, T. J., and Moore, C. B. (1988) *J. Am. Chem. Soc. 110*, 8336-8341.

59. Agrawal, N., Mihai, C., and Kohen, A. (2004) *Anal. Biochem. 328*, 44-50.

60. Agrawal, N., Mihai, C., and Kohen, A. (2003) *Anal. Biochem. 322*, 179-184.

61. Changchien, L.-M., Garibian, A., Frasca, V., Lobo, A., Maley, G. F., and Maley, F. (2000) *Prot. Expres. Pur. 19*, 265-270.

62. Rucker, J., Cha, Y., Jonsson, T., Grant, K. L., and Klinman, J. P. (1992) *Biochemistry 31*, 11489-11499.

63. Northrop, D. B. (1975) *Biochemistry 14*, 2644-2651.

64. Northrop, D. B. (1977) *University Park Press, Baltimore, MD.*, 122-152.

65. Northrop, D. B. (1991) *Enzyme mechanism from isotope effects (Cook, P. F.. Ed.)*, 181-202.

66. Streitwieser, A., Jagow, R. H., Fahey, R. C., and Suzuki, F. (1958) *J. Am. Chem. Soc. 80*, 2326-2332.

67. Bahnson, B. J., Colby, T. D., Chin, J. K., Goldstein, B. M., and Klinman, J. P. (1997) *Proc. Natl. Acad. Sci. USA 94*, 12797-12802.

68. Chin, J. K., and Klinman, J. P. (2000) *Biochemistry 39*, 1278-1284.

69. Cook, P. F. (1991) in *Enzyme mechanism from isotope effects* (Cook, P. F., Ed., Ed.) pp 203-230, CRC Press, Boca Raton, FL.

70. Cleland, W. W. (1991) in *Enzyme Mechanism from Isotope Effects (Cook, P. F., Ed.)* pp 247-268, CRC Press, Boca Raton, FL.

71. Stern, M. J. W., R. E. J. (1974) *J. Chem. Phys. 60*, 2808-2814.

72. Schneider, M. E., and Stern, M. J. (1972) *J. Am. Chem. Soc. 94*, 1517-1522.

73. Sutcliffe, M. J., and Scrutton, N. S. (2002) *Eur. J. Biochem. 269*, 3096-3102.

74. Fersht, A. (1998), W. H. Freeman, New York.

75. Charlier, J., and Plapp, B. V. (2000) *J. Biol. Chem. 275*, 11569-11575.

76. Basran, J., Sutcliffe, M. J., and Scrutton, N. S. (2001) *J. Biol. Chem. 276*, 24581-24587.

77. Maglia, G., and Allemann, R. K. (2003) *J. Am. Chem. Soc. 125*, 13372-13373.

78. Antoniou, D., and Schwartz, S. D. (2001) *J. Phys. Chem. B 105*, 5553-5558.

79. Knapp, M. J., Rickert, K., and Klinman, J. P. (2002) *J. Am. Chem. Soc. 124*, 3865-3874.

80. Bruno, W. J., and Bialek, W. (1992) *Biophys. J. 63*, 689-699.

81. Agrawal, P. K., Billeter, S. R., and Hammes-Schiffer, S. (2002) *J. Phys. Chem. B 106*, 3283-3293.

82. Marcus, R. A. (1982) *Faraday Discuss. Chem. Soc. 74*, 7-15.

83. Marcus, R. A., and Sutin, N. (1985) *biochem. Biophys. Acta 811*, 265-322.

84. Agrawal, P. K., Webb, S. P., and Hammes-Schiffer, S. (2000) *J. Am. Chem. Soc. 122*, 4803-4812.

85. Alhambra, C., Sanchez, M. L., Corchado, J. C., Gao, J., and Truhlar, D. J. (2001) *Chem. Phys. Lett. 347*, 512-518.

86. Cui, Q., Elstner, M., and Karplus, M. (2002) *J. Phys. Chem. B 106*, 2721-2740.

87. Cui, Q., and Karplus, M. (2001) *J. Am. Chem. Soc. 123*, 2284-2290.

88. Ostovic, D., Roberts, R. M. G., and Kreevoy, M. M. (1983) *J. Am. Chem. Soc. 105*, 7629-7631.

89. Hermes, J. D., and Cleland, W. W. (1984) *J. Am. Chem. Soc. 106*, 7263-7264.

90. Bibbs, J. A., Demuth, H. U., Huskey, W. P., Mordy, C. W., and Schowen, R. L. (1988) *J. Mol. Catal. 47*, 187-197.

91. Wolfenden, R., Snider, M., Ridgway, C., and Miller, B. (1999) *J. Am. Chem. Soc. 121*, 7419-7420.

92. Doll, K. M., Bender, B. R., and Finke, R. G. (2003) *J. Am. Chem. Soc. 125*, 10877-10884.

93. Doll, K. M., and Finke, R. G. (2003) *Inorg. Chem. 42*, 4849-4856.

94. Padmakumar, R., and Banerjee, R. (1997) *Biochemistry 36*, 3713-3718.

95. Slieker, L. J., and Benkovic, S. J. (1984) *J. Am. Chem. Soc. 106*, 1833-1838.

96. Jaffe, J. J., and R., C. L. (1980) *J. Parasitol 66*, 721-762.

97. Kohen, A., and Limbach, H. H. (2005) *Isotope effects in chemistry and biology*, Talyor & Francis CRC Press:, New York.

98. Sikorski, R. S., Wang, L., Markham, K. A., Rajagopalan, P. T. R., Benkovic, S. J., and Kohen, A. (2004) *J. Am. Chem. Soc. 126*, 4778-4779.

99. Osborn, M. J., Talbert, P. T., and Huennekens, F. M. (1960) *J. Am. Chem. Soc. 82*, 4921-4927.

100. Kallen, R. G., and Jencks, W. P. (1966) *J. Biol. Chem. 241*, 5851-5863.

101. Agrawal, N., Hong, B., Mihai, C., and Kohen, A. (2004) *Biochemistry 43*, 1998-2006.

102. Reid, E. B., and Siegel, J. R. (1954) *J. Chem. Society*, 520-524.

103. Blakley, R. L. (1960) *Nature 188*, 231?32.

104. Kanaan, N., Marti, S., Moliner, V., and Kohen, A. (2007) B*iochemistry.*

105. Kohen, A., and Jensen, J. H. (2002) J. *Am. Chem. Soc.* 1*24,* 3858-3864.

106. J., J. J., and Chrin, L. R. (1980) J. *Parasitol* 6*6,* 53-58.

107. Fritz, T. A., Liu, L., Finer-Moore, J. S., and Stroud, R. M. (2002) B*iochemistry* 4*1.*

108. Barrett, J. E., Lucero, C. M., and Schultz, P. G. (1999) *J. Am. Chem. Soc.* 1*21,* 7965-7966.

109. Hammes-Schiffer, S. C., Kiefer, P. M. H., J. T. (Chapter21), Truhlar, D. G. C., Warshel, A. e. a. C., and Kuznetsov, A. M. U., J. (Chapter 26) (2006) I*sotope Effects in Chemistry and Biology,* Taylor & Francis, CRC Press: Boca Raton, FL.

110. Hammes-Schiffer, S. (2006) A*cc. Chem. Res.* 3*9,* 93-100.

111. Rickert, K. W., and Klinman, J. P. (1999) B*iochemistry* 3*8,* 12218-12228.

112. Wang, L., Tharp, S., Selzer, T., Benkovic, S. J., and Kohen, A. (2006) B*iochemistry* 4*5,* 1383-1392.

113. Wang, L., Goodey, N. M., Benkovic, S. J., and Kohen, A. (2006) P*hyl. Trans. R. Soc. B.* 3*61,* 1307-1215.

114. Basran, J. e. a. C., and Kohen, A. C. (2006) in I*sotope Effects in Chemistry and Biology,* Taylor &Francis, CRC Press., Boca Raton, FL.

115. Kealey, J. T., Eckstein, J., and Santi, D. V. (1995) C*hemistry & Biology* 2*,* 609-614.

116. Ma, J. C., and Dougherty, D. A. (1997) C*hem. ReV. 97,* 1303-1324.

117. Cleland, W. W. C. (2006) in I*sotope Effects in Chemistry and Biology* (Eds., Ed.) pp 915-930, Taylor & Francis, CRC Press:, Boca Raton, FL.

118. Saxl, R. L., Reston, J., Nie, Z., Kalman, T. I., and Maley, F. *(2003)* Biochemistry 4*2, 4544-4551.*

119. Saxl, R. L., Changchien, L.-M., Hardy, L. W., and Maley, F. (2001) Biochemistry 40, 5275-5282.

120. Newby, Z., Lee, T. T., Morse, R. J., Liu, Y., Liu, L., Venkatraman, P., Santi, D. V., Finer-Moore, J. S., and Stroud, R. M. (2006) Biochemistry 45, 7415-7428.

121. Phan, J., Mahdavian, E., Nivens, M. C., Minor, W., Berger, S., Spencer, H. T., Dunlap, R. B., and Lebioda, L. (2000) *Biochemistry 39*, 6969-6978.

122. Hong, B., Haddad, M., Maley, F., Jensen, J. H., and Kohen, A. (2006) *J. Am. Chem. Soc. 128*, 5636 - 5637.

123. Matthews, D. A., Villafranca, J. E., Janson, C. A., Smith, W. W., Welsh, K., and Freer, S. (1990) *J. Mol. Biol. 214*, 937-948.

124. Fauman, E. B., Rutenber, E. E., Maley, G. F., Maley, F., and Stroud, R. M. (1994) *Biochemistry 33*, 1502-1511.

125. Liu, Y., Barrett, J. E., Schultz, P. G., and Santi, D. V. (1999) *Biochemistry 38*, 848-852.

126. Hardy, L. W., Graves, K. L., and Nalivaika, E. (1995) *Biochemistry 34*, 8422-8432.

127. Pogolotti, A. L., Weill, C., and Santi, D. V. (1979) *J. Am. Chem. Soc. 18*, 2794-2798.

128. Carreras, C. W., Climie, S. C., and Santi, D. V. (1992) *Biochemistry 31*, 6038-6044.

129. Huang, W., and Santi, D. V. (1994) *J. Biol. Chem. 269,* 31327-31329.

130. Hayatsu, H., Wataya, Y., Kai, K., and Iida, S. (1970) *Biochemistry 9,* 2858-2865.

131. Wataya, Y., and Hayatsu, H. (1972) *J. Am. Chem. Soc*. 94, 8927-8928.

132. Wataya, Y., and Hayatsu, H. (1972) *Biochemistry 11*, 3583-3588.

133. Cleland, W. W. (1980) *Methods in Enzymol. 64,* 104-125.

134. Roberts, S. A., Hyatt, D. C., Honts, J. E., Changchien, L., Maley, G. F., Maley, F., and Montfort, W. R. (2006) *Acta Cryst. F62*, 840-843.

135. Klinman, J. P., Humphriesg, H., and Voe, J. G. (1980) *J. Biol. Chem. 255*, 11648-11651.

136. Cook, P. F., and Cleland, W. W. (1981) *Biochemistry 20*, 1790-1796.

137. Cleland, W. W. (1987) pp 61-113, Elsevier, Amsyerdam.

138. Maglia, G., and Allemann, R. K. (2003) *J. Am. Chem. Soc. 125*, 13372-13373.

139. Miller, S. M., and Klinman, J. P. (1985) *Biochemistry 24*, 2114-2127.

140. Nagel, Z. D., and Klinman, J. P. (2006) *Chem. Rev. 106*, 3095-3118.

141. Marcus, R. A. (2007) *J. Phys. Chem. B 111*, 6643-6654.